Inaugural dissertation

for

obtaining the doctoral degree

of the

Combined Faculty of Mathematics, Engineering and Natural Sciences

of the

Ruprecht - Karls - University

Heidelberg

Presented by

Aya Abouissa, M.Sc.

born in: Alexandria, Egypt

Oral examination:

Dynamic Endothelial Cell-Driven Cross-Talk in Response to Neonatal vs. Adult Cardiac Pressure Overload: Unraveling Compensatory and Maladaptive Mechanisms

Referees:

Prof. Dr. Marc Freichel

Prof. Dr. Joerg Heineke

Declaration of Originality

I, Aya Abouissa, hereby declare that the presented work in this thesis entitled *'Distinct Endothelial Cell-Driven Responses to Neonatal vs. Adult Cardiac Pressure Overload: Unraveling Adaptive and Maladaptive Pathways'* is my own independent work and has been completed without any unauthorized assistance. I affirm that all references and sources used in the development of this work have been properly cited, and any collaboration with others has been clearly acknowledged.

I certify that this submission meets the standards of originality required by Heidelberg University's Faculty of Biosciences. This work has not been submitted, in whole or in part, for any other degree or qualification at this or any other institution.

Signature: Aya Abouissa

Place/ Date:

1. Abstract

Background: Cardiac pressure overload (PO) is a common detrimental stimulus triggering pathological cardiac remodeling and heart failure (HF) in adult patients, mainly secondary to aortic valve stenosis or chronic arterial hypertension. Despite modern and advanced therapeutic options, HF remains the leading cause of high mortality worldwide. The paucity of regeneration in the adult mammalian heart in response to injury is a key therapeutic barrier in cardiovascular medicine. Upon PO, the adult murine myocardium undergoes significant pathological remodeling, hallmarked by capillary rarefaction, enhanced myocardial apoptosis and interstitial fibrosis. In contrast, our group has previously shown that the neonatal murine heart retains a transient regenerative window during the first postnatal week when subjected to neonatal transverse aortic constriction (nTAC), an in-vivo murine model of PO induction through aortic ligation in neonates. One-day old mice (P1) hearts exposed to nTAC completely adapt in response to injury and maintain cardiac function with minimal signs of myocardial fibrosis. However, nTAC in P7 mice leads to HF. A major contributor to full heart regeneration and adaptation in P1 mice is the rapid and enhanced heart revascularization through angiogenesis in response to nTAC, while this capacity is significantly diminished in P7 mice.

Hypothesis: A highly synchronized endothelial-derived intercellular communication between the different cell compartments of the heart is hypothesized in response to PO, to prevent the shift from the compensatory phenotype observed in P1 mice, to the development of cardiac maladaptation in P7 and adult mice.

Methods: For this purpose, bulk RNA sequencing was first utilized to determine the RNA transcriptomic changes in endothelial cells (ECs) during subacute and chronic phases of PO in adult mice. Additionally, in neonatal mice, single-cell RNA sequencing was used to identify EC sub-populations that play a key role in the transition from an adaptive to a maladaptive response to nTAC. EC-secreted ligands specific to each surgical time point were identified, and their potential autocrine and paracrine effects were analyzed in vitro.

Results: Upon PO induction in adult mice, my experiments show that ECs transiently express collagen and matrix remodeling genes, along with cell cycle-related genes, during the initial short-term response to the surgery. In addition, the upregulation of inflammatory genes by ECs peaked during the subacute phase of PO and remained elevated throughout the chronic stage. Intercellular communication of these EC-secreted matrix proteins triggered cardiomyocytes' hypertrophy, ECs proliferation and migration, along with fibroblasts' migration.

On the other hand, endothelial cells that I isolated from neonatal murine hearts, which exhibit an adaptive response to nTAC, enriched certain EC subpopulations linked to vasculature development and sprouting angiogenesis. Upon analysis, I could identify three interesting EC-secreted ligands. In direct cell contact 2D and 3D co-culture models, overexpression of these candidates in ECs enhanced cardiomyocytes' proliferation and cytokinesis as well as maintained proper cardiomyocyte's contraction. On the contrary, the downregulation of these genes in ECs lead to an opposite maladaptive phenotype in cardiomyocytes.

Conclusion: Conclusively, my work shows that cardiac ECs exhibit a great age- and timepoint-specific dynamic plasticity in response to PO. These observations might shed light on the potential crucial role of EC-derived angiocrine factors in promoting compensatory mechanisms to cardiac pressure overload.

2. Zusammenfassung

Hintergrund: Die Drucküberlastung des Herzens ist ein häufiger schädlicher Stimulus, der bei erwachsenen Patienten ein pathologisches kardiales Remodeling und eine Herzinsuffizienz (HI) auslöst. Hauptsächliche Ursache hierfür sind eine Aortenklappenstenose oder chronischer arterieller Bluthochdruck. Trotz moderner und fortschrittlicher therapeutischer Möglichkeiten ist die HI nach wie vor eine der häufigsten Todesursachen weltweit. Die unzureichende Regenerationsfähigkeit des erkrankten adulten Herzens ist dabei eines der größten therapeutischen Hindernisse in der kardiovaskulären Medizin. Nach PO durchläuft das adulte Mausmyokard einen pathologischen Remodelingprozess, der durch verminderte Kapillarisierung, verstärkte myokardiale Apoptose und interstitielle Fibrose gekennzeichnet ist. In einem in-vivo Mausmodell der PO-Induktion durch Aortenligatur bei Neugeborenen, der neonatalen transversalen Aortenkonstriktion (nTAC), konnte unsere Gruppe bereits zeigen, dass das neonatale Mäuseherz während der ersten postnatalen Woche ein vorübergehendes Regenerationsfenster behält. Ein Tag alte Mäuseherzen (P1), die einer nTAC ausgesetzt sind, passen sich vollständig an die Druckbelastung an und behalten ihre kontraktile Effizienz ohne eine Herzfibrose zu entwickeln. Bei P7-Mäusen führt die nTAC jedoch zu einer HI. Ein Hauptfaktor für die vollständige Regeneration und Anpassung des Herzens bei P1-Mäusen ist die schnelle und gesteigerte Revaskularisierung des Herzens durch Angiogenese als Reaktion auf nTAC, während diese Fähigkeit bei P7-Mäusen deutlich vermindert ist.

Hypothese: Wir postulieren, dass als Reaktion auf PO eine geordnete endotheliale interzelluläre Kommunikation zwischen den verschiedenen Zellkompartimenten des Herzens notwendig ist, um den Übergang von einem kompensatorischen Phänotyp, der bei P1-Mäusen als Reaktion auf PO beobachtet wird, zur Entwicklung einer kardialen Maladaptation bei P7- und erwachsenen Mäusen zu verhindern.

Methoden: Es wurden zunächst Bulk-RNA-Sequenzierungen eingesetzt, um die RNA-Transkriptomveränderungen in Endothelzellen (ECs) während der subakuten und chronischen Phasen von PO in erwachsenen Mäusen zu analysieren. Zusätzlich wurde bei neugeborenen

Mäusen die Einzelzell-RNA-Sequenzierung verwendet, um EC-Subpopulationen zu identifizieren, die eine Hauptrolle beim Übergang von einer adaptiven zu einer maladaptiven Reaktion auf nTAC spielen. Die von den EC sekretierten Liganden, wurden identifiziert, und ihre potenziellen autokrinen und parakrinen Wirkungen wurden in vitro analysiert.

Ergebnisse: Bei der Induktion von PO in adulten Mäusen exprimieren die ECs während der initialen kurzfristigen Reaktion auf den Eingriff vorübergehend Kollagen- und Matrix-Remodeling-Gene sowie zellzyklusrelevante Gene. Darüber hinaus erreichte die Hochregulierung von Entzündungsgenen durch ECs während der subakuten Phase der PO ihren Höhepunkt und blieb während der chronischen Phase erhöht. Die interzelluläre Kommunikation dieser von den ECs sekretierten Matrixproteine führte zur Hypertrophie der Kardiomyozyten, zur Proliferation und Migration der ECs und zur Migration der Fibroblasten.

Andererseits reicherten Endothelzellen aus neonatalen Mäuseherzen mit adaptiver Reaktion auf nTAC bestimmte EC-Subpopulationen an, die mit Gefäßentwicklung und Angiogenese verbunden sind. Es wurden drei interessante Liganden identifiziert, die von diesen ECs produziert werden. In 2D- und 3D-Kokulturmodellen mit direktem Zellkontakt verstärkte die Überexpression dieser Kandidaten in ECs die Proliferation und Zytokinese der Kardiomyozyten und hielt die Kontraktionsfähigkeit der Kardiomyozyten aufrecht. Im Gegensatz dazu führte die Herunterregulierung dieser Gene in ECs zu einem gegenteiligen maladaptiven Phänotyp in Kardiomyozyten.

Schlussfolgerung: Mein Arbeit zeigt, dass kardiale ECs eine große alters- und zeitpunktspezifische dynamische Plastizität als Reaktion auf PO aufweisen. Diese Beobachtungen könnten Aufschluss über die potenziell zentrale Rolle aus EC stammender angiokriner Faktoren für die kardiale Kompensation nach Druckbelastung geben.

3. Acknowledgment

I would like to express my deepest gratitude to everyone who supported me throughout this journey.

First and foremost, I want to thank my thesis supervisor, Prof. Dr. Joerg Heineke, for his unwavering guidance, patience, and encouragement. His expertise and insight have been invaluable, and I am profoundly grateful for the opportunity to do my doctoral thesis under his mentorship. This work would not have been possible without your support.

I would also like to extend my sincere thanks to Prof. Dr. Thomas Wieland, my faculty supervisor for the HBIGS, for his valuable guidance throughout the doctoral program, and for being part of the Thesis Advisory Committee meetings. My sincere gratitude also for Prof. Dr. Marc Freichel for accepting to be part of my Defense Examination Committee. I deeply appreciate you for taking the time to review my work and provide thoughtful feedback. A special thanks for Dr. Chi-Chung Wu and Dr. Mahak Singhal for accepting the invitation to be examiners for my doctoral thesis defense and I am looking forward to their expertise that would greatly enhance the rigor and quality of the examination process.

A special thank you to our collaborators, especially to Prof. Dr. Gergana Dobreva, for being an essential part during my Thesis Advisory Committee meetings. Her contributions have greatly enriched my research and her shared knowledge has been essential in bringing this work to fruition. My sincere gratitude for Dr. Julio Cordero for his valuable guidance with bioinformatic analysis. I also extend my genuine appreciation for Dr. Adel El-Sherbiny, Dr. Karin Haack and Arthur Mathes for generously sharing their laboratory expertise with me.

I would also like to acknowledge the support and resources provided by the Heidelberg Biosciences International Graduate School (HBIGS), which has played a critical role in my academic and professional development. My special thankfulness to Dr. Rolf Lutz and Ms. Martina Galvan for their precious guidance throughout my PhD journey.

I am incredibly grateful to my lab colleagues for their camaraderie, assistance, and the collaborative spirit that made our lab such a great place to work. Special appreciations go to our lab technical assistants Nina Weinzierl, Elvira Wink and Dr. Manuela Fuhrmann for their great support and generous teaching of all the required techniques and for their special

motherly care. Our friendship and deep bond that we developed throughout these years will remain in my heart forever. My deep appreciations for Dr. Amelie Schober for her generous, clear support and laboratory help, your knowledge and expertise have helped me refine my work and will bring it even more forward. Special thanks to my former PhD colleagues Shruthi, Merve and Steve, thank you for being really good colleagues and friends and I really appreciate the spirit we had together and commonly sharing our experiences and struggles while supporting each other through our journey. And my outstanding gratitude for my current PhD colleague Javier, who despite his relatively new presence in our group, has made a big difference in the lab spirit. I do really appreciate our special bond, funny jokes, recharging gossips and most of all our shared support on all aspects. I am deeply thankful for our relatively young yet strong friendship. Finally yet importantly, I would like to express my appreciation for my former M.Sc. student Mhd Amin Alzabibi for his great support and work along with my project and his ultimate and remarkable motivation.

To my family, words cannot express how grateful I am for your unconditional love and support. You have been my foundation throughout this journey, and I am forever thankful for your belief in me. Specially my mom, Prof. Dr. Noha Nafee, who I inherited the “researcher gene” from and who, despite being miles away and all her busy schedules, always finds a way to be present in my best and hardest times, supporting me continuously with her warm hugs, sincere advices and beautiful prayers. In addition, I am very thankful for my dad Amr, my aunt and cousins for your long-distance heartful support and our cheering long phone calls.

To my miles-away childhood besties, Rodaina and Ebtehal, who despite the distance separating us since primary school, we always find a way to connect, feel and understand each other even without talking. Thank you for continuously checking on me, being there through my hardest times and keeping me in your heart and mind. Our special ARE-bond will remain my unbreakable safe-zone forever. To my friends, Rahma, Karima and Nada, thank you for your constant encouragement, for listening when I needed to talk, and for helping me find balance. Special thanks to Maksood, your companionship has been a precious source of my strength.

Finally, to my beloved cat, Marshmallow, thank you for your comforting presence and for always being there to brighten my days, especially during the most challenging moments. You provided much-needed hugs, joy and relaxation.

This thesis is as much yours as it is mine.

4. Table of Content

5. List of Figures

6. List of Tables

7. Abbreviations

α-SMA	Alpha-Smooth Muscle Actin
AAV	Adeno-Associated Viruses
ACE2	Angiotensin Converting Enzyme 2
ACE inhibitors	Angiotensin-Converting-Enzyme inhibitors
AO	Aorta
ARBs	Angiotensin Receptor Blockers
ARNIs	Angiotensin Receptor Neprilysin Inhibitors
AS	Aortic Stenosis
bmp	Beats per Minute
BP	Biological Processes
BSA	Bovine Serum Albumin
CM	Cardiomyocytes
CVDs	Cardiovascular Diseases
DNA	Deoxyribonucleic Acid
EC	Endothelial Cells
ECM	Extracellular Matrix
EF	Ejection Fraction
EndMA	Endothelial-to-Mesenchymal Activation
EndMT	Endothelial-to-Mesenchymal Transition
eNOS	endothelial Nitric Oxide Synthase
EtOH	Ethanol
FACS	Fluorescence-Activated Cell Sorting
FB	Fibroblasts
FCS	Fetal Calf Serum
GO	Gene Ontology
HCl	Hydrochloric acid
HF	Heart Failure
HFpEF	Heart Failure with Preserved Ejection Fraction
HFrEF	Heart Failure with Reduced Ejection Fraction

HR	Heart Rate
HW/BW	Heart Weight to Body Weight ratio
IB4	Isolectin B4
KCl	Potassium Chloride (Kaliumchlorid)
Ki67	Antigen Kiel 67 (MKi67)
LCCA	Left Common Carotid Artery
L-Glu	L-glutamine
LVEDA	Left-Ventricular End-Diastolic Area
LV-EF	Left-Ventricular Ejection Fraction
LV-FS	Left-Ventricular Fractional Shortening
LVID	Left-Ventricular Internal Diameter
LVPW	Left-Ventricular Posterior Wall thickness
mRNA	Messenger Ribonucleic Acid
NO	Nitric Oxide
NRCM	Neonatal Rat Cardiomyocytes
NRFB	Neonatal Rat Fibroblasts
nTAC	Neonatal Transverse Aortic Constrition
O.C.T.	Optimal Cutting Temperature embedding medium
PBS	Phosphate-Buffered Saline
PFA	Paraformaldehyde
PI3K	Phosphotidylinositol 3 Kinase
PO	Pressure Overload
P/S	Penicillin/ Streptomycin
PW	Pulse Wave Doppler
qRT-PCR	Quantitative Real-Time Polymerase Chain Reaction
RAAS	Renin-Angiotensin-Aldosterone System
RCCA	Right Common Carotid Artery
RNA	Ribonucleic Acid
ROS	Reactive Oxygen Species
RT	Room Temperature
s.c.	Subcutaneous Injection
scRNAseq	Single-Cell RNA Sequencing

SGLT2i	Sodium-Glucose Co-Transoporter-2 Inhibitors
snRNAseq	Single-Nucleus RNA Sequencing
SNS	Sympathetic Nervous System
TAC	Transverse Aortic Constriction
TAZ	Transcriptional Co-Activator With PDZ-Binding Motif
TGF-β	Transforming Growth Factor Beta
TF	Transcription Factor
UMAP	Uniform Manifold Approximation and Projection
w/v	Weigh per Volume
YAP	Yes-Associated Protein
µm	Micrometer

8. Chapter 1: Introduction

8.1. Cardiovascular Diseases (CVDs) and Heart Failure (HF)

8.1.1. Epidemiology of CVDs

Cardiovascular diseases (CVDs) encompass various disorders impacting the heart and blood vessels, such as heart failure, coronary artery disease, arrhythmias, and stroke. These conditions are primarily triggered by chronic arterial hypertension, atherosclerosis, and other factors that impair blood flow and heart function. Despite modern advancements in diagnostic and therapeutic options, cardiovascular diseases (CVDs) continue to be the leading cause of mortality worldwide. They account for approximately 17.9 million deaths annually, representing about 32% of all global deaths, even surpassing cancer.[1,2]

Although age, gender, ethnicity, and lifestyle are the primary factors driving the global prevalence of reported CVDs, morbidity and mortality rates are influenced by genetic predisposition, comorbidities, environmental triggers, as well as the socioeconomic conditions of the country. Although the prevalence and impact may vary, CVDs affect both genders while men tend to develop CVDs at a younger age compared to women.[3]

Hypertension is a significant risk factor for cardiovascular diseases (CVDs), affecting nearly half of middle-aged men (over 45 years old) and increasing the prevalence of CVDs in men to 30%.[3] Conversely, women typically encounter CVDs later in life, often after menopause when the protective effects of estrogen diminish. Despite this later onset, CVDs continue to be the primary cause of death for women, with approximately one in three women succumbing to heart disease or stroke. [4]

While CVDs are relatively uncommon in children compared to adults, they can have profound implications for their health and development. Congenital heart defects are the most prevalent type of CVD in children, affecting approximately 1% of newborns worldwide. [5] However, the rising prevalence of risk factors like high blood pressure and elevated cholesterol levels among children is influenced by childhood obesity, sedentary lifestyles, and poor dietary habits. These factors may increase the likelihood of CVDs in adulthood. [6]

Even though 85% of CVDs related deaths were due to heart attack and stroke, heart failure (HF) significantly impacts the prevalence and burden of CVDs globally. It impacts around 26 million

individuals globally and is a leading cause of hospitalizations and mortality, contributing substantially to healthcare expenses. [7]

8.1.2. Heart Failure

Heart failure (HF) is a complex clinical syndrome characterized by the inability of the heart to pump oxygenated blood efficiently to meet the body's metabolic needs. This condition usually arises due to structural or functional abnormalities in the heart, which hinder its ventricular ability to fill with or to eject blood. [8] This leads to heart failure, classified into two main types: heart failure with preserved ejection fraction (HFpEF) and heart failure with reduced ejection fraction (HFrEF). This typically involves an abnormality in the myocardium that causes dysfunction in ventricular diastole and/or systole, respectively. [9]

HFpEF is a subtype of heart failure characterized by symptoms of HF in the presence of a preserved left ventricular ejection fraction (LV-EF) of 50% or higher. It is associated with diastolic dysfunction, characterized by myocardial stiffness that hinders proper relaxation and filling during the diastole. [10] Strategies for managing HFpEF prioritize symptom control, managing associated conditions, and encouraging lifestyle changes, although specific targeted therapies are currently more limited compared to those available for HFrEF, with empagliflozin being the first drug with proven benefit in HFpEF.[9]

On the other hand, HFrEF is a form of heart failure characterized by impaired left ventricular systolic function, leading to a reduced LV-EF typically below 40%. [8] HFrEF is usually manifested by different stages: acute and chronic phases. Episodes of acute heart failure exacerbations are marked by the sudden onset or worsening of symptoms, often necessitating hospitalization for intensive management and stabilization. In contrast, chronic heart failure refers to a persistent condition where symptoms endure and deteriorate over time despite treatment, significantly affecting patients' quality of life and life expectancy. [11]

Generally, HFpEF and HFrEF share the same clinical phenotype. Common symptoms often include dyspnea, fatigue, exercise intolerance, and fluid retention due to inadequate cardiac output and increased filling pressures. [9] Although they share many clinical similarities, HFpEF and HFrEF are distinct disorders within the spectrum of heart failure, with different pathogenesis requiring unique tailored treatment modalities.

8.1.3. Pathophysiology of Heart Failure

Although HFpEF and HFrEF are within the same disease spectrum, they differ significantly in their pathophysiological triggers. The major risk factors for HFpEF include obesity, arterial hypertension, metabolic syndrome, renal dysfunction, and atrial fibrillation. [10] Conversely, HFrEF often results from myocardial damage, such as that caused by myocardial infarction, chronic hypertension, or cardiomyopathies. [11]

Generally, HF pathophysiology involves a cascade of complex interactions that lead to the heart's inability to pump blood effectively, failing to fulfill the body's metabolic demands. Central to this condition is the interplay between structural and functional cardiac abnormalities, neurohormonal dysregulation, and systemic responses, all of which contribute to the progressive nature of the disease. At the core of heart failure is the initial myocardial injury or stress, often resulting from conditions such as ischemic heart disease, uncontrolled hypertension, valvular heart disease, or cardiomyopathies. This injury leads to impaired myocardial contractility, increased cardiac pressure overload, reduced cardiac output, and ventricular remodeling—a maladaptive process that includes ventricular dilation, myocardial hypertrophy, and interstitial fibrosis. [12,13]

Following injury and impaired myocardial function, the reduced cardiac output triggers compensatory mechanisms aimed at maintaining adequate perfusion. Among these mechanisms, the activation of the renin-angiotensin-aldosterone system (RAAS) and the sympathetic nervous system (SNS) are paramount. While initially beneficial, chronic activation of these systems exacerbates heart failure. The RAAS promotes vasoconstriction, sodium and water retention, and stimulates aldosterone and angiotensin II production, which in turn lead to increased blood volume and pressure, further straining the heart. [12] On the other hand, the SNS increases heart rate and contractility, however, prolonged stimulation induces direct cardiotoxic effects, including increased myocardial oxygen demand, fibrosis, and apoptosis. Persistent SNS and RAAS signaling results in elevated circulating levels of the neurohormones norepinephrine and angiotensin II, respectively, further deteriorating heart function and symptoms.

The interplay between these mechanisms results in a vicious cycle of worsening heart function and symptoms, such as dyspnea, fatigue, and fluid retention. These pathophysiological insights have guided the development of targeted therapies for heart failure, including RAAS inhibitors

(like Angiotensin-converting-enzyme inhibitors and angiotensin receptor blockers, ACE inhibitors and ARBs, respectively), beta-blockers, and mineralocorticoid receptor antagonists, which aim to mitigate neurohormonal activation, reduce cardiac workload, and prevent adverse remodeling. Although new treatment modalities are evolving including a combination of angiotensin receptor blockers plus neprilysin inhibitors (ARNIs), sodium-glucose co-transoporter-2 inhibitors (SGLT2i), soluble guanylate cyclase stimulators and myosin activators, the morbidity and mortality of heart failure remains high, and therefore new therapeutic targets need be identified to develop treatments that extend beyond the current treatment algorithms.

8.2. Cardiac Pressure Overload (PO)

8.2.1. Pathophysiology of cardiac PO

Cardiac pressure overload (PO) is a condition characterized by increased resistance against which the heart must contract and pump the blood, often resulting from chronic arterial hypertension [14] valvular heart diseases such as aortic stenosis (AS). [15-18] This pathological state necessitates increased myocardial force generation to maintain cardiac output, leading to several compensatory and maladaptive changes within the myocardium.

The most prominent adaptation is left ventricular hypertrophy (LVH), characterized by the thickening of the ventricular wall and increased muscle mass. This hypertrophy is a response to increased afterload and is initially beneficial as it helps normalize wall stress and maintain stroke volume. [14,19] At the cellular level, this involves cardiomyocyte hypertrophy, enhanced sarcomere organization, and changes in extracellular matrix composition, including increased collagen deposition, which collectively contribute to thickened ventricular walls. [14,18]

However, prolonged pressure overload induces pathological remodeling. The hypertrophic myocardium becomes stiff and less compliant, impairing diastolic filling and leading to diastolic dysfunction. [14,15] This diastolic dysfunction can progress to HFpEF, where the heart maintains a normal ejection fraction but cannot adequately fill during diastole, leading to congestive symptoms.

Additionally, the hypertrophied myocardium has increased oxygen demand, which can outstrip supply, particularly in the presence of concurrent coronary artery disease, leading to ischemia

and fibrosis. [10,18] At a certain stage of disease progression, even eliminating the pressure overload cannot adequately improve heart failure. [20]

8.2.2. Cellular and Molecular Changes in Cardiac Pressure Overload

Numerically, endothelial cells (EC), cardiomyocytes (CM), and fibroblasts (FB) are the three main cell types in the adult heart. CMs make up about 30% of the total cell count, ECs are approximately three times more numerous than cardiomyocytes, and FB represent a less abundant fraction. [21] Cardiac remodeling in response to PO is characterized by an interplay between all the constituting cell types.

8.2.2.1. Contribution of Adult Cardiomyocytes to PO and HF

Cardiomyocyte hypertrophy in response to PO is a crucial adaptive mechanism that allows the heart to cope with increased hemodynamic demands. This hypertrophic response is driven by various stimuli, including mechanical stress exerted on the myocardium, primarily due to conditions such as chronic arterial hypertension and AS, which increase the afterload against which the heart must pump. [15,23] Additional stressors include neurohormonal activation (particularly RAAS and SNS), and autocrine/paracrine growth factors such as transforming growth factor-beta (TGF-β) and insulin-like growth factor-1 (IGF-1).

Pathological cardiac hypertrophy can manifest in two distinct forms: concentric and eccentric hypertrophy, each associated with different hemodynamic stressors and clinical implications. Concentric hypertrophy is an initial compensatory mechanism to the increased pressure overload associated with chronic arterial hypertension and AS. This form of hypertrophy is characterized by an increase in CMs width by adding new sarcomeres side-by-side in parallel to existing sarcomeres. This increase in ventricular wall thickness to overcome persistent afterload pressure further leads to significantly reduced chamber radius. Histologically, pressure overload-induced hypertrophy is characterized by an increase in left ventricular wall thickness without a corresponding increase in chamber size. [15] At the cellular level, concentric hypertrophic cardiomyocytes exhibit an increased cross-sectional area and enhanced organization of sarcomeres, which are arranged in parallel to generate greater contractile force. This structural remodeling helps the heart maintain stroke volume and cardiac output despite the elevated hemodynamic afterload. [15,22,23]

Eccentric hypertrophy, on the other hand, arises from volume overload conditions. This type of hypertrophy allows the heart to accommodate increased blood volume and maintain cardiac output by dilating the chamber and elongating cardiomyocytes. At the cellular level, eccentric hypertrophic cardiomyocytes exhibit a serial arrangement of sarcomeres leading to an elongated phenotype of cardiomyocytes. This type of hypertrophy is marked by an increase in ventricular chamber size, resulting in overall dilation of the ventricle. [22,23]

The net increase in wall thickness associated with concentric cardiac hypertrophy is initially considered an early adaptive response to PO. According to the law of Laplace, this thickening reduces wall stress and consequently lowers oxygen demand. [22,24] However, over time, persistent pathological PO can become maladaptive and result in increased myocardial stiffness, impaired diastolic function and a reduced ventricular compliance predisposing to arrhythmias and HF. Concentric cardiac hypertrophy often transitions into eccentric hypertrophy in the final disease state.

On the molecular level, the hypertrophic response involves complex intracellular signaling cascades and structural changes within the cardiomyocytes, upon exposure to increased mechanical load. Augmented ventricular load results in greater wall stress for each CM, which is a key factor in myocardial energy consumption. Moreover, the hypertrophied myocardium has higher metabolic demands and is more susceptible to ischemic injury. On the cell membrane, mechanical stretch receptors, such as integrins and mechanosensitive ion channels, initiate signaling through pathways including the mitogen-activated protein kinase (MAPK) pathway, the phosphoinositide 3-kinase (PI3K)/Akt pathway, and the nuclear factor of activated T-cells (NFAT) pathway. These pathways promote gene transcription and protein synthesis, leading to the concentric enlargement of CM. Key transcription factors such as GATA4, NFAT, and myocyte enhancer factor 2 (MEF2) are upregulated, driving the expression of genes associated with hypertrophy, thereby elucidating an initial compensatory response preserving the contractile function. [15,23,25,26] The preliminary adaptive hypertrophy is characterized by augmented synthesis of contractile proteins such as myosin heavy chain and actin, increased ribosomal biogenesis, and enhanced protein translation.

On the other hand, calcineurin activation by increased calcium levels results in the translocation of NFAT to the nucleus and the activation of prohypertrophic genes. This aberrant activation drives eccentric hypertrophy to injury and cardiac dilation, which leads to a

decompensated state that is characterized by a strongly reduced cardiac functional performance. [15,25]

Concurrently, neurohormonal activation plays a significant role in cardiomyocyte hypertrophy. The RAAS and SNS are activated in response to reduced cardiac output and blood pressure. Angiotensin II, a key effector of RAAS, binds to its receptors on cardiomyocytes, stimulating hypertrophic growth via the activation of the MAPK pathway and upregulation of growth-promoting genes. Similarly, catecholamines released by the SNS act on beta-adrenergic receptors, Sfurther enhancing hypertrophic signaling. [12,15]

Moreover, the hypertrophied myocardium is at an increased risk of arrhythmias due to electrical remodeling, including changes in ion channel expression and distribution. The altered electrophysiological properties, coupled with structural remodeling, create a substrate for reentrant circuits and increased susceptibility to ventricular arrhythmias and sudden cardiac death. [23] Additionally, CMs initially adapt to the increased hemodynamic demand by inducing certain metabolic changes and switching from fatty acids to glucose consumption. [27]

A major contributor to pathogenic remodeling after heart injury is the limited ability of adult cardiomyocytes to proliferate. The regenerative capacity of adult cardiomyocytes is significantly constrained compared to other tissues, which poses a substantial challenge for heart repair following injury. [27,28] In adult mammals, the turnover rate of cardiomyocytes is extremely low, with an annual renewal rate of approximately 1% at a young age, decreasing to about 0.45% in older adults. This limited regenerative ability is primarily because most CMs exit the cell cycle shortly after birth and rarely re-enter it, resulting in their inability to proliferate sufficiently in response to cardiac injury, where a substantial loss of cardiomyocytes leads to scar formation and compromised cardiac function. [28]

Several molecular mechanisms underpin this limited regenerative capacity. For instance, the cell cycle regulatory proteins such as cyclins and cyclin-dependent kinases (CDKs) are downregulated in CMs shortly after birth, inhibiting their proliferation. Additionally, the Hippo signaling pathway, which is known to regulate organ size by controlling cell proliferation and apoptosis, is highly active in adult cardiomyocytes and acts as a brake on their proliferation. The upregulation of cell cycle inhibitors like p21 and p27 further prevents cardiomyocytes from dividing. [27,29]

8.2.2.2. Functional Involvement of Non-Cardiomyocytes to the Pathophysiology of Pressure Overload

Cardiac Endothelial Cells (ECs)

Endothelial cells are the most numerous cell type in the adult heart. [21,44] They play a crucial role in maintaining cardiovascular homeostasis by regulating vascular tone, blood flow, and barrier function. In the context of cardiac PO, ECs contribute significantly to the pathological maladaptation of the adult heart by various mechanisms. Initially, endothelial dysfunction is a hallmark of CVDs and is characterized by a diminished capacity of ECs to perform their normal functions. Specifically, under PO, decreased nitric oxide (NO) bioavailability leads to impaired vasodilation, increased vascular resistance, and subsequent cardiac stress. [45-47] Additionally, increased oxidative stress, driven by reactive oxygen species (ROS) such as superoxide anions, contributes to endothelial dysfunction. ROS can further reduce NO bioavailability by converting NO to peroxynitrite, exacerbating vascular stiffness and inflammation. [45,48]

Interestingly, in PO conditions, angiogenesis can be maladaptive. Although initial angiogenic responses aim to compensate for increased myocardial demands, sustained pressure overload often leads to insufficient angiogenesis and capillary rarefaction. [49,50] This inadequacy results in myocardial hypoxia and fibrosis, further contributing to cardiac dysfunction. [51]

In addition to their autocrine role in PO, ECs act in a paracrine manner and play a central role in mediating inflammatory responses in the injured adult heart. In response to ischemia, activated ECs produce pro-inflammatory cytokines (e.g., IL-6, TNF-α) and chemokines that recruit immune cells to the myocardium. This inflammatory milieu exacerbates CMs injury and fibrosis. Likewise, ECs upregulate adhesion molecules (e.g., ICAM-1, VCAM-1) that facilitate the adhesion and transmigration of leukocytes into the cardiac tissue, amplifying the inflammatory response and contributing to adverse remodeling. [52] As a complementary approach, ECs adapt to PO by enhancing the secretion of endothelin-1 and neuregulin-1, which potently induce CMs hypertrophy.

On the other hand, Endothelial-to-Mesenchymal Activation (EndMA) is a process whereby ECs temporally lose their endothelial characteristics and acquire a mesenchymal, fibroblast-like phenotype. In response to PO, ECs gradually undergo EndMA where they co-express endothelial markers (e.g., VE-Cadherin, CD31) as well as mesenchymal markers (e.g., α-SMA,

vimentin). These transformed cells contribute to the pool of myofibroblasts, which produce excessive extracellular matrix components, leading to myocardial fibrosis and stiffness. Under PO, elevated levels of TGF-β activate downstream Smad-dependent pathways as well as Sox9-derived Ccn2 secretion in ECs that drive the transition and promote fibrosis. [53-55]

Therefore, improving the integrity and functionality of cardiac endothelial cells could be crucial in enhancing the myocardial response to pressure overload and reducing maladaptive remodeling.

Cardiac Fibroblasts (FBs)

Cardiac fibroblasts, being the third most abundant cells in the adult heart [21,44], play a critical role in maintaining the structural and functional integrity of the myocardium. Physiologically, FBs maintain extracellular matrix (ECM) homeostasis, providing a structural scaffold for CMS, distributing mechanical forces throughout the cardiac tissue, and mediating electrical conduction. [56] Under conditions of cardiac PO, FBs undergo significant changes that contribute to pathological cardiac remodeling and HF in adults. This response includes several mechanisms leading to FBs activation and proliferation. Initially, increased mechanical stressed from PO is sensed by cardiac FBs, leading to their activation. This involves mechano-transduction pathways that convert mechanical signals into biochemical responses, promoting fibroblast proliferation and survival. [56,57] Furthermore, factors such as transforming growth factor-beta (TGF-β), upregulated in pressure overload conditions, bind to receptors on FBs, initiating signaling cascades that result in their activation and proliferation. [57]

Subsequently, a subfraction of activated FBs differentiate into myofibroblasts, which have distinct characteristics and play a pivotal role in fibrosis. Myofibroblasts express alpha-smooth muscle actin (α-SMA) and have enhanced contractile properties. They are highly synthetic and produce large amounts of ECM proteins, particularly collagen types I and III. [57,58]

Additionally, one of the most critical roles of FBs in the context of pressure overload is ECM remodeling, which over time becomes maladaptive. Activated myofibroblasts significantly increase the synthesis of ECM components, such as collagens, fibronectin, and proteoglycans. This excessive ECM deposition leads to myocardial fibrosis, which stiffens the heart and impairs its contractile function. [44,59]

While the initial reparative fibrosis is essential for preventing ventricular wall rupture, an excessive fibrotic response and reactive fibrosis outside the injured area are harmful, as they progressively impair cardiac function and can ultimately lead to heart failure. Therefore, identifying factors that balance the fibrotic response to cardiac injury is crucial for proper heart regeneration and adaptation.

8.3. Pivotal Adaptation of Neonatal Mice to Cardiac Pressure Overload

In comparison, neonatal murine hearts exhibit an extraordinary regenerative capacity that starkly contrasts with the limited reparative abilities of their adult counterparts. This adaptive potential is particularly evident within the first days of life, during which neonatal hearts can recover from significant injuries without permanent damage or scar formation. This regenerative capacity is primarily attributed to the cardiomyocytes retaining their ability to proliferate within three days after birth. However, starting from the fourth postnatal day, CMs transition from a hyperplastic state to a hypertrophic phenotype, as part of the normal heart growth process. [61]

Experimental studies in mice and pigs have demonstrated that neonatal hearts can fully regenerate following partial surgical resection or myocardial infarction, and entirely restore heart function within weeks. [30-32] In mice, this regenerative capacity peaks within the first three days after birth, but gradually decreases and ends by the seventh postnatal day.

In this context, multiple neonatal cardiac injury models have been developed to study the heart's regenerative capacity in response to various injurious stimuli. In 2011, Porrello and his colleagues have demonstrated that surgical resection of 15% of the left ventricular apex in 1-day old (P1) mice completely regenerates within 21 days. Following a robust inflammatory response, pre-existing resident CMs proliferated and completely restored normal cardiac function in response to the injury. In contrast, subjected to the same injury, P7 mice failed to regenerate and the resected part was replaced by a scar fibrotic tissue. [30,62] Since then, this regenerative window was also verified in other neonatal in-vivo murine models inducing direct ischemic injury on the myocardium through cryoinjury and coronary artery ligation. [63-65]

In our group, we pioneered a novel neonatal model to induce cardiac pressure overload in newborn mice. [66] In this model, we perform neonatal transverse aortic constriction (nTAC) by

ligating the aorta between the brachiocephalic artery and the left common carotid artery (LCCA). This procedure induces pressure overload on the heart, simulating aortic stenosis and arterial hypertension in patients. We discovered that performing nTAC in P1 mice during their regenerative phase resulted in an adaptive response and maintained proper cardiac function and ejection fraction (EF). This cardiac adaptation was primarily attributed to increased CMs proliferation and enhanced myocardial angiogenesis.[35,66] In contrast, nTAC in P7 mice (non-regenerative stage) induced a maladaptive phenotype hallmarked by increased interstitial fibrosis and CMs hypertrophy, resulting in significant cardiac dysfunction.

This regenerative ability in neonates is characterized by substantial cardiomyocyte proliferation and repair following injury leading to the formation of new myocardial tissue. [26,31,32] One crucial aspect contributing to this age-specific phenomenon is the unique molecular and cellular environment present in the neonatal heart, which supports and promotes cardiomyocyte proliferation and tissue regeneration. [26,31,32] This includes the interplay between ECs and FBs to potentiates CMs proliferation and adaptation to cardiac PO in neonates.

The underlying mechanisms that enable this robust regenerative response involve several cellular and molecular processes. In the first few days after birth, neonatal cardiomyocytes retain the ability to re-enter the cell cycle and proliferate in response to myocardial damage, thereby facilitating complete cardiac regeneration without scar formation. One crucial aspect contributing to this age-specific phenomenon is the unique molecular and cellular environment present in the neonatal heart, which supports and promotes cardiomyocyte proliferation and tissue regeneration. [26,31,32] We demonstrated that pharmacological inhibition of angiogenesis in P1 mice subjected to nTAC resulted in reduced CMs proliferation and increased cardiac fibrosis, creating a maladaptive phenotype similar to that seen in P7 mice undergoing nTAC.[35] This highlights the crucial role of endothelial cells and angiogenesis in supporting cardiac regeneration and adaptation in response to nTAC.

Additionally, the ECM composition in the neonatal heart plays a completely different role that supports regeneration. Following neonatal injury, the ECM provides structural support and biochemical signals that are crucial for cell proliferation, migration, and differentiation. Hence, in neonates, the ECM is more dynamic and less fibrotic compared to adults, which helps in effective tissue remodeling and regeneration after injury. [44,60]

Cardiomyocytes proliferation

Cardiomyocyte proliferation and cytokinesis are essential processes for maintaining heart function, particularly in response to cardiac injury or stress. During early development, cardiomyocytes undergo rapid proliferation, contributing to heart growth and development. In adult hearts, the capacity for cardiomyocyte proliferation is significantly limited, which poses challenges for regeneration after injury such as myocardial infarction. Effective proliferation and cytokinesis of cardiomyocytes can potentially lead to the formation of new cardiac muscle cells, thereby improving cardiac repair and function. Studies have shown that enhancing cardiomyocyte proliferation through various pathways, including the manipulation of cell cycle regulators, as well as transcription and growth factors, can lead to improved cardiac outcomes. [26,28,33-35]

Additionally, cytokinesis, the final step of cell division where one cell splits into two, is crucial for ensuring that newly formed cardiomyocytes are structurally and functionally integrated into the existing myocardium. Disruption in cytokinesis can result in binucleated cells or cell cycle arrest, undermining the heart's regenerative capacity. [33,36] Therefore, understanding the underlying mechanisms and promoting cardiomyocyte proliferation and cytokinesis hold significant potential for developing regenerative therapies to treat heart diseases and improve cardiac function.

Hippo-YAP signaling pathway

One of the pivotal pathways involved in this regenerative capacity is the Hippo-YAP signaling pathway. This pathway, initially discovered in Drosophila, is highly conserved across species and involves a series of kinase cascades that ultimately control the activity of the transcriptional co-activators Yes-associated protein (YAP) and transcriptional co-activator with PDZ-binding motif (TAZ). In the context of the heart, the Hippo pathway helps to maintain the balance between cell growth and death, which is vital for heart development, homeostasis, and regeneration. The core components of the Hippo pathway include the kinases MST1/2 and LATS1/2, which phosphorylate and inhibit YAP/TAZ. When YAP/TAZ are phosphorylated, they are retained in the cytoplasm and degraded, preventing them from entering the nucleus to activate gene transcription involved in cell proliferation and survival. [37-39]

Studies have shown that the Hippo pathway negatively regulates cardiomyocyte proliferation. [40] In neonatal cardiomyocytes, the inhibition of the Hippo pathway leads to the activation of YAP, a transcription co-activator that promotes cardiomyocyte proliferation and inhibits apoptosis. This pathway plays a significant role in enabling cardiomyocytes to divide and replace lost cells, thereby facilitating heart regeneration. [38,39,41]

The Hippo pathway also plays a role in regulating apoptosis in the heart. Activation of the Hippo pathway can lead to increased cardiomyocyte apoptosis, which is detrimental to heart function and regeneration. Conversely, inhibition of the pathway in cardiomyocytes can reduce apoptosis and promote cell survival, aiding in tissue repair and regeneration. [39,42]

Additionally, genetic manipulation of the Hippo pathway in animal models has demonstrated its impact on heart size and function. Overactivation of YAP can lead to heart overgrowth, while its inhibition can result in reduced heart size and impaired function. These findings highlight the delicate balance required for optimal heart regeneration and the potential therapeutic applications of targeting the Hippo pathway for cardiac repair. However, the precise control of YAP/TAZ activity is crucial to avoid adverse effects such as uncontrolled cell proliferation and tumorigenesis. [41,43]

Thus, identifying new pathways and factors that enhance cardiomyocyte proliferation and cytokinesis would be highly beneficial for promoting cardiac regeneration after injury and maintaining proper function.

8.4. Hypothesis and Aims of the Study

In response to sustained PO induction in adults, cardiac maladaptive remodeling occurs, preliminary highlighted by capillary rarefaction, enhanced myocardial apoptosis and interstitial fibrosis. However, PO in neonatal mice during the first day after birth elicits an adaptive compensatory mechanism, hallmarked by enhanced angiogenesis and cardiomyocytes proliferation with minimal fibrosis.

Hence, a major contribution of cardiac endothelial cells governing this transition from an adaptive to maladaptive phenotype is highly hypothesized. An EC-derived cross-talk with the main cardiac cell types is assumed.

Therefore, the major aims of my study are listed as:

1. To study how cardiac ECs contribute to the maladaptive phenotype of adult mice to cardiac pressure overload during the early and chronic phase.
2. To investigate how ECs promote the adaptive response of neonatal mice in response to PO.
3. To determine the potential EC-secreted angiocrines responsible for this cardiac adaptation.
4. To test the effect of these ligands on the behavior and function of the three main cardiac cell types

9. Chapter 2: Materials and Methods

9.1. Animal Experimental Models

9.1.1. Animal Use and Welfare

All procedures performed in this study involving the care and use of animals were ethically approved by the local state authorities (the Lower Saxony State Office for Consumer Protection and Food Safety and the Regional Council Karlsruhe, Germany, files no. 33.12-42502-04-17/2706, 3.12-42502-04-17/2588, I-22/03). All animal experiments described in this study were carried out in accordance to the Guide for the Care and Use of Laboratory Animals published by the National Research Council (NIH Publication No. 85-23, revised 1996) and the German animal protection code.

For the adult murine cardiac pressure overload experiments, male wildtype C57Bl6N mice (from Charles River Laboratories) at the age of 8 to 10 weeks were interbred in-house and used for cardiac TAC or sham surgeries. For neonatal murine cardiac pressure overload experiments, adult males and females wildtype ICR/CD1 mice (from Charles River Laboratories) were interbred in-house and their pups were used for surgeries. For neonatal rat cardiomyocytes and fibroblasts' isolation experiments, adult males and females wildtype Sprague-Dawley rats (from Janvier) were bred in-house and their 1-3 days old pups were used for experiments.

All animals were maintained in a 12-h light-dark cycled room under controlled temperature (22± 2°C) and humidity (35-60%) with unlimited access to water and standard diet.

9.1.2. Transverse Aortic Constriction in Adult Mice

Transverse aortic constriction (TAC) is a well-established in-vivo experimental model to induce heart failure with reduced ejection fraction (HFrEF) hallmarked with cardiac hypertrophy secondary to pressure overload (PO) in mice. [67,68]

In 8-10 weeks old mice, TAC was induced through a ligation around the aortic arch between the right innominate and left common carotid arteries (RCCA and LCCA, respectively) as described previously. TAC was maintained for 1 week or 8 weeks to simulate the subacute and chronic phases of cardiac PO, respectively. Briefly, anesthesia was induced with 3-4% isoflurane

in an induction chamber. Subcutaneous (s.c.) injection of 0.02 mg/kg atropine and 0.1 mg/kg buprenorphine was used as an appropriate analgesic. Following oral intubation, anesthesia was maintained via a mask connected to a small animal ventilator (MiniVent Type 845, Harvard Apparatus) supplying 1.5-2% of isoflurane in 1 Lpm oxygen. Mice were stabilized onto a heat-controlled surgery table to maintain the body temperature at 37°C during the procedure. Upper left sternal thoracotomy was followed by partial removal of the thymus to visualize the aortic arch. TAC was induced through a ligature around a 26-guage needle that is subsequently removed after the second constriction (Figure 1). In sham-operated mice, the same procedure and medications was applied without aortic ligation. At the end of the surgery, the chest wall was sutured followed by application of surgical glue and mice were injected with 0.1 mg/kg atropine for heart stimulation.

Post-operatively, mice received additional analgesia in drinking water during the following week.

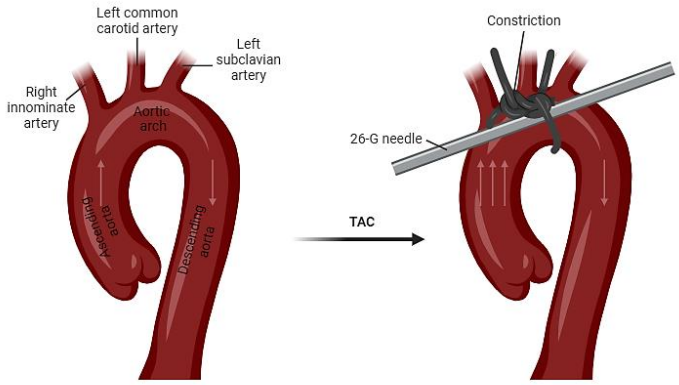

Figure 1 Schematic representation of adult transverse aortic constriction (TAC) procedure.

Illustration depicting the constriction site in the aortic arch between the innominate artery and the left common carotid artery using a 26-gauge needle. Couple of days following needle removal, the increased doppler flow can be measured in the right common carotid artery branch of the innominate artery. *Illustration created by using www.biorender.com.*

9.1.3. neonatal Transverse Aortic Constriction (nTAC)

Similar to adult TAC, our lab established an in-vivo murine model to induce cardiac pressure overload in neonatal mice named as neonatal transverse aortic constriction (nTAC). The detailed protocol was published in the online scientific journal Nature Protocols. [35,66] In

summary, I performed nTAC surgery on ICR/CD1 mice (Charles River Laboratories) during their first 24 hours after birth (1-day old, P1) or after the 7th postnatal day (P7), in which the aortic arch was ligated between the RCCA and LCCA (Figure 2). Following a brief induction of anesthesia with 4% isoflurane in 1 Lpm oxygen, neonatal mice were placed in an ice-water bath for 2-4 minutes to induce hypothermia. Subsequently, I fixed the pups on a covered ice pack in supine position during the whole surgery to maintain anesthesia. Under the microscope, a medial sternotomy was created from the neck side until the second rib without removing the thymus. Once visualized, I inserted a 10-0 suture needle (Ethicon, EH7467G) under the aortic arch between the right and left common carotid arteries (RCCA and LCCA, respectively). Next, three knots were tied around a 32G needle (Hamilton, 22032-01) before the latter was gently pulled out. At the end, I sutured the thorax then the skin with 8-0 absorbable sutures (coated Vicryl, Ethicon, V542G). Finally, the mice were placed under a heating red-light lamp until recovery before being returned to their mother. Two days after surgery, I measured blood flow velocity with Doppler echocardiography to ensure the success of the surgery.

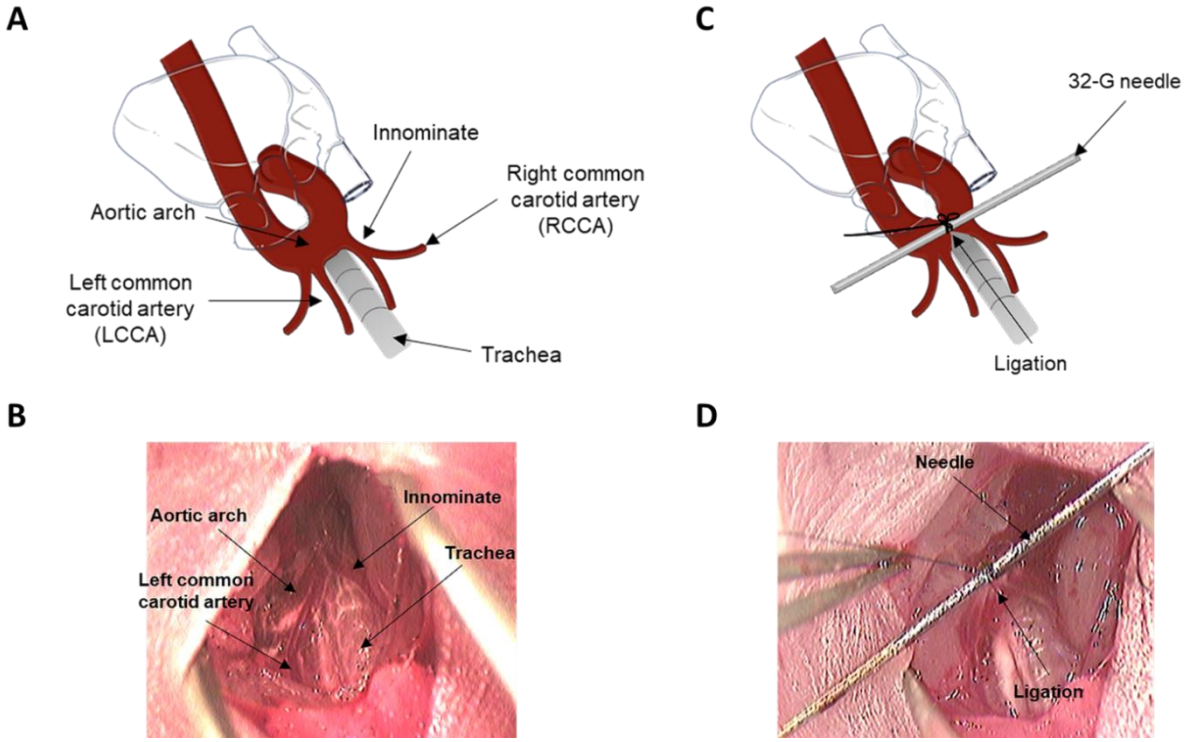

Figure 2 Schematic illustration of neonatal transverse aortic constriction (nTAC) procedure.

(**A-B**) Scheme and microscopic visualization depicting the aortic arch following chest opening and thymus removal in neonatal mice. (**C-D**) The surgical needle is placed parallel to the transverse aorta. The suture is ligated between the innominate artery and the left common carotid artery using a 32-gauge needle. *Illustration adapted from Nat Protoc 16, 775–790 (2021).* [66]

9.2. Transthoracic Echocardiography (Echo)

Sedation was induced in adult mice with the initial application of 3% isoflurane in an induction chamber then stabilized with 1-2% isoflurane via a mask. During the procedure, I placed the mice on a heating pad in the supine position in order to maintain their body temperature at 37°C. Warmed echo gel was applied on the shaved chest. The mouse limbs were taped onto the metal ECG leads and ECG was incessantly recorded. I performed non-invasive transthoracic echocardiography with a 30MHz transducer (Vevo MX-550D, Visualsonics) from Vevo 3100 system (FUJIFILM VisualSonics, Toronto, Canada). The respiration and heart rates (HR) were continuously recorded, the latter maintained between 400-500 bmp. Subsequently, I analyzed the data using the cardiac measurement packages of VevoLab 5.5.0 software (FUJIFILM).

9.2.1. Left Ventricular View

I imaged the mouse heart in B-mode and M-mode. Both parasternal long-axis (PSLAX) and short-axis (PSAX) views immediately under the papillary muscles level were recorded. Left-ventricular posterior wall thickness (LVPW) at diastole and systole as well as left-ventricular end-diastolic area (LVEDA) were measured from M-mode images at the level of the papillary muscles. To assess cardiac contractility, LV ejection fraction and fractional shortening (LV-EF and LV-FS, respectively) were calculated in PSLAX mode (Figure 3).

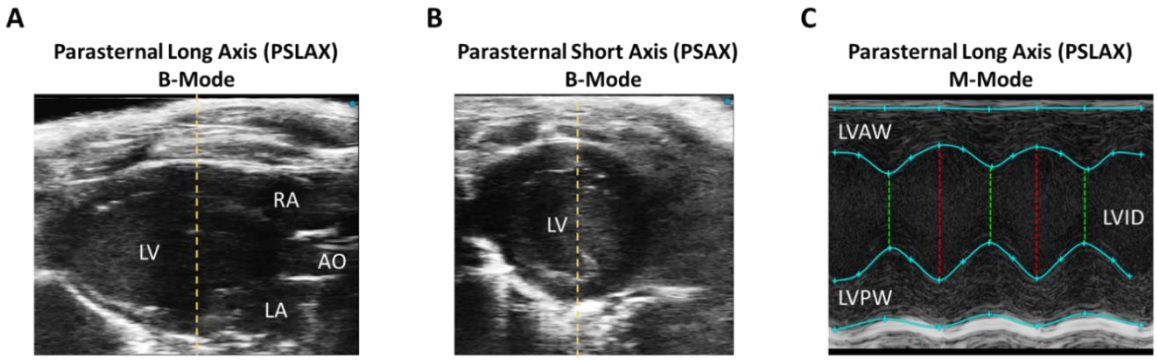

Figure 3 Parasternal axis visualization modes for echocardiographic measurements in mice.

(**A-B**) Echocardiographic visualization in B-Mode showing (**A**) parasternal long axis (PSLAX) and (**B**) parasternal short axis (PSAX) views. (**C**) M-Mode image of PSLAX view with tracings of the anterior and posterior walls of the left ventricle. Cardiac systolic function parameters, including LV ejection fraction [LV-EF, %], LV end-diastolic area [LVEDA], and LV posterior wall thickness [LVPW], were measured in M-Mode by detecting at least three consecutive contractions. The yellow dashed line indicates the measurement plane under the papillary muscle level. Abbreviations: LV = Left ventricle, LA = Left atrium, RA = Right atrium, AO= aorta, LVAW = LV anterior wall, LVPW = LV posterior wall, LVID = LV internal diameter.

9.2.2. Carotid Flow Measurement

In order to ensure the success to TAC and nTAC surgeries and to evaluate the strength of aortic constriction, I recorded pulse wave-Doppler (PW-Doppler) in the B-mode tracing from the apical four chamber view at the level of carotid bifurcation. Two to three day after surgeries, the peak blood flow velocity was measured and calculated as a ratio between the right and left common carotid arteries (RCCA and LCCA). Following TAC, RCCA/LCCA ratio at least doubles (Figure 4).

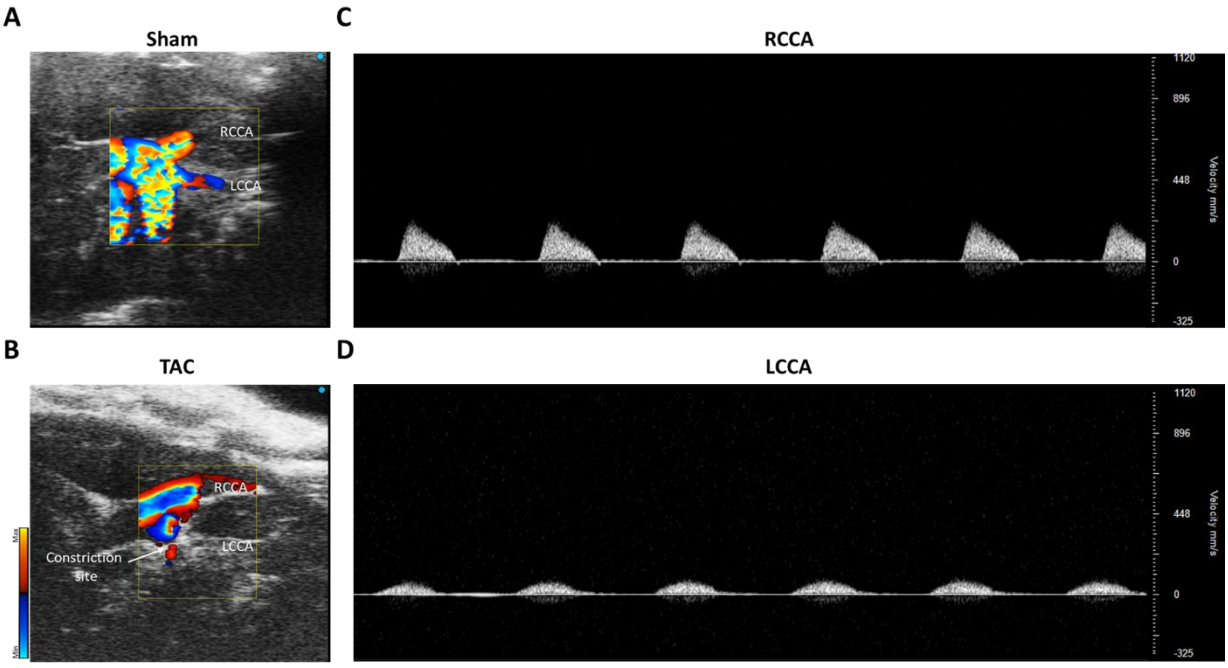

Figure 4 Pulse Wave Doppler Mode visualization in mice.

(**A-B**) Color Doppler Mode images of the aortic arch view showing a patent aortic arch in sham (**A**) and ligated aortic arch in TAC mice (**B**). (**C-D**) Pulse Wave (PW) Doppler Mode waveform of (**C**) Right common carotid artery (RCCA) and (**D**) Left common carotid artery.

9.3. Organ Harvest and Embedding

For organ harvesting at the end of the experiments, mice were weighed and euthanized. I collected the heart and lungs and immediately washed them in cold PBS for blood removal. Subsequently, the hearts were additionally washed in 0.5% (w/v) KCl in PBS to induce cardiac relaxation. I cut out right and left atria. Excess liquid was dried on a tissue paper and organs' weight was recorded.

For embedding, I cut the hearts transversally into half. The upper part was embedded in a cryomold containing optimal cutting temperature (O.C.T.) embedding medium (Tissue-Tek O.C.T., 16-004004) which was placed onto a pre-cooled n-pentane bath in liquid nitrogen to allow for gradual tissue freezing without ice-crystals formation. The basal section was further dissected into four equal parts then snap-frozen in liquid nitrogen for later RNA and protein isolations.

9.4. Primary Cells Isolation

All microbeads, solutions and reagents used in the following section are summarized in the Table 1. below.

Table 1 List of reagents used for primary cells isolation from Miltenyi

Target	Company	Cat no.
Anti-mouse CD146 (LSEC) MicroBeads	Miltenyi Biotec	130-092-007
Debris Removal Solution	Miltenyi Biotec	130-109-398
Dynabeads	Invitrogen	11035
gentleMACS C Tubes	Miltenyi Biotec	130-096-334
gentleMACS Octo Dissociator with Heaters	Miltenyi Biotec	130-096-427
MACS BSA Stock Solution	Miltenyi Biotec	130-091-376
MACS LS-Columns	Miltenyi Biotec	130-042-401
MACS MS-Columns	Miltenyi Biotec	130-042-201
MACS MultiStand	Miltenyi Biotec	130-042-303
MACS Rinsing Solution	Miltenyi Biotec	130-091-222
Neonatal Cardiac Endothelial Cell Isolation Kit, mouse	Miltenyi Biotec	130-104-183
Neonatal Cardiac Fibroblast Isolation Kit, mouse	Miltenyi Biotec	130-101-372
Neonatal Cardiomyocyte Isolation Kit, mouse	Miltenyi Biotec	130-100-825
Neonatal Heart Dissociation Kit, mouse and rat	Miltenyi Biotec	130-098-373
Octo-MACS Separator	Miltenyi Biotec	130-042-109
QuadroMAC Separator	Miltenyi Biotec	130-091-051
Red Blood Cell Lysis Solution (10×)	Miltenyi Biotec	130-094-183

9.4.1. Isolation of Adult Murine Endothelial Cells

Cardiac endothelial cells were isolated from adult murine hearts using MACS-magnetic Dynabeads from Miltenyi Biotec. Summarily, following euthanasia, I briefly injected the murine hearts with Heparin (300 U/ml in PBS, Ratiopharm, N68542.06) and washed them in ice-cold 1x PBS (PAN Biotech, P04-53500) to pump the blood out then both atria were removed. Heart ventricles were minced into smaller tissue pieces then digested with the enzyme solution consisting of collagenase I (500 U/ml, Worthington - LS004196) and DNase I (150 U/ml, Worthington - LS002139) in RMPI 1649 Medium (Thermo Scientific, 31870025) for 1 hour at 37°C. Subsequently, digested tissues were homogenized and filtered through 70µm cell strainers to remove undigested tissue clumps. Next, I washed the strainers with pre-warmed fetal bovine serum (FBS, Thermo Scientific, 10270106) and MACS buffer with BSA (MACS Rinsing Solution, 130-091-222 and MACS BSA Stock Solution, 130-091-376) to stop the digestion. Following multiple washing rounds, the tissue lysates were incubated with anti-CD146 coated microbeads (Miltenyi Biotec, 130-092-007) for 30 minutes at 4°C to label cardiac EC then positively captured with Miltenyi magnetic MS columns (Miltenyi Biotec, 130-042-201). After multiple washing steps and elution, enriched EC populations were passed through a fresh MS column for a second positive enrichment. Captured EC were then eluted and were either used immediately for flow cytometry or snap-frozen in liquid nitrogen and stored at -80°C for later RNA and protein isolation.

9.4.2. Isolation and Culture of Neonatal Rat Ventricular Cardiomyocytes (NRCM) and Fibroblasts (NRFB)

Neonatal rat ventricular cardiomyocytes (NRCM) and fibroblasts (NRFB) were isolated from 1-3 days old Sprague-Dawley rats following an in-house protocol. Briefly, after euthanasia, hearts from 40-80 neonatal rats were collected and rinsed in ice-cold 1x ADS (pH 7.35) to pump the blood out. Following atria removal, I minced the ventricles into smaller pieces in 1x ADS then digested for 9-11 rounds with the enzymatic digestion solution consisting of Collagenase Type II (Worthington, LS004176) and Pancreatin (Sigma, P3292). NRCM were then separated from NRFB based on their density by centrifugation in a Percoll gradient (Sigma, 17-0891-01).

9.4.3. Isolation of Neonatal Murine Cardiac Cells *(endothelial cells, cardiomyocytes and fibroblasts)*

Neonatal murine cardiac endothelial cells

During this study, I isolated neonatal cardiac endothelial cells (EC) from 1, 3, 7 and 10 days old neonatal mice' hearts using MACS-magnetic microbeads from Miltenyi Biotec. In summary, neonatal pups were euthanized by decapitation. Their hearts were collected and briefly rinsed in 1x PBS to pump out the blood by gentle squeezing with sterile forceps. I removed the atria, the vessels and the remaining connective tissues, then the ventricles were minced with a blade in 1x ADS. Subsequently, the ventricles were dissociated using Neonatal Heart Dissociation Kit (Miltenyi Biotec, 130-098-373) following the manufacturer's protocol, consisting of enzymatic digestion in gentleMACS C Tubes (Miltenyi Biotec, 130-096-334). Following complete aspiration of 1x ADS and addition of the enzymes mix, the C tubes were inverted and attached with the cap down onto the sleeve of the gentleMACS Octo Dissociator with the heating function (Miltenyi Biotec, #130-096-427) and the program 37C_mr_NHDK_1 was run for 1 hour approximately. Subsequent to the dissociation procedure, I further proceeded with the cell suspension to perform red blood cells' lysis (Red Blood Cell Lysis Solution (10×), Miltenyi Biotec, 130-094-183).

Next, I negatively selected the endothelial cells by magnetically labelling non-endothelial cells populations using Non-Cardiac Endothelial Cell Depletion Cocktail, which were captured with Miltenyi magnetic LS columns (Miltenyi Biotec, 130-042-401). Following seven times wash with cold homemade buffer consisting of 1x DPBS with 0.5% BSA and 230 U/ml DNase I (Worthington, LS002139), I incubated the flow-through containing endothelial cells with Cardiac Endothelial Cell Isolation Cocktail. Neonatal cardiac endothelial cells were then captured with Miltenyi magnetic MS columns (Miltenyi Biotec, 130-042-201). The flow-through containing unlabeled cells was collected with seven times wash with cold buffer for cardiomyocytes isolation. Subsequently, I eluted the enriched endothelial cells population by pushing the plunger through the magnetic column. I either used these EC directly for FACS and scRNAseq or cultured or stored them for RNA isolation at -80°C until further use.

Endothelial cells from 10-days old pups were subjected to debris removal following heart dissociation and RBCs lysis using Debris Removal Solution ((Miltenyi Biotec, 130-109-398)

following the manufacturer's instructions, to remove dead cardiomyocytes after enzymatic digestion.

Neonatal murine cardiac fibroblasts

I isolated neonatal cardiac fibroblasts (FB) from 1, 3, 7 and 10 days old neonatal murine hearts with Neonatal Cardiac Fibroblast Isolation Kit (Miltenyi Biotec, 130-101-372). The same heart dissociation protocol was applied as mentioned above. Nevertheless, I optimized the isolation protocol and isolated cardiac fibroblasts with double-negative selection steps followed by double-positive enrichments in ice-cold PEB buffer, prepared by diluting MACS BSA Stock Solution (Miltenyi Biotec, 130-091-376) 1:20 with autoMACS® Rinsing Solution (Miltenyi Biotec, 130-091-222). During negative selection, I incubated the dissociated cell suspension with Non-Cardiac Fibroblast Depletion Cocktail permitting the capture of non-fibroblasts population inside Miltenyi magnetic MS columns. This step was repeated twice with a second labeling with the same cocktail to enhance cells purity. The flow-through consisting of cardiac fibroblasts and cardiomyocytes was subsequently incubated with Cardiac Fibroblast Isolation Cocktail then captured with Miltenyi magnetic MS columns. Once more, I repeated this step two times to improve the positive selection of fibroblasts. The enriched neonatal cardiac fibroblasts trapped inside the column were then eluted by firmly plunging the column and were either directly cultured or stored at -80°C for subsequent RNA isolation and sequencing. Same as from endothelial cells, the flow-through containing unlabeled cells was collected with four times rinsing with cold buffer for cardiomyocytes isolation.

Notably, neonatal murine cardiac fibroblasts from 10-days old pups were subjected to debris removal after ventricular digestion and RBCs lysis with the same solution as I described above.

Neonatal murine cardiomyocytes

Similar to neonatal cardiac endothelial cells and fibroblasts, I isolated cardiomyocytes from 1, 3, 7 and 10 days old neonatal mice pups' hearts using Neonatal Cardiomyocyte Isolation Kit (Miltenyi Biotec, 130-100-825). Neonatal ventricles from TAC- and sham-operated hearts by myself were dissociated with the same technique described above. Cardiomyocytes from 1- and 3-days old pups were isolated from the same hearts as EC and FB obtained from the flow-through of their positive-enrichment. Following centrifugation, I incubated the flow-through with Neonatal Cardiomyocyte Isolation Cocktail to capture any remaining cell contaminants in

the MS columns. The flow-through from this selection contained the enriched neonatal cardiomyocytes population. On the other hand, cardiomyocytes from 7- and 10-days old pups were isolated from separate operated hearts without any debris removal. Next, enriched cardiomyocytes were either cultured or stored at -80°C for later RNA isolation and sequencing.

9.5. Cell Manipulation and Laboratory Studies

9.5.1. Cell Culture and Maintenance

Cell lines

For the in-vitro validation of the first part of my study, I cultured the mouse embryonic cell line C166 (ATCC, CRL-2581), from passages 9-10, in Dulbecco's Modified Eagle's Medium (DMEM, PAN Biotech, P04-03500) with 10% FBS, supplemented with 1% L-glutamine (L-Glu,) and 1% penicillin/ streptomycin (P/S).

For lentivirus production, I cultured HEK293T epithelial-like cells (ATCC, CRL-3216), from passages 4-5, in DMEM with 10% heat-inactivated FBS (at 56°C for 30 min with mixing) in addition to 1% L-Glu and 1% P/S.

To study the ligands in vitro, I cultured Human Umbilical Vein Endothelial Cells (HUVECs, PromoCell, C-12200), from passage 2, in Endothelial cells growth medium containing the Supplement Mix (Promocell, C-22010) with 10% FBS, supplemented with 1% L-Glu and 1% P/S.

Primary cells

Following isolation, I cultured NRCM overnight in “plating medium” consisting of 80% DMEM High Glucose, 20% Medium 199 (PAN Biotech, P04-07050) and 10% FBS, complemented with 1% L-Glu and 1% P/S. On the second day, following washing with 1xDPBS, I switched the medium to “maintenance medium” consisting of DMEM with/without 10% FBS (based on the experimental setup), in addition to 1% L-Glu and 1% P/S.

Similarly, on the day of isolation, I cultured NRFB in DMEM containing 10% FBS, 1% L-Glu and 1% P/S for two hours then the cells were washed before being supplemented with fresh medium for overnight incubation. On the following days, I washed the cells twice with pre-warmed 1x PBS before changing the media.

Cells were cultured and maintained at 37°C, 5% CO2 with 100% humidity.

9.5.2. Cryopreservation and Thawing the Cells

For cryopreservation, I washed the cells twice with 1x DPBS and dissociated them with 0.25% trypsin/PBS (Thermo Scientific, 15090046) for 3 min in the incubator. Afterward, I harvested the cells using twice the amount of trypsin in cell-specific medium containing FBS. After centrifugation at 200xg for 3-5 minutes, cells were resuspended in a cell-specific medium containing 10% DMSO and 10% FCS. Then I transferred the cell suspension into cryovials (1 ml) and gradually frozen in an isopropanol-containing container at -80°C overnight, which was then transferred into liquid nitrogen for long-term storage.

During thawing, cells were transferred from liquid nitrogen on dry ice then thawed gradually in the water bath at 37°C. Following sterilization, I mixed the cells with pre-warmed culture media and centrifuged at 200xg for 3 minutes to remove DMSO. After discarding the supernatant, cells were resuspended and homogenized in cell-specific medium and were plated into corresponding plates at 37°C, 5% CO2 with 100% humidity.

9.5.3. Establishment of Stable HUVEC Cell Line by Lentiviral Transfection

For this procedure, I cultured HEK293T cells from passages 4-5 in 6-well plates until reaching 50-60% confluence. For transfection, a plasmids' mix (3µg in total) consisting of 1.5µg plasmids amplified from the lentiviral library (overexpressing or downregulating with shRNA the genes of interest) along with 0.975µg packaging plasmid (CMVΔR8.74) and 0.525µg envelop plasmid (VGV.G) were mixed in 100µl serum-free medium without antibiotics Opti-MEM (Gibco, 31985-062) per transfected-well. Afterwards, I added X-tremeGENE HP DNA Transfection Reagent (Roche, 06 366 236 001) dropwise to the mix at ratio of 3:1 (9µg Fugene added to 3µg plasmids' mix) and incubated it for 20 minutes at RT following gentle mixing by inverting the tube. After removing half of the medium of cultured HEK293T cells, I added the prepared plasmids' mix onto the cells drop by drop. The cells were incubated for 48 hours to produce the virus at 37°C with 5% CO_2 with another half of the medium added on the second day. Two days thereafter, I harvested the supernatant of the HEK293T cells and centrifuged it at 4200 rpm for 20 minutes at RT to pellet the remaining cells. Subsequently, the supernatant containing the virus was

filtered with 0.45 µm filter and added to HUVECs (from passage 2) pre-seeded the day before in another 6-well plate at a density of 0.75×10^5 - 1×10^5 cells per well. In order to enhance the efficiency of the lentiviral infection, I added Polybrene (Sigma, TR-1003-G) to the virus-containing medium at a concentration of 8µg/ml before being incubated at 37°C with 5% CO_2. After 24 hours, the medium of the transduced HUVECs containing the virus was changed to normal HUVECs' medium (Endothelial cells growth medium + Supplement Mix (Promocell, C-22010) + 10% FBS). On the subsequent days, I changed the HUVECs' medium daily with an incremental increase in Puromycin (Sigma, P7255) concentration from 0.5 to 2 µg/ml to select only the transfected HUVECs harboring the resistant gene following lentiviral transfection. Consequently, the transfected HUVECs were directly used for co-culture experiments or frozen in liquid nitrogen in HUVECs medium with 10% DMSO (Cell Signaling, 12611) and 10% FBS.

9.5.4. Co-culture Experiments

For co-culture experiments, I plated lentiviral-transfected HUVECs the day before at a density of 0.4×10^5 per cm^2. Once a HUVECs monolayer has formed, NRCM and NRFB, isolated from P1-P3 rat pups, were co-cultured onto of HUVECs at a density of 0.52×10^5 and 0.26×10^5 per cm^2, respectively. During experiments, I prepared co-culture medium by mixing 50% HUVECs-specific medium and 50 % NRCM/NRFB-medium.

9.5.5. Cardiac 3D-Organoids Formation

Cardiac organoids consist of multiple cardiac cells (cardiomyocytes, endothelial cells and fibroblasts) which self-organize to form three-dimensional in-vitro structures, with the aim to recapitulate the structural and functional characteristics of a native heart. For this purpose, the three-dimensional co-culture model developed by Wagner et al. was adapted with slight modifications. [69,70] During this experiment, I used neonatal rat ventricular cardiomyocytes (NRCM) and fibroblasts (NRFB), isolated according to the protocol mentioned above. A cell suspension was adjusted to contain 0.32×10^5 NRCM and 0.064×10^5 NRFB per cardiosphere in plating medium (consisting of 68% DMEM High Glucose, 17% Medium 199, 10% Horse Serum (Sigma, H1138) and 5% FBS). In order to keep the cells in humidified atmosphere, I filled the bottom part of a 10cm cell culture dish with 1x DPBS. Next, I distributed the cell suspension as

droplets of 30µl on the inner surface of the lid of the cell culture dish and incubated them inverted for 4-5 days at 37°C and 5% CO_2. Subsequently, the formed heterotypic spheroids were collected and singularized in an Ultra-Low Adhesion U-Bottom (Corning, 7007) then left to recover for 3-5 hours at 37°C and 5% CO_2. Afterwards, 0.10×10^5 HUVECs previously transfected with lentivirus were added to each spheroid in 100µl EBM (consisting of Endothelial cells growth medium + Supplement Mix + 10% FC´BS) and left overnight in the incubator to accommodate. On the next day, I prepared cardiosphere culture medium (CSM) with mixing 50% EBM and 50 % maintenance medium (composed of 90% DMEM High Glucose, 10% Medium 199 and 1% Horse-Serum). Half the medium was removed from each well and replaced with 100µl CSM containing 1:500 200mM Phenylephrine (PE, Sigma, P6126) to reach a final concentration of 200µM per well. On the subsequent days, I changed the medium every second day by removing half the medium and adding 100µl CSM containing 1:1000 PE. Ten days after HUVECs addition, I recorded cardiac organoids' spontaneous beating before harvesting them for immunofluorescent staining.

9.6. Immunofluorescence and Histological Analysis

Using a rotary cryotome (Thermo Fisher, HM355S), hearts embedded in Tissue-Tek O.C.T. compound (Tissue-Tek, 16-004004) were sectioned by myself on tissue slides (Thermo Scientific - Menzel Glaser, 24 x 60 mm) into 7µm or 12µm cryosections for immunofluorescent or Picro-Sirius red staining, respectively. The cut slices were left to dry for 30 minutes at room temperature (RT) then stored at -80°C until further usage.

9.6.1. Immunofluorescence Staining

All microbeads, solutions and reagents used in the following section are summarized in the Table 2. below.

Table 2 List of antibodies for immunofluorescent staining and FACS

Target	Company, Cat no.	Application
Anti-mouse CD31 Antibody	Miltenyi Biotec, 130-119-653	1:50, FACS
Anti-mouse CD45 Antibody	Miltenyi Biotec, 130-123-879	1:50, FACS
Feeder Cells Antibody, anti-mouse	Miltenyi Biotec, 130-120-802	1:50, FACS
FITC anti-mouse CD102 Antibody	BioLegend, 105606	1:100, FACS
Isolectin B4 antibody (IB4)	Vector Lab, FL-1201	1:50, IF
Mouse monoclonal anti-cardiac Troponin T antibody [1C11]	Abcam, ab8295	1:200, IF
ProLong Gold Antifade Mountant	Thermo Scientific, P36934	
Purified Mouse Anti-Human CD144	BD Pharmingen, 555661	1:100, IF
Purified Rat anti Mouse CD102	BD Pharmingen, 553326	1:200
Purified Rat Anti-Mouse CD31	BD Pharmingen, 553370	1:100
Rabbit anti-aurora B	Sigma, A5102	1:100, IF
Rabbit monoclonal anti-CD146	Abcam, ab75769	1:100, IF
Rabbit monoclonal anti-phospho-smad3 (S423+S425)	Abcam, ab52903	1:100, IF
Rabbit polyclonal anti-Fibronectin	Sigma-Aldrich, F3648	1:100, IF
Rabbit polyclonal anti-Ki67	Abcam, ab15580	1:100, IF
VectaShield Hardset Antifade Mounting Medium with DAPI	Vector Lab, H-1500	

Tissue slides

For immunofluorescence staining, I fixed tissue slides for 20 minutes at RT in 4% paraformaldehyde (PFA). Following three rounds of washing with 1x PBS for 5 minutes each, the slides were permeabilized using freshly-prepared 0.3% Triton-X (Triton X 100 reinst, Carl Roth, 3051.3) in PBS for 20 minutes at RT. The tissues were washed three more times with 1x PBS as described before and blocked with 3% Bovine serum albumin (BSA, Sigma, 10735108001) in PBS for 1 hour at RT. The slides were subsequently incubated with the respective primary antibodies at 4°C overnight, covered with parafilm to preserve the moisture in a humidity chamber filled with Millipore water. On the next day, I washed slides once with 0.01% Triton-X in PBS then twice with 1x PBS at RT for 5 minutes each to remove excess unbound antibodies. The slides were then incubated with the corresponding secondary antibodies for 1 hour at RT. Applying the previously described washing protocol, I then

mounted the slides with mounting medium containing DAPI to visualize the nuclei (VECTASHIELD HardSet Antifade Mounting Medium With DAPI, Vector Lab, H-1500). In the dark, the slides were then left to air dry for 2 hours at RT.

Cardiac organoids

Following spontaneous beating measurement, I collected the cardiac organoids in one tube per condition and fixed them with 4% PFA in a laboratory rotator for 1 hour at RT. Following PFA removal and one-time wash with 1x DPBS, spheroids were permeabilized with 0.2% Triton X-100 in PBS for 1 hour at RT while rotating. Subsequently, I washed the organoids once with PBST (1x PBS containing 1% Tween 20 and 0.002% Triton X-100) and blocked with 5% BSA in PBST for 1 hour at RT with continuous rotation. Following blocking, cardiospheres were incubated overnight at 4°C on a rotator with the primary antibodies at a concentration of 1:100 w/v in 5% BSA/PBST. On the following day, I removed the supernatant and washed the organoids three times with PBST for 20 minutes each then once briefly with 5% BSA/PBST. Next, cardiac spheroids were incubated with secondary antibodies and DAPI at a concentration of 1:100 and 1:1000 w/v, respectively, in blocking buffer for 4 hours at RT in the dark on a rotator. After three times wash with PBST for 20 minutes each, I carefully spread spheroids on a glass slide and mounted them with ProLong Gold Antifade Mountant (Thermo Scientific, P36934) under cover glass then I left them to dry for 2 hours in the dark before being stored at 4°C until imaging.

9.6.2. Picro-Sirius Red Staining

Picro-sirius red staining is a well-established in-vitro method for the detection of collagen fibers deposition in the extracellular matrix in tissues. In brief, defrosted tissue slides were fixed with ice-cold absolute acetone (Roth, 5025.6) for 10 minutes then air-dried at RT for 5 minutes. Then I immersed the slides in picric acid solution with formaldehyde (150 ml saturated picric acid solution (Sigma, P6744) + 50 ml 37% formaldehyde solution (Roth, 7398.4) for 30-45 minutes at RT. A brief rinse in 70% ethanol (EtOH) was followed by immersion into direct red in picric acid solution (200 ml saturated picric acid solution + 0.2g Direct red dye (Direct Red 80, Sigma Aldrich, 365548)) for 1 hour at RT. Subsequently, I briefly rinsed the slides once for 2 minutes

with 10 mM hydrochloric acid (HCl) then once in 70% EtOH for another 2 minutes. Tissue slides were then dehydrated twice in absolute EtOH for 5 minutes each and finally washed two times 5 minutes in Roticlear solution (Roth Chemicals, A538.2). Lastly, I mounted the slides with RotiMount (Roth Chemicals, HP68.1) under cover slips.

9.6.3. Tissue Imaging

For immunofluorescence staining, images were acquired using Leica DMi8 Fluorescence microscope or Leica TCS SP8 confocal microscope. The images were visualized with Leica Application suite X (LAS X) version 3.7. Subsequently, I analyzed the images and quantified them using Fiji ImageJ.

For picro-sirius red histological imaging, tissue slides were scanned in bright-field with 20X magnification using Zeiss Axio Scan.Z1. Then I analyzed the images with ZEN 2.6 Blue Edition, Carl Zeiss. I calculated the scarred area as the percentage of red-stained fibrotic area in relation to total transverse left-ventricular area using Adobe Photoshop 22 and Fiji ImageJ.

9.7. Contraction analysis

Using Leica DMi8 microscope, I acquired movies of spontaneous beating of cardiac organoids and cardiomyocytes co-cultured with HUVECs with 10x objectives for 30-60 seconds. I quantified the beating rate and beating amplitudes using the ImageJ macro MYOCYTER. [71] Spontaneous contraction was determined by counting the number of beats per minute.

9.8. RNA Studies

9.8.1. RNA Isolation

I performed RNA isolation from tissue samples using TRIzol reagent (Invitrogen, 15596-018) followed by NucleoSpin RNA isolation Mini kit (Macherey-Nagel, 740955.250) according to the manufacturer's protocol. Briefly, tissue pieces were lysed with TRIzol reagent using Tissue Lyser II (Qiagen) and magnetic beads for 2 minutes then I mixed the samples with chloroform (Honeywell, C2432) and incubated them for 5 minutes at RT. The two-phases solution was then centrifuged. Subsequently, I transferred the top aqueous phase into isopropanol and mixed it

well by vortexing. Afterwards, I loaded the lysate onto NucleoSpin® RNA Columns (light blue ring) and centrifuged it then discarde the flowthrough. Following desalting of the column silica membrane using MDB solution, remaining DNA was digested with DNase reaction mixture for 20 minutes at RT. I then washed the silica membrane containing the RNA and dried it on three rounds. Finally, I eluted the RNA using 30-60 µl RNase-free water (Thermo, AM9937). I kept the isolated RNA on ice through the whole procedure till being stored at -80°C until further use.

I isolated RNA from cells using NucleoSpin RNA isolation Mini kit (Macherey-Nagel, 740955.250) only. Cells were initially lysed with RA1 solution and β-mercaptoethanol (Sigma, M3148). The rest of the protocol was applied as mentioned above.

9.8.2. cDNA Generation

cDNA was generated by using Maxima H minus First stand cDNA synthesis kit (Thermo Scientific, K1652) according to the manufacturer's protocol. In brief, I added 500ng of template RNA to the primers mix containing dNTP. Following the initial incubation at 65°C, I added Maxima H Minus Enzyme mix. The mixture was then incubated in the thermal cycler according to the following table.

Table 3 cDNA preparation cycler program

Step	Temperature	Time
1	65°C	5 min
2	25°C	10 min
3	50°C	15 min
4	85°C	5 min

9.8.3. Quantitative real-time PCR (qRT-PCR)

Quantitative real-time PCR (qRT-PCR) was accomplished using Maxima SYBR Green mix (Thermo Scientific, K0253) and PowerUp SYBR Green Master Mix (Thermo Scientific, A25743) with ROX as reference dye following the manufacturer's protocol on AriaMx Real-time PCR System (Agilent, G8830a). I normalized the gene expression to *Gapdh* mRNA expression. Primer sequences used in the experiments are listed in the Table 4. below.

Table 4 List of primers used for qRT-PCR

	Forward primer	Reverse primer
m*Gapdh*	5'-CGTCCCGTAGACAAAATGGT-3'	5'-GAATTTGCCGTGAGTGGAGT-3'
m*Myh7*	AGGCAAGGCAAAGAAAGGCTCATC	GCGTGGAGCGCAAGTTTGTCATAA
m*Nppa*	ATTGACAGGATTGGAGCCCAGAGT	TGACACACCACAAGGGCTTAGGAT
h*Apln*	GACCCATGCCTTTCTGAAGCA	CTCCAGAGAAGCAGACCAATCT
h*Bmp7*	GAGTGTGCCTTCCCTCTGAACT	AGGACGGAGATGGCATTGAGCT
h*Ccl21*	CTGCTCCATCCCAGCTATCC	GAGCTCCTTTGGGTCTGCAC
h*Cldn11*	AACCTGCATTGCCAGTTGAC	CCGCCTGTACTTAGCCACAC
h*Col4a1*	TGTTGACGGCTTACCTGGAGAC	GGTAGACCAACTCCAGGCTCTC
h*Cxcl11*	AGCCTCCATAATGTACCCAAGT	GTTGTCCTTTATTTTCTTTCAGGGT
h*Cxcl12*	CTCAACACTCCAAACTGTGCCC	CTCCAGGTACTCCTGAATCCAC
h*Dll1*	TGCCTGGATGTGATGAGCAGCA	ACAGCCTGGATAGCGGATACAC
h*Efnb3*	CCTGTCTACTGGAACTCGGC	CCGATCTGAGGGTACAGCAC
h*Fgf11*	TCCTCATCCTGCTGTCCAAGGT	ATTCGCCTGGAGGTAGAAACCC
h*Fgf23*	AGAGGATGCTGGCTTTGTGG	AGACGTCGTACCCGTTTTCC
h*Gapdh*	ACCTGACCTGCCGTCTAGAA	ACCCTGTTGCTGTAGCCAAA
h*Il6*	AGACAGCCACTCACCTCTTCAG	TTCTGCCAGTGCCTCTTTGCTG
h*Inhba*	GCTCAGACAGCTCTTACCACA	AAAAGGCCCTGCTTTTCCTCC
h*Nts*	CAGCAGGGCTTTTCAACACTGG	CTCATACAGCTGCCGTTTCAGAA
h*Thbs4*	AGACGTCGTACCCGTTTTCC	TGCACCTTCCCATCGTTCTT
h*Tnfa*	ACTTTGGAGTGATCGGCCC	CATTGGCCAGGAGGGCATT
h*Tnfsf13*	ACAGGCCCAAGGATATGGTG	CCTTCTCGAGACACCACCTG

9.9. In-vitro Studies and Cellular Assays

9.9.1. Coating of Cell-culture Plates

To investigate the effect of different coating matrices on NRCM cell size, I coated 6-well cell culture plates with various matrices: 0.5% w/v gelatin, 5 µg/cm² fibronectin (Sigma, F2006), and 10 µg/cm² Col1a1 (Corning, CLS354236). The plates were incubated for 1-2 hours at 37°C with 5% CO_2 to ensure proper coating. After incubation, I completely aspirated the solutions before culturing NRCM at a density of 3.5×10^5/well.

9.9.2. Wound Closure Scratch Assay

Aiming at studying the effect of different coating matrices on endothelial cells and fibroblasts' migration, I performed a scratch assay. Therefore, I plated NRFB and C166 Endothelial cells at a density of 5.5×10^5/well and 3.5×10^5/well, respectively, in 6 well coated plates until confluency (24 hours). Once reached, I "scratched" the cell monolayer using a p200-pipette tip as a straight line and gently washed the cells once with 1x PBS to remove excess scrapped cells before being incubated with fresh medium. The scratch was imaged by myself with a bright-field microscope with 5x magnification at baseline and after 18 hours. I calculated the cellular migration as ((scratch area at the first timepoint - scratch area at 18 hours timepoint) / scratch area at the first timepoint) * 100 (wound closure percentage).

9.9.3. DNA Synthesis Colorimetric Assay

For the quantification of endothelial cells proliferation, ELISA-based Cell Proliferation BrdU kit (Roche, 11647229001) was used. This colorimetric immunoassay assesses cellular proliferation based on the quantification of BrdU incorporation during DNA synthesis in mitosis. For this experiment, I plated C166 Endothelial cells at a seeding density of 1×10^3 and 2×10^3/well in 96-well flat-bottomed cell culture plates pre-coated with the various extracellular matrix proteins. Based on the manufacturer's protocol, 24 hours after cells' seeding, I added BrdU labelling solution to the cells and incubated them at 37°C for another day to permit enough BrdU incorporation in dividing cells. After fixation, I added anti-BrdU-POD working solution followed by Substrate Solution. Once color development started, the absorbance of the samples was measured in an ELISA reader at 370 nm. Adequate controls (blank control "no cells" and background control "no BrdU") were also included.

9.9.4. Tube Formation Assay

This experiment was used to assess the ability of endothelial cells to form capillary-like structures (tubes) following overexpression or downregulation (with shRNA) of the genes of interest, with the appropriate support of extracellular matrix. For this purpose, I plated lentiviral transfected-HUVECs at subconfluent densities on Matrigel-coated plates. On the day

preceding the experiment, Matrigel (Corning, 354234) was thawed at 4°C and a sterile 96-wells flat bottom plate was pre-cooled at -20°C overnight. Next day, I pipetted 50µl Matrigel to each well on ice and pulse-centrifuged it for 10 seconds until homogenous then incubated it for 1 hour at 37°C. Subsequently, I plated the transduced HUVECs on the Matrigel-coated wells at a density of 25×10^3 cells/well in a total of 100µl medium/well and incubated them at 37°C with 5% CO_2. After 24 hours, the formed tubes were labelled with BCECF/AM Ester (Sigma, B8806) at a dilution of 1:100 for 30 minutes before imaging. Subsequently, I imaged each well in the middle using a fluorescent (GFP) and bright-field microscope with 5x magnification. The images were visualized with Leica Application suite X (LAS X) version 3.7. Subsequently, I quantified closed loops and tubes lengthes manually using Fiji ImageJ.

9.10. Flow Cytometry

Following MACS separation, I briefly washed enriched adult cardiac EC with 1x PBS containing 2% FCS and 2mM EDTA then incubated them with Purified rat anti-mouse CD16/CD32 (Fc block solution, BD Biosciences, 553141) for 5 minutes at 4°C. Next, the cells were labelled by incubation at 4°C for 20 minutes with the directly conjugated anti-mouse antibodies: CD31-PE (Miltenyi Biotec, 130-119-653), CD45-PerCP (Miltenyi Biotec, 130-123-879), anti-feeder cells-APC (Miltenyi Biotec, 130-120-802) and CD102/ICAM-2-FITC (BioLegend, 105606). Subsequent to washing, the labelled cells were counted by FACS LSR II from BD. I analyzed the obtained data with FlowJo software (version 10).

Similarly, after MACS isolation, enriched neonatal cardiac endothelial cells populations were FACS sorted for alive single cells by staining with SYTOX™ Blue Dead Cell Stain (1:2000, Thermo Scientific, S34857), which were subsequently used for scRNA-sequencing. The purity of the sorted cells was checked with CD31-PE (Miltenyi Biotec, 130-119-653) as described above.

9.11. RNA Sequencing

9.11.1. Bulk RNA Sequencing

RNA isolated from adult cardiac EC at different TAC time points was sent for bulk RNA sequencing at the Helmholtz Center for Infection Research in Braunschweig. Total RNA quality and integrity was checked using Agilent Bioanalyzer 2100 (Agilent Technologies, Waldbronn,

Germany). Dynabeads™ mRNA DIRECT™ Micro Purification Kit (Thermo Scientific, 61021) was used for mRNA purification followed by RNA sequencing library generation from 100ng initial total RNA using ScriptSeq v2 RNA-Seq Library Preparation Kit (Epicentre Biotechnologies, Madison, WI, USA, SCL6H) according to manufacturer's protocol. The prepared RNA libraries were sequenced using TruSeq SBS Kit v3-HS (50 cycles, single ended run, Illumina, FC-401-3002) on Illumina HiSeq 2500 sequencing system, reaching 3 x10^7 reads per sample on average.

The quality and integrity of the RNA isolated from neonatal cardiac EC, CM and FB from different indicated nTAC timepoints were checked and controlled using Agilent Bioanalyzer 2100 (Agilent Technologies, Germany) for size distribution detection. Quantified libraries were prepared and pooled by BGI, Hong Kong. Bulk RNA sequencing from different cardiac cells was conducted as single-ended with a 50-base read length by BGI using the Illumina HiSeq 2500.

9.11.2. 10x Genomics scRNA-Sequencing Library Preparation

Following MACS isolation, enriched neonatal cardiac endothelial cells populations from indicated time points (10dSham, 10d1dTAC and 3dp7dTAC) were FACS sorted for alive single cells by staining with SYTOX™ Blue Dead Cell Stain and then resuspended at a density of 1000 cells/µl in 0.04% BSA (UltraPure BSA, Thermo Scientific, AM2616). Single cell suspensions were loaded onto a 10X Chromium Controller (10X Genomics, 1000127) following the manufacturer's protocol, utilizing the proprietary technology of 10X Genomics. For library preparation, 5000 cells were used for the Chromium Next GEM Single Cell 3' Kit v3.1 (10xGenomics, 1000128) according to manufacturer's protocol (10xGenomics, CG000204, Rev D). Briefly, the initial step involved creating an emulsion where individual cells were encapsulated into oil droplets along with gel beads coated with unique primers containing 10X cell barcodes, unique molecular identifiers (UMIs), and poly(dT) sequences. Barcoded full-length cDNA was generated through multiple reverse transcription reactions. Subsequently, the emulsions were disrupted using a recovery agent, and cDNA was cleaned up using DynaBeads MyOne Silane Beads (10xGenomics, 2000048). Next, bulk cDNA amplification was performed according to the Table 5. below. I purified the amplified cDNA product using the SPRIselect Reagent Kit (Beckman Coulter, B23318). Sequencing libraries were first fragmented for 14 cycles before the adaptor ligation and single indexing using Single Index Plate T Set A (10xGenomics, 1000213). I quantified the library and assessed its quality using Bioanalyzer

High Sensitivity DNA Analysis Kit (Agilent, 5067-4626) and High Sensitivity D5000 ScreenTape System (Agilent, 5067-5592 & -5593). Single-indexed libraries were equimolarly pooled (1.7 pM) and sequenced on the Illumina NextSeq 500/550 using paired-end 28x91 bp sequencing mode with the NextSeq 500/550 High Output Kit v2.5 (150 cycles, Illumina, 20024907).

Table 5 cDNA amplification cycler program

Step	Temperature	Time	
1	98°C	3 min	
2	98°C	15 sec	12 cycles
3	63°C	20 sec	
4	72°C	1 min	
5	72°C	1 min	
6	4°C	Hold	

9.12. RNA-sequencing Data Bioinformatic Analyses

9.12.1. Bulk RNA sequencing Analysis

For bulk RNA-seq data analysis,I used the Trim Galore! wrapper tool to trim the sequences and to address base call quality and adaptor contamination, removing reads shorter than 20 nucleotides from the *fastq* files. Subsequently, the trimmed reads were aligned with the short-read aligner STAR to the reference genome (mm10). I used the R package "Rsubread" to determine feature counts. For data cleaning, only genes with counts greater than 5 in at least two samples were considered for further analysis. I normalized the library size of the samples to counts per million (cpm) reads for adult EC data and to reads per kilobase per million mapped reads (RPKM) in the neonatal cardiac cells data, and then transformed into log2 values. Subsequently, I selected the differentially expressed genes (DEGs) with EdgeR package of R. Significant changes in gene expression between compared groups were filtered using the Wald test based on a p-value < 0.05 and a fold change (FC) > 1.5 for upregulated genes and FC < 0.75 for downregulated genes in the corresponding conditions. I used either CompareCluster or Metascape online tool to conduct gene ontology (GO) biological process (BP) analysis across different conditions using the enrichGO databases, with a p-value threshold of <0.05 and Bonferroni correction for the p-values. Heatmaps displaying the differentially regulated genes were generated using the ComplexHeatmap program, based on the z-score values of the

log2CPM for each gene. Motif analyses were conducted using findMotifs.pl from Homer with the settings -500-end 100-len 8,10-p 8. This analysis focused on the sequences of significantly upregulated genes from -500 bp to +100 bp around their transcriptional start site (TSS), considering motifs with a p-value < 0.05 as significant. Receptor-Ligands interaction analysis was performed based on the database from Nitchet and Skelly et al. (2018). In order to sort the ligand-receptor pairs by relevance, a LIG_REC_Score was calculated based on the expression level of both the ligand and receptor in the donor and recipient cells. For the adult samples, I quantified the score based on the sum of CPM of ligands expressed in ECs that were upregulated after TAC with a Log2FC > 1 and a p-value < 0.05, along with the CPM of the corresponding receptors in the receiver cells. Receptors were filtered to be expressed in TAC more than in sham with a Log2FC > 0.1. In comparison, I calculated the score for the neonatal conditions based on ligands enriched in regenerating ECs with a log2FC > 0.58 and a p-value < 0.05, along with the unfiltered sum of RPKM of the corresponding receptors in the receiver cells. The resulting LIG_REC value was normalized using the z-score, which was then used to generate circos plots for visualizing interactions.

9.12.2. scRNA-Sequencing Bioinformatic Analysis

To process the *fastq* files from single-cell RNA sequencing, I used Cell Ranger Single Cell Software Suite version 3.1.0 (10x Genomics) to conduct quality control, sample de-multiplexing, barcode processing, and single-cell 3' gene counting. I mapped the sequencing reads to the reference genome mm10 (version 3.0.0) using the Cell Ranger suite with default parameters. The sequencing libraries had an average of 91.8 $\pm$ 0.87 % of reads confidently mapped to the reference genome, with 1364 $\pm$ 279 median genes per cell and 3316 $\pm$ 1082 unique molecular identifiers (UMIs) per cell. I analyzed a total of 8980 cells from all three conditions, as detailed in Table 10.2.2. For data integration and analysis, I used the Seurat package (version 4.0.2) in R (version 4.0.5). Initially, I filtered the dataset to include cells expressing a minimum of 200 genes and less than 25% mitochondrial counts. Subsequently, the matrix was log-normalized and scaled for further analysis. After filtering, I performed the subsequent analyses with 8874 cells. Unsupervised clustering was performed on the data set with a resolution of 0.5 utilizing 10 dimensions following the Satja Lab Tutorial (https://satijalab.org/seurat/v3.1/pbmc3k_tutorial.html). I conducted the differential

expression analysis of genes using the "FindAllMarkers" function in the Seurat package, employing the statistical test "Bimod" for focused analyses. Genes with adjusted P values <0.05 were identified as differentially expressed genes. I generated the transcriptional profiles per cluster using Seurat, and gene ontology terms associated with these profiles were obtained through the "Express Analysis" feature of the Metascape functional annotation tool for further analysis. For sleepwalk analysis, I used the UMAP embedding stored in the Seurat data object along with the PCA coordinates to calculate the feature-space distances, based on S. Ovchinnikova and S. Anders, 2020. [72] 3D-UMAP plot was generated using Babyplots R package.[73]

9.13. Statistical Analysis

I conducted the data analysis and statistical evaluations using GraphPad Prism software (version 8). Data are represented as mean and error bars indicate standard error of the mean (SEM). The figure legends provided details regarding the number of replicates for both animal experiments and cell culture experiments. Initially, I performed statistical analysis to assess the data for normality to ensure appropriate selection of statistical tests. For data following a Gaussian distribution, a two-tailed unpaired Student's t-test was employed to compare between two groups. For comparison of more than two groups, one-way ANOVA followed by a post hoc Sidak’s multiple comparison test was utilized. Statistical significance was defined as p-values < 0.05.

Me, as the principal investigator, was blinded through the various surgical treatments, echocardiography, organ weight determination, all histological and immunofluorescence quantifications, as well as in vitro ligand testing and contractility measurement.

10. Chapter 3: Results

All the results presented below reflect the work I did completely on my own for my PhD study.

10.1. Section 1: *Contribution of endothelial cells to the maladaptive response of adult mice to cardiac pressure overload*

The following section summarizing the work performed for the first part of my thesis has been published in the open access journal iScience under the title "*Analysis of myocardial cellular gene expression during pressure overload reveals matrix based functional intercellular communication*" (Froese, N*, Cordero, J* and Abouissa, A* et al., 2022). [74] ***The figures shown below from the published article represent the part I completed entirely on my own and reflect my individual contribution to the paper.***

(*equally contributing first authors)

10.1.1. Phenotypic characterization of subacute and chronic pressure overload in adult murine hearts

As an in-vivo experimental model of subacute and chronic cardiac pressure overload (PO), transverse aortic constriction (TAC) was performed for 1-week or 8-weeks in adult mice, respectively (Figure 5-A). I could notice that the heart weight to body weight ratio (HW/BW) was significantly augmented in 1-week TAC operated mice versus sham and this ratio increased further in 8-weeks TAC mice, as a hallmark of cardiac hypertrophy secondary to PO (Figure 5-B).

Additionally, I observed that the left ventricular ejection fraction (EF), an echocardiographic measurement of systolic heart function, was initially preserved in the subacute phase of TAC, but decreased significantly in chronic PO with no observable difference in the heart rate (Figure 5- C-D).

Interstitial myocardial fibrosis was significant in both 1- and 8-weeks TAC operated hearts compared to sham, as revealed by Picro-Sirius red histological staining (Figure 6- A-B).

Additionally, I detected a significant upregulation in the expression of cardiac hypertrophy associated genes (*Nppa* and *Myh7*) in the subacute and chronic phases of adult TAC, as analyzed by qPCR from isolated murine cardiomyocytes (Figure 6- C-D).

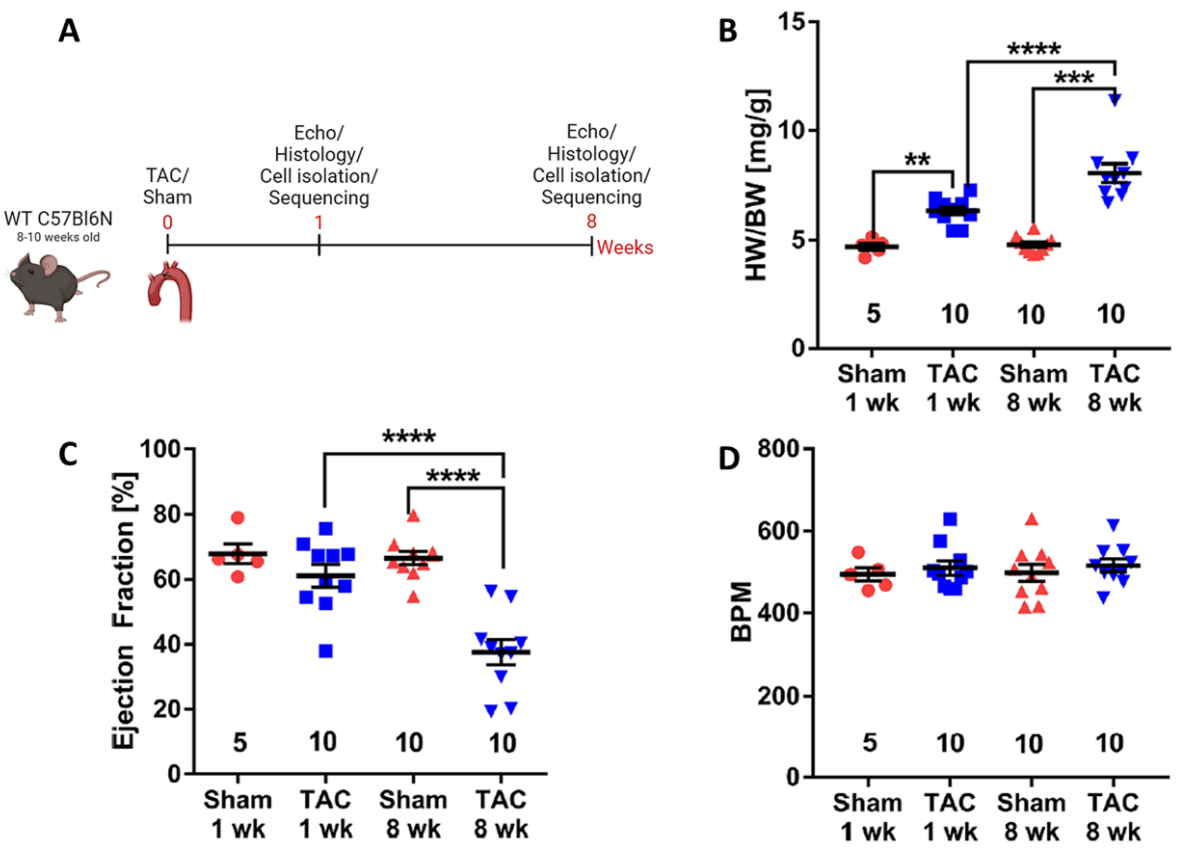

Figure 5 In-vivo characterization of subacute and chronic pressure overload in adult mice.

(**A**) Schematic representation of the experiment timeline of adult mice subjected to TAC (transverse aortic constriction) or sham surgeries. (**B**) Heart weight to body weight ratio (HW/BW) of hearts isolated from mice subjected to TAC and sham surgeries for 1- and 8 weeks. (**C**) Left ventricular ejection fraction (EF%) and (**D**) heart rate (as beats per minute, BPM) determined by transthoracic echocardiography in 1-week sham (n=5), 1-week TAC, 8-weeks sham and 8-weeks TAC (n=10 for each group). Data shown as mean ± SEM. **p<0.01, ***p<0.001, ****p<0.0001 (one-way ANOVA/Sidak's multiple-comparisons test). The graphs used in this figure are adapted from the published article [74] and represent the data acquired by myself.

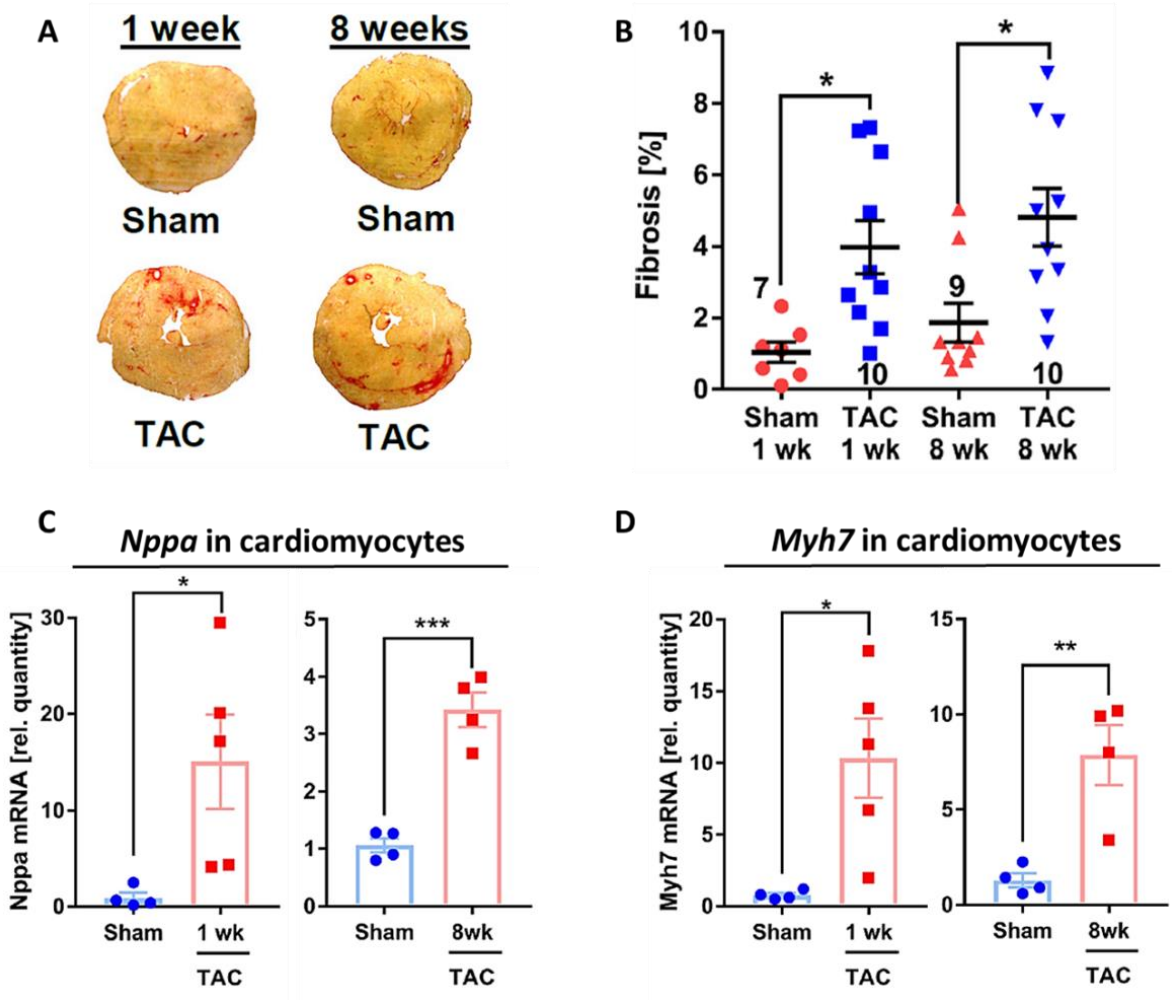

Figure 6 Phenotype characterization of subacute and chronic pressure overload on the cellular level.

(**A**) Representative images of Picro-Sirius red histological staining of adult murine hearts 1-week and 8-weeks following sham and TAC surgeries. (**B**) Interstitial myocardial fibrosis quantification from the Picro-Sirius red staining in heart sections from 1-week sham (n=7), 8-week sham (n=9), 1-week TAC and 8-week TAC (n=10 each). *p<0.05 (one-way ANOVA/Sidak's multiple-comparisons test). (**C**) Relative mRNA levels of Natriuretic Peptide A (Nppa) and (**D**) Myosin Heavy Chain 7 (Myh7) measured by qPCR in cardiomyocytes isolated from TAC and sham mice 1-week and 8-weeks after surgeries. *p<0.05, **p<0.01, ***p<0.001 (two-tailed unpaired t-test). Data presented as mean ± SEM. The graphs used in this figure are adapted from the published article [74] and represent the data acquired by myself.

10.1.2. Isolation of cardiac endothelial cells from adult murine hearts

Following enzymatic digestion of TAC and sham-operated murine hearts, cardiac endothelial cells (EC) were positively labelled with anti-CD146 coupled magnetic microbeads and captured by Miltenyi columns from the digested cell mixture (Figure 10.1.2A-A). I repeated this procedure twice to ensure the purity of enriched EC population which was verified by flow cytometry. The analysis revealed that around 93% of the enriched population were double-positive for known EC markers: Pecam1 (CD31) and ICAM1 (CD102) (Figure 10.1.2A-B).

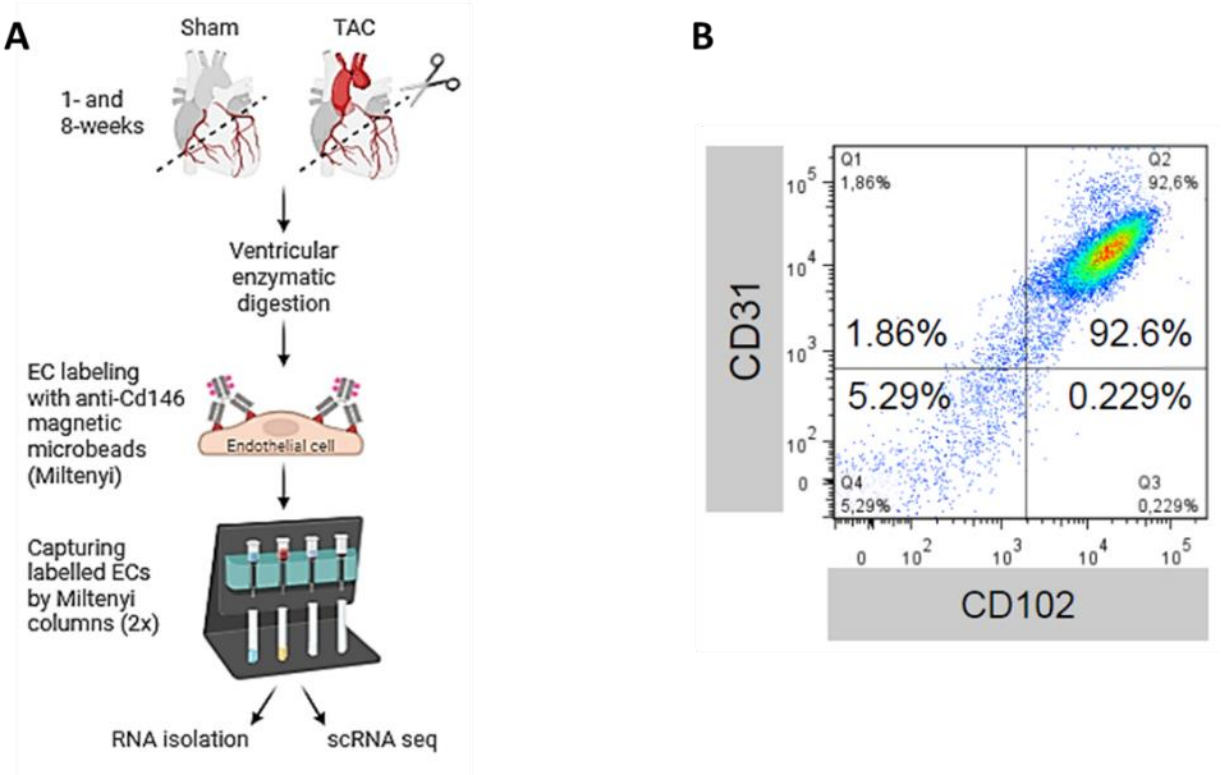

Figure 7 Cardiac endothelial cells isolation and purification from adult murine hearts.

(**A**) Schematic of the experimental design of ventricular endothelial cells (EC) labeling and isolation using Miltenyi columns for bulk and single-cell RNA sequencing. (**B**) Flow cytometric analyses of isolated endothelial cells stained for endothelial markers CD31 and CD102. The numbers in each quadrant represent the percentage of cells localized in a particular quadrant. *Illustration created by using* www.biorender.com. The graph used in panel B is adapted from the published article [74] and represent the data acquired by myself.

For further validation, I verified the co-expression of CD146 protein with the EC marker Isolectin B4 (IB4) by immunofluorescent staining in heart sections isolated from mice after subacute and chronic TAC and sham. I confirmed the co-localization of the two proteins by the overlap between both fluorescent channels (Figure 10.1.2B-A).

Subsequently, RNA was isolated from the EC enriched populations obtained from all TAC and sham conditions then sent for bulk RNA sequencing. Initial bioinformatic analysis revealed that the isolated cardiac EC expressed high levels of *Cdh5* (VE-Cadherin), *Pecam1* (CD31), *Flt1* (VEGF-receptor 1) and *Kdr* (VEGF-receptor 2) under all conditions (Figure 10.1.2B-B). Additionally, preliminary analysis showed that EC isolated from 1-week TAC hearts co-expressed extracellular matrix genes *(Col1a1, Col3a1, Vim* and *Postn)* along with the aforementioned EC specific genes, with negligible fibroblasts' marker *(Pdgfrα)* expression, suggesting a transient transition to fibroblasts-like gene expression profile (Figure 10.1.2B-B).

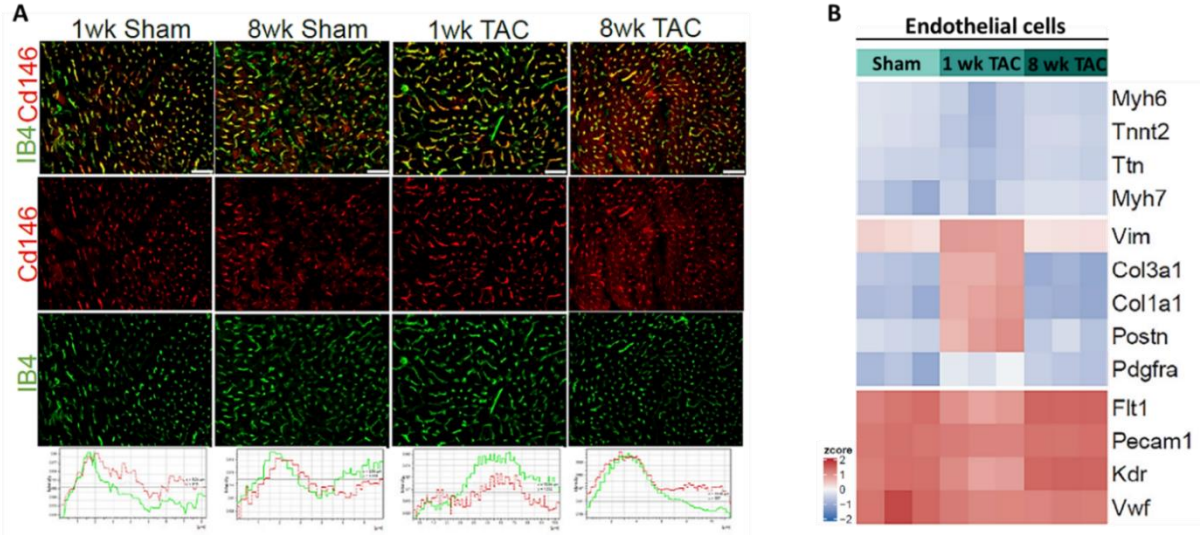

Figure 8 Ex-vivo validation of isolated cardiac endothelial cells' purity and identity.

(**A**) Immunofluorescence staining of murine heart sections following 1-week and 8-weeks sham and TAC surgeries for endothelial cell markers Cd146 (red) and IB4 (green). The fluorescence overlap between both channels is plotted below the images showing the co-localization of both markers (n=3 per condition). Scale bar, 50µm. (**B**) Heatmap showing the expression of cell-type marker genes in bulk RNA sequencing from cardiac endothelial cells isolated following sham and TAC surgeries. The graphs used in this figure are adapted from the published article [74] and represent the data acquired by myself.

10.1.3. Effect of induced pressure overload on cardiac endothelial cells' gene expression

Bulk RNA sequencing analysis of murine cardiac EC of different conditions revealed that the most dynamic changes in gene-expression occur one week after TAC. Bioinformatically, these changes were divided into 8 distinct clusters of specific gene-expression profiles (Figure 10.1.3A-A). The differential expression profile of these clusters was mapped over time (Figure 10.1.3A-B). I noticed that clusters expressing genes related to cell cycle regulation and mitotic division (cluster 1) as well as extracellular matrix organization (cluster 1 and 7) were transiently upregulated one week after TAC, and then returned to sham level eight weeks thereafter (Figure 10.1.3B-A).

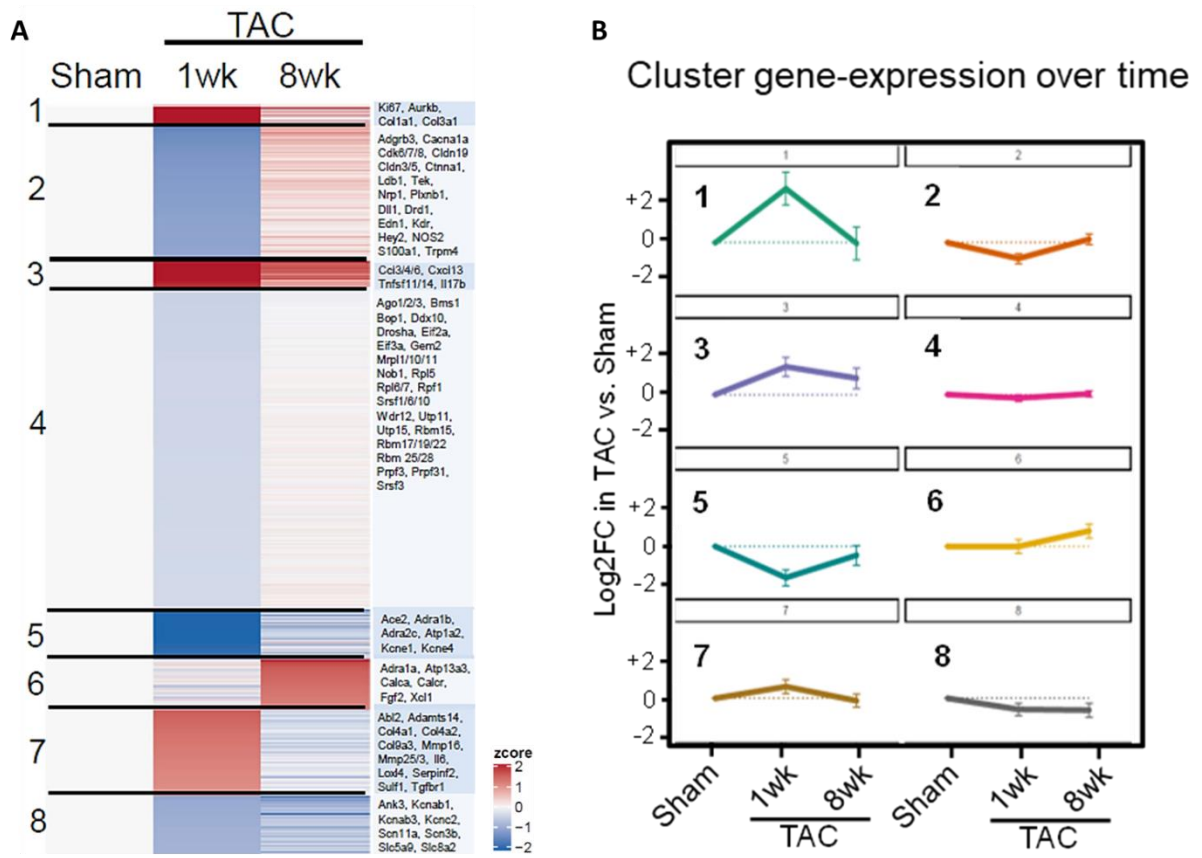

Figure 9 Bioinformatic clustering of cardiac endothelial cells after bulk RNA sequencing shows highest activity in response to 1-week TAC.

(**A**) Heatmap of differentially expressed genes in cardiac endothelial cells (EC) isolated from sham, 1-week and 8-weeks TAC obtained from bulk RNA sequencing. Based on their unique genetic expression pattern, EC were classified into eight distinct clusters. (**B**) Bar graph visualizing the dynamic change in cluster gene regulation over time in the three different surgical conditions. Data are presented as mean ± SEM. The graphs used in this figure are adapted from the published article [74] and represent the data acquired by myself. The heatmap and plots were analyzed by myself with the help of Dr. Cordero, J.

Subsequently, I verified the transient induction of cardiac EC mitotic activity on the protein level through immunofluorescent staining of heart sections, where I could see higher numbers of double Ki67-positive (pan proliferation marker) and IB4-positive (EC marker) cells in 1-week TAC compared to 8-weeks TAC and sham (Figure 10.1.3B-B).

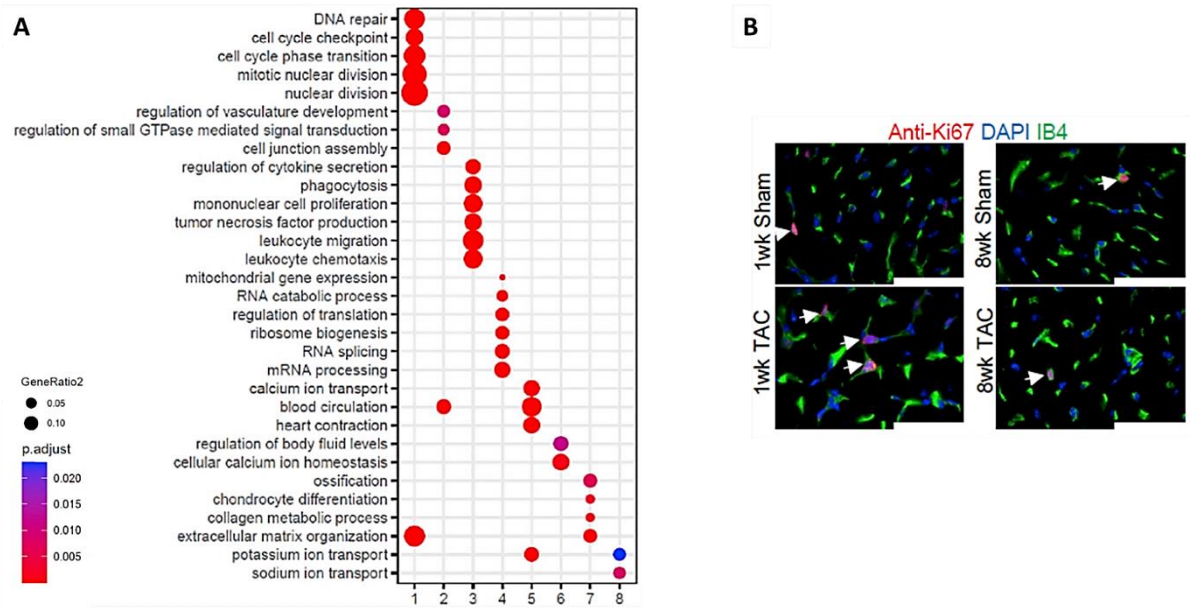

Figure 10 Cardiac endothelial cells' proliferation is enhanced one week after TAC induction in adult mice.

(**A**) Dot plot summarizing the top expressed gene ontology terms (GO, biological process) from the 8 endothelial cells' clusters. (**B**) Immunofluorescence staining for the pan proliferation marker (Ki67) and the endothelial cells' marker (IB4) in mouse heart sections from the different surgical timepoints (n=3 per condition). The white arrows mark Ki67-positive endothelial cells. Scale bar, 50µm. The graphs used in this figure are adapted from the published article [74] and represent the data acquired and analyzed by myself.

Additionally, I noticed that the expression of genes related to cellular inflammation (grouped in cluster 3) was significantly induced in the subacute phase of TAC and remained elevated throughout chronic pressure overload. On the other hand, genes associated with cell junction and vasculature development (cluster 2), mRNA splicing and processing (cluster 4) along with blood circulation and heart contraction (cluster 5) were transiently downregulated in 1-week TAC then achieved the sham level 8 weeks after TAC. Chronic TAC selectively induced genes related to cellular calcium homeostasis (cluster 6) while genes belonging to ions' transport were downregulated in both subacute and chronic phases of TAC (cluster 8) (Figure 10.1.3A – A-B, Figure 10.1.3B-A).

10.1.4. Transcription factors of cardiac endothelial cells exhibits a dynamic response to induced cardiac pressure overload in adult mice

From bulk RNA sequencing, binding sites for transcription regulators in the promoter regions of the differentially regulated genes in the eight aforementioned clusters were analyzed. In concordance with mitosis-related genes enriched in cluster 1, binding motifs for transcription factors associated with cell cycle regulation (such as E2F transcription factors and CHR motifs) were expressed within the same cluster (Figure 10.1.4–A). Similarly, SMAD binding motifs were enriched, the latter are known for induction of extracellular matrix genes expression. As an example, I observed the increase in nuclear abundance of phosphorylated (activated) SMAD3 in cardiac EC significantly only in 1-week TAC and I could confirm its expression in dissected heart sections by immunofluorescent staining (Figure 10.1.4 – B-C).

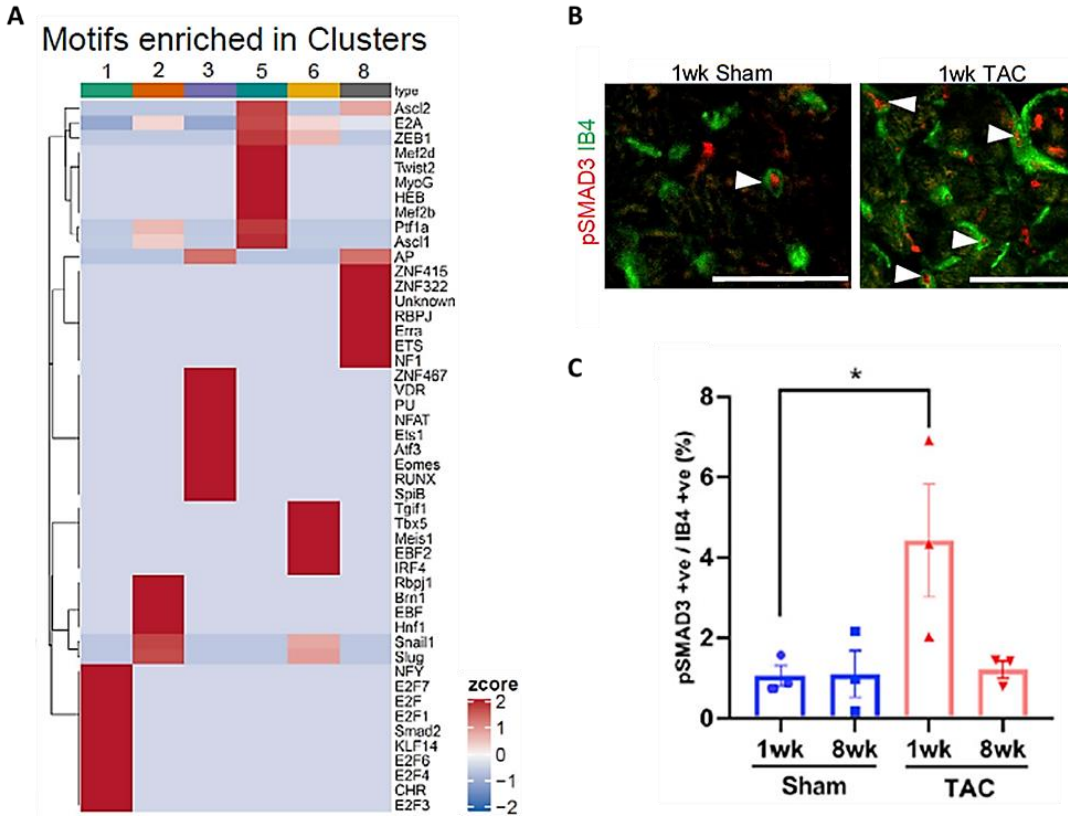

Figure 11 Cardiac pressure overload induces significant genetic transcriptional changes in adult mice during the subacute phase.

(**A**) Heatmap of top ten enriched transcription factor binding motifs in the promoter region of regulated genes in the eight cardiac endothelial cells' clusters. (**B**) Immunofluorescence staining for phospho(p)-SMAD3 (red) and the endothelial cells' marker (IB4, green) in murine heart sections from the different surgical timepoints. The white arrows point at pSMAD3-positive endothelial cells. Scale bar, 50µm. (**C**) Quantitative analysis of pSMAD3-positive ECs in heart sections from adult mice following different surgical timepoints (n=3 per condition). *p<0.05 (one-way ANOVA/Sidak's multiple-comparisons test). Data presented as mean ± SEM. The images and graphs used in this figure are adapted from the published article [74] and represent the data acquired by myself.

On the other hand, cluster 3 enriched binding motifs for transcription factors are usually found in the promotor region of known inflammatory genes (such as NFAT, RUNX and ETS transcription factors).

10.1.5. Cardiac endothelial cells interact with their surrounding in distinctive paracrine and autocrine manners during subacute and chronic phases of cardiac pressure overload

Next the potential interaction of cardiac endothelial cells (EC) with its surrounding environment in response to different TAC timepoints was investigated. For this purpose and based on bulk RNA sequencing data, I studied the ligands secreted from cardiac EC and their interacting receptors expressed on the three main cardiac cell types (cardiomyocytes (CM), fibroblasts (FB) and EC). In order to identify the potential interactions, significantly upregulated EC-derived ligands by at least two folds were designated as “GAIN” while downregulated ones were noted as “LOSS”. A ligand-receptor score was assigned to each ligand-receptor pair to prioritize the interaction within each category. This score was calculated based on the expression levels of each ligand and receptor in addition to the fold-change regulation of the EC-secreted ligand in response to TAC. The analysis revealed that the expression of numerous autocrine and paracrine EC-derived ligands (>150 factors) was enhanced during the subacute TAC phase (in comparison to sham), while a significantly lower fraction of ligands was downregulated (Figure 10.1.5–A). I observed the same trend in 8-weeks TAC endothelial cells- derived ligands although with far less total number of factors (Figure 10.1.5–B).

Potential EC-expressed gained and lost ligand-receptor interactions in subacute and chronic cardiac pressure overload are presented in Figures 10.1.5 – C-D. I noticed that endothelial cells strongly upregulated the transcription of several extracellular matrix glycoproteins and collagens (such as *Fn1*, *Col1a1* and *Col3a1*), which interacted with different integrin receptors expressed on the cell surface of CM and FB as well as EC in a paracrine and autocrine manner. Additionally, in response to subacute and chronic TAC, cardiac EC increased the expression of inflammatory stimulants (like *Il1b*) along with known growth factors (as *Ctgf* and *Igf1*).

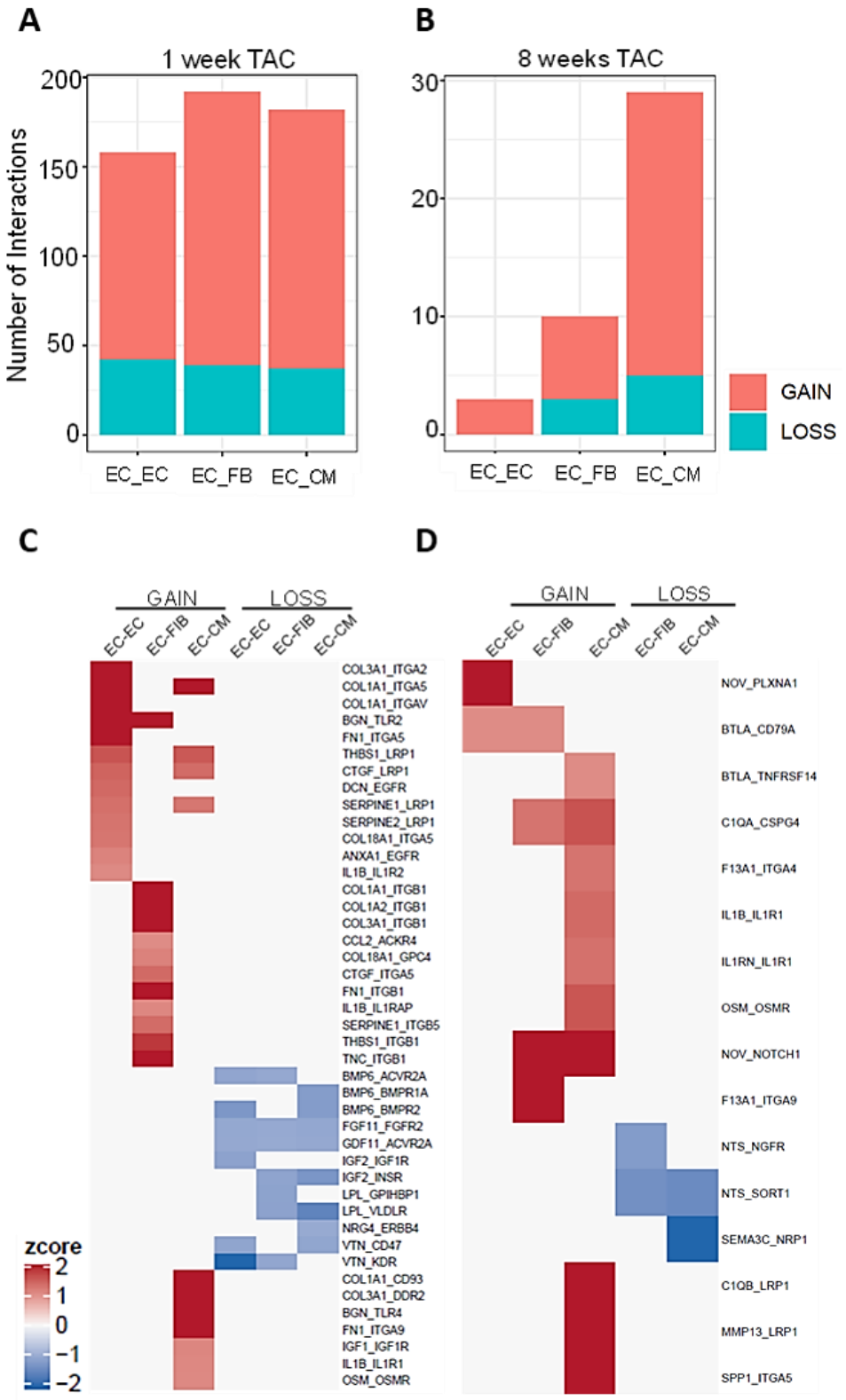

Figure 12 Subacute and chronic phases of cardiac pressure overload are associated with disctinctive interactions of endothelial cells with their surrounding environment.

(**A and B**) Quantification of endothelial cells (EC)-derived ligands upregulated (GAIN) and downregulated (LOSS) in response to 1-week (**A**) and 8-weeks (**B**) TAC. (**C and D**) Examples of gained (red) and lost (blue) ligand-receptor interactions between EC, cardiomyocytes (CM) and fibroblasts (FB) during the subacute (**C**) and chronic (**D**) phases of TAC.

10.1.6. In-vitro validation of the effect of EC-derived ligands on other cardiac cell types

By immunofluorescent staining, I could verify the increase in fibronectin abundance specifically in EC (detected one week after TAC) as seen by the strong overlap in fibronectin protein expression and IB4-stained endothelial cells in subacute TAC heart sections (Figure 10.1.6A–A). However, I observed that this co-expression was strongly reduced in the chronic TAC samples, where fibronectin was more localized to other cell types with less evidence in EC (Figure 10.1.6A–B).

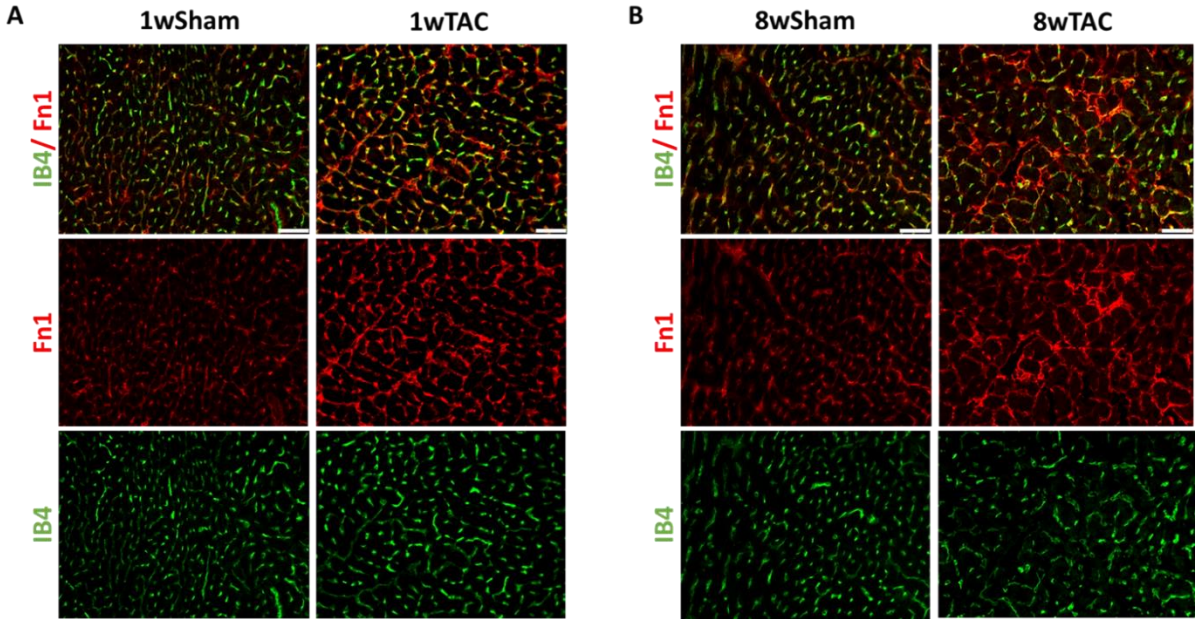

Figure 13 Enhanced fibronectin secretion by endothelial cells is solely observed during the subacute phase of cardiac pressure overload.

(**A and B**) Immunofluorescence staining for fibronectin (red) and the endothelial cells marker IB4 (green) in murine heart sections following 1-week (**A**) and 8-weeks (**B**) of TAC and sham surgeries (n=3 per condition). Scale bar, 50µm. The images used in this figure are adapted from the published article [74] and represent the data acquired by myself.

Initially, I further tested the paracrine functional impact of EC-derived ligands on adjacent cardiomyocytes in-vitro, since most secreted factors were related to extracellular matrix proteins. For this purpose, I cultured neonatal rat cardiomyocytes (NRCM) on cell culture plates pre-coated with the various matrices (such as Gelatin, consisting of denatured collagen), Collagen 1 and Fibronectin), previously detected from the ligand-receptor analysis. Interestingly, I noted that only Fibronectin coating induced NRCM hypertrophy, while gelatin

and collagen exhibited no difference in comparison to uncoated surfaces (Figure 10.1.6B – A-B).

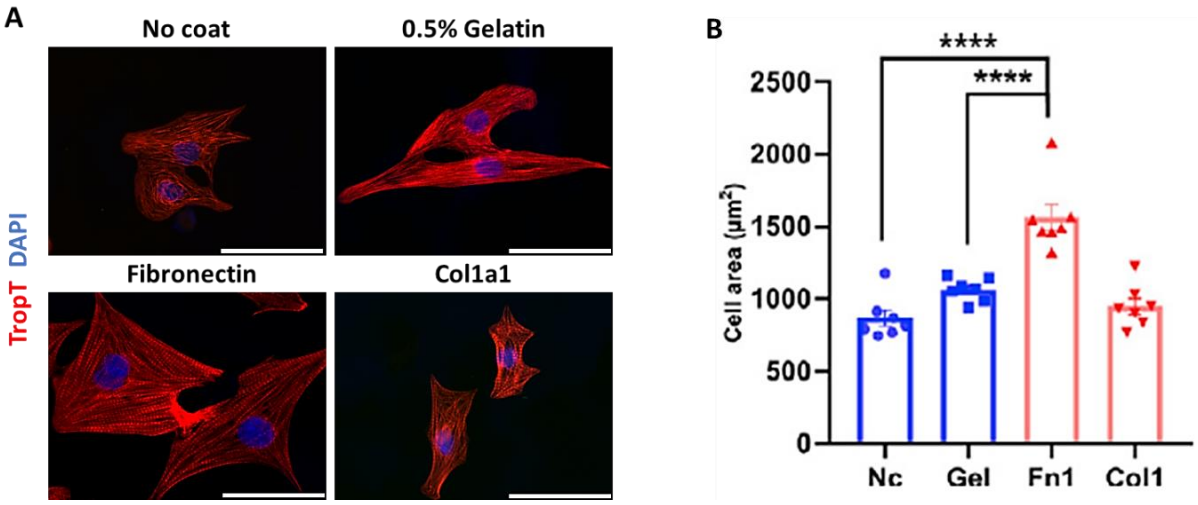

Figure 14 Fibronectin induces a hypertrophic response in neonatal rat cardiomyocytes.

(**A**) Isolated neonatal rat cardiomyocytes (NRCM) plated on different matrices (0.5% gelatin, Collagen and Fibronectin versus no coat) and stained for the cardiomyocytes-marker troponin-T (red) showing the paracrine effect of these factors on NRCM size. Scale bar, 50µm. (**B**) Quantification of NRCM cell area plated on different extracellular matrix proteins (n=7 per condition). Data presented as mean ± SEM. ****p<0.0001 (one-way ANOVA/Sidak's multiple-comparisons test). The images and graphs used in this figure are adapted from the published article [74] and represent the data acquired and analyzed by myself.

Similarly, I further investigated the paracrine effect of the aforementioned matrix proteins on fibroblasts' migratory function. In this context, I plated neonatal rat fibroblasts (NRFB) on the pre-coated cell culture dishes with the same matrices mentioned above. Following scratching, I monitored the wound closure over time. I noticed that only Fibronectin coating enhanced NRFB migration in comparison to Collagen, Gelatin and no coating (Figure 10.1.6C – A-B).

Next, I studied the autocrine impact of the secreted matrix deposition-related ligands on endothelial cells' function in various in-vitro models. In contrast to NRFB, Fibronectin, Collagen as well as Gelatin induced C166 endothelial cells migration and shortened wound closure time compared to no coat (Figure 10.1.6D – A-B). On the other hand, both Fibronectin and Collagen separately lead to a significant increase in C166 EC proliferation unlike Gelatin and no coat, as indicated by enhanced BrDU incorporation by ELISA (Figure 10.1.6D – C).

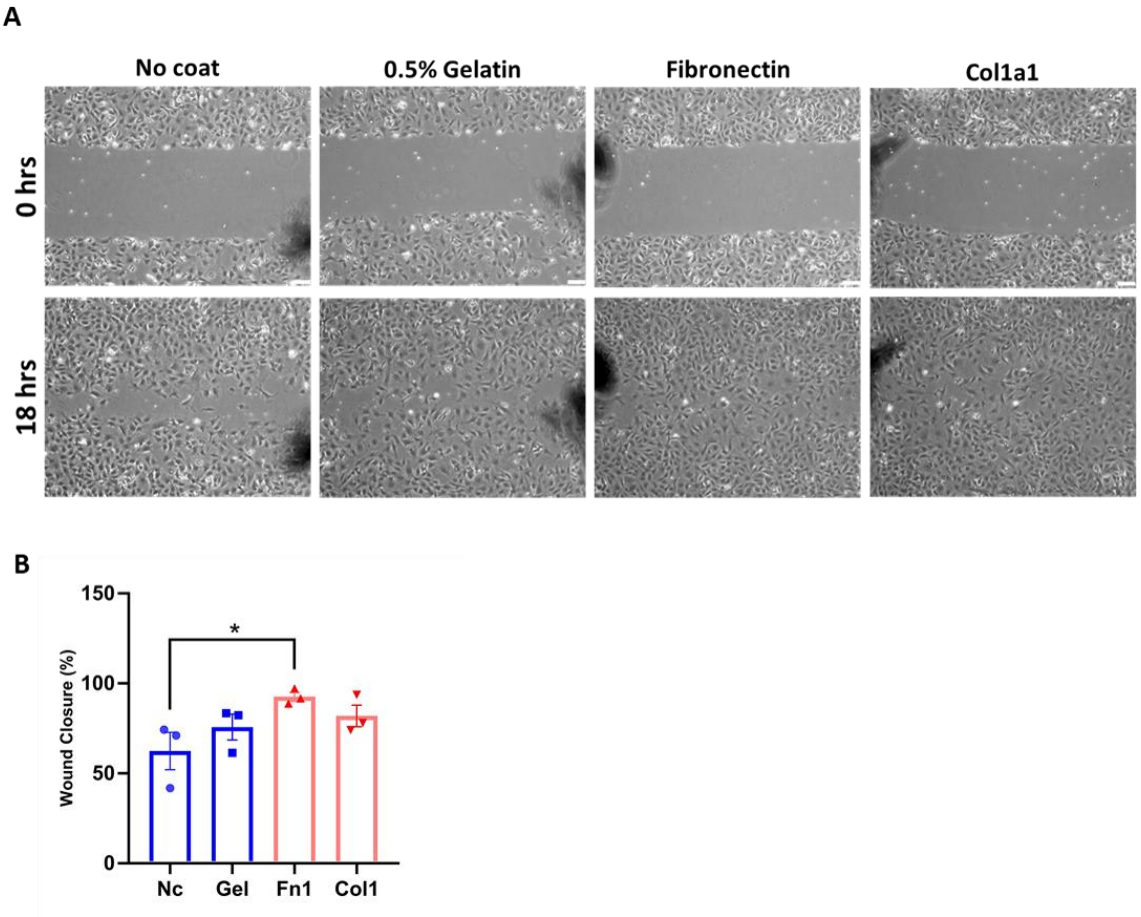

Figure 15 Fibronectin enhances the in-vitro migration of neonatal rat fibroblasts.

(**A**) Representative images from the scratch assay of isolated neonatal rat fibroblasts (NRFB) plated on different matrix coats (0.5% gelatin, Collagen and Fibronectin versus no coat). Scale bar, 50µm. (**B**) Wound closure quantification of NRFB 18 hours after being plated on different extracellular matrices (n=3 per condition). Data presented as mean ± SEM. *p<0.05 (one-way ANOVA/Sidak's multiple-comparisons test). The images and analyzed graphs used in this figure are adapted from the published article [74] and represent the data acquired solely by myself.

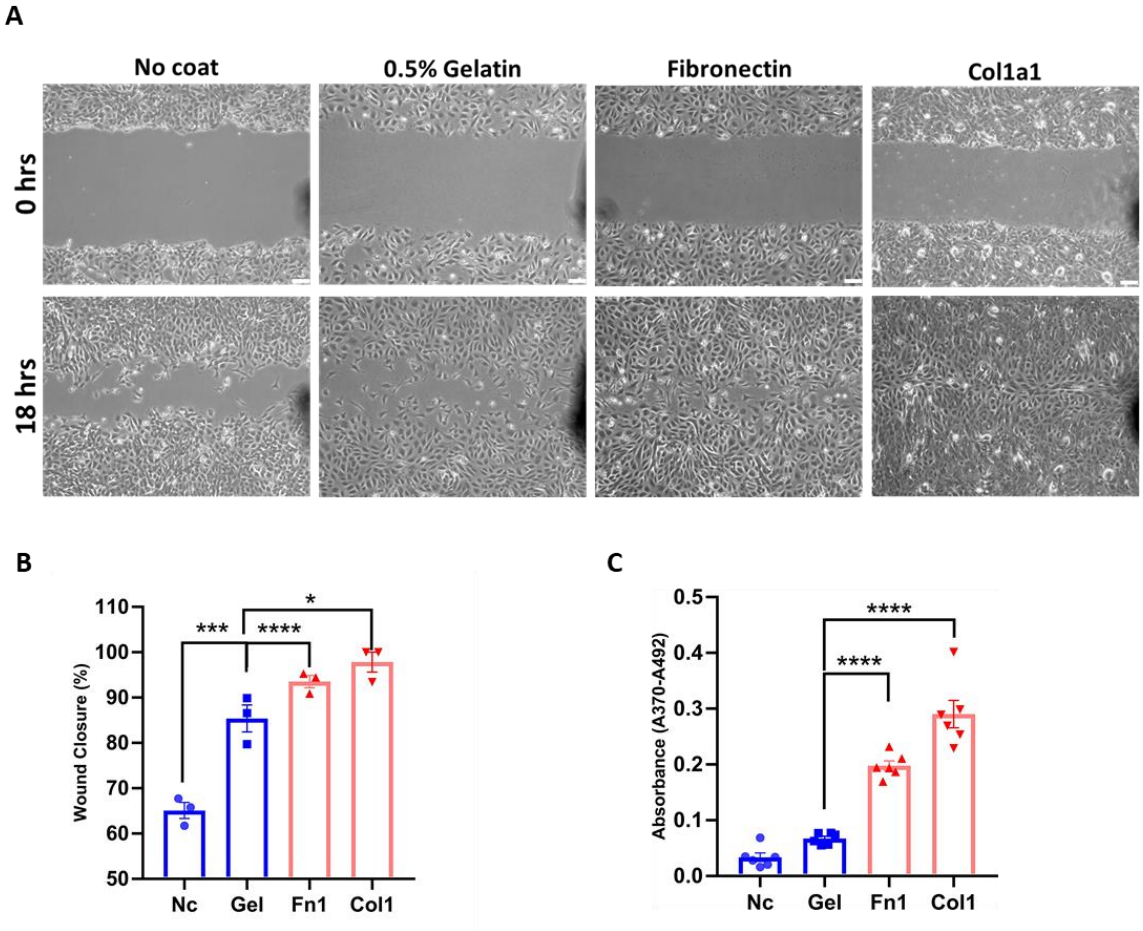

Figure 16 Fibronectin and collagen induce endothelial cells' proliferation and migration in-vitro.

(**A**) Representative images from the scratch assay of endothelial cells (C166) plated on different matrix coats (0.5% gelatin, Collagen and Fibronectin versus no coat). Scale bar, 50µm. (**B**) Wound closure quantification of C166 endothelial cells after being plated on different extracellular matrices (n=3 per condition). Data presented as mean ± SEM. *p<0.05, ***p<0.001, ****p<0.0001 (one-way ANOVA/Sidak's multiple-comparisons test). (**C**) Quantified data of C166 endothelial cells' proliferation following plating on different matrices measured with BrDU incorporation by ELISA (n=7 per condition). ****p<0.0001 (one-way ANOVA/Sidak's multiple-comparisons test). Data are shown as mean ± SEM. The images and analyzed graphs used in this figure are adapted from the published article [74] and represent the data acquired solely by myself..

10.2. Section 2: *Investigating the role of endothelial cells to the adaptive response of neonatal mice following induced cardiac pressure overload*

In contrast to the maladaptive role of endothelial cells after adult TAC discussed in the previous section, our group found that neonatal transverse aortic constriction (nTAC) performance in 1-day old (P1) mice induced a universal adaptive response to cardiac pressure overload. Enhanced cardiac revascularization accompanied by increased cardiomyocytes' (CM) proliferation were the main hallmarks of cardiac compensation and maintenance of the heart's contractile function with minimal fibrosis in response to nTAC at P1. Nevertheless, this capacity significantly decreased when nTAC was performed in 7-days old mice (P7), where pressure overload induction lead to fibrotic maladaptation and heart failure. [35,66]

Hence, my main aim for the second part of my thesis was to decipher the contributing role of cardiac endothelial cells (EC) to the adaption to nTAC in P1 mice and what governs the transition to the maladaptive response observed in P7 mice. *The following section reports the work performed by myself intending to study the adaptive role of EC on the transcriptome and secretome level after nTAC.*

10.2.1. Establishment of an isolation and purification technique of cardiac endothelial cells from neonatal mouse hearts intended for single cell RNA sequencing

I performed neonatal transverse aortic constriction (nTAC) on neonatal P1 and P7 mice, by ligating the aortic arch between the right and left common carotid arteries (RCCA and LCCA, respectively), as described in chapter 9. At the 10th postnatal day (P10), I isolated cardiac endothelial cells (EC) from mice subjected to neonatal transverse aortic constriction at P1 (10 days post 1-day old nTAC, shortened as 10dp1dTAC) and at P7 (3 days post 7-days old nTAC, 3dp7dTAC), as well as their sham controls, using antibodies-coupled microbeads and Miltenyi columns (Figure 10.2.1 – A). I slightly adjusted the company's protocol to improve the purity of the enriched cells population. In brief, negative depletion of non-endothelial cell fraction was followed by a positive selection of neonatal cardiac endothelial cells captured in the magnetic MACS columns. However, I increased the number of cold buffer washes to seven times instead of three. The additional washing steps improved the purity of the enriched EC population.

Following enrichment, I further checked endothelial cells' purity by flow cytometry. The analysis revealed that around 98-99% of the enriched population was CD31-positive (Pecam1, known EC marker) (Figure 10.2.1 – D). Single viable FACS-sorted neonatal cardiac endothelial cells isolated from all three conditions (10dp1dTAC, 3dp7dTAC and 10dSham) were subjected to single cell RNA sequencing (scRNAseq) (Figure 10.2.1 – A-C).

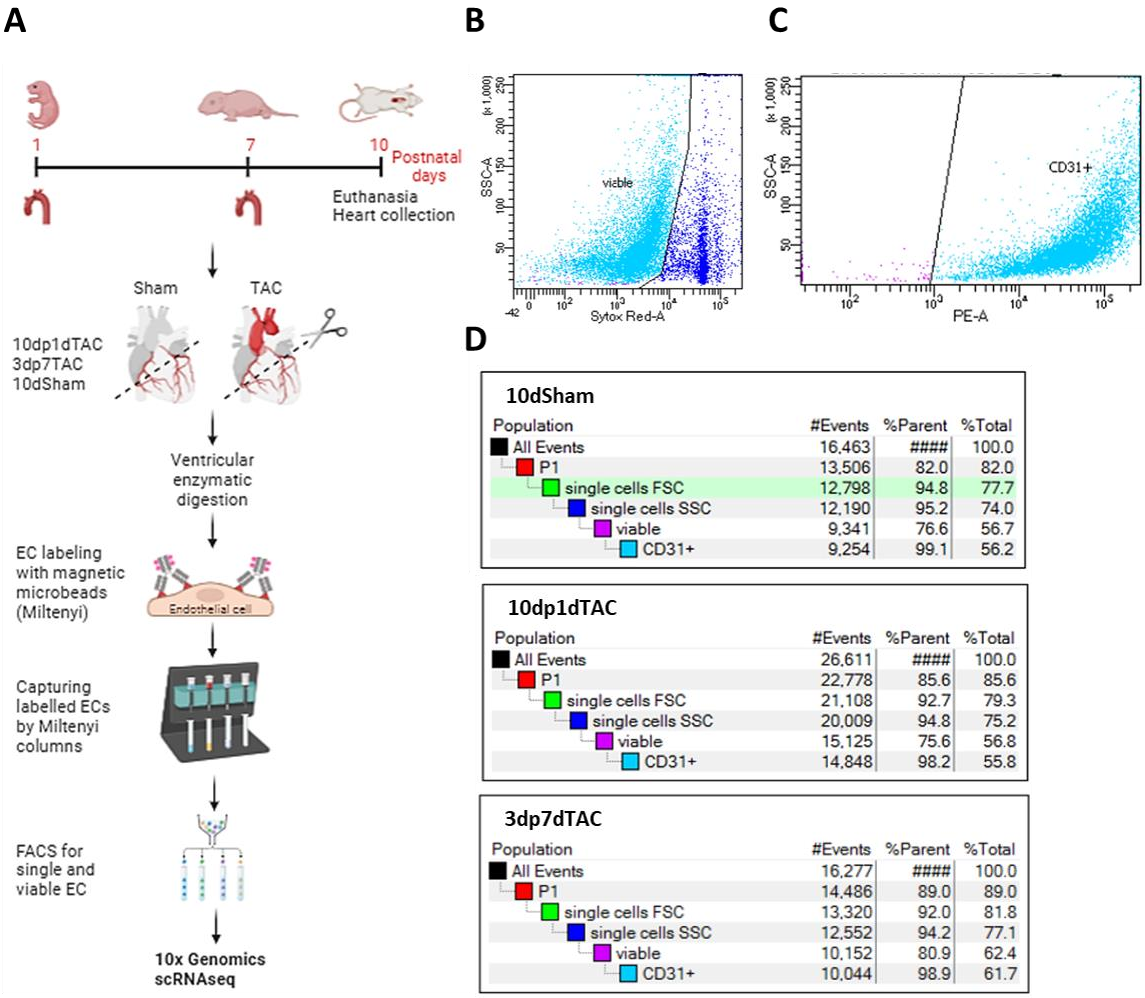

Figure 17 Ventricular endothelial cells isolation and purification from neonatal murine hearts following nTAC.

(**A**) Schematic representation of experimental design for the single-cell RNA analyses. TAC or sham surgeries were performed on P1 and P7 neonatal pups. Heart ventricles (indicated by the dashed lines) were collected at the 10th post-natal day and cardiac endothelial cells (EC) were purified with Miltenyi columns for scRNAseq. n = 8–12 pups were used for ventricular EC collection for each time point. (**B**) FACS sorting of enriched cardiac EC for single viable cells by staining with SYTOX™ Red Dead Cell Stain. (**C**) Flow cytometric representation of isolated ventricular EC stained for the conjugated endothelial marker CD31-PE. (**D**) Flow cytometric quantifications showing the percentage of single viable CD31-positive EC from the three surgical timepoint (10dSham, 10dp1dTAC and 3dp7dTAC) prior to scRNAseq. *Illustration created by using www.biorender.com.* The graphs represent the data analyzed and interpreted solely by myself.

10.2.2. Cardiac endothelial cells' heterogeneity in response to neonatal TAC

Following MACS isolation and FACS sorting, neonatal cardiac endothelial cells (EC) from all three conditions (10dp1dTAC, 3dp7dTAC and 10dSham) were subjected to single cell RNA sequencing (scRNAseq) with the aim to understand the contribution of individual EC populations to cardiac adaptation after nTAC. Using 10x Genomics Chromium platform along with next generation sequencing (NGS) from Illumina, around 9000 total single-cells were acquired from all three samples (see Table 10.2.2, below). I could observe that adaptive endothelial cells (10dp1dTAC) showed the highest number of total genes' expression (15549 features) in comparison to maladaptive (3dp7dTAC) and sham (14628 and 14945, respectively). From the unsupervised graph-based clustering using R package Seurat computational tools, I could detect a total of 14 distinct clusters (Figure 10.2.2A) and I visualized the spatial distribution of these clusters in space through uniform manifold approximation and projection (UMAP) (Figure 10.2.2B-A). The majority of the clustered populations were double positive for the known EC markers: Pecam1 (CD31) and Cdh5 (VE-Cadherin) with minor contaminant cells types subsequently removed from the analysis (Figure 10.2.2B – B-C).

Table 6 Single cell RNA sequencing metrics from all conditions

	10dSham	10dp1dTAC	3dp7dTAC
Estimated number of cells	2729	3992	2259
Filtered number of cells	2709	3948	2217
Number of reads	102,897,734	97,493,793	97,028,804
Reads with valid barcodes	97.8%	97.8%	94.1%
Q30 bases in RNA read	93.0%	92.9%	93.0%
Reads mapped to genome	95.9%	96.1%	95.6%
Reads mapped confidently to genome	92.2%	92.4%	90.8%
Median UMI per cell	2,494	2,912	4,541
Median genes per cell	1,126	1,294	1,671
Total genes detected	17,529	18,156	17,199
Total genes detected after filtration	14,945	15,549	14,628

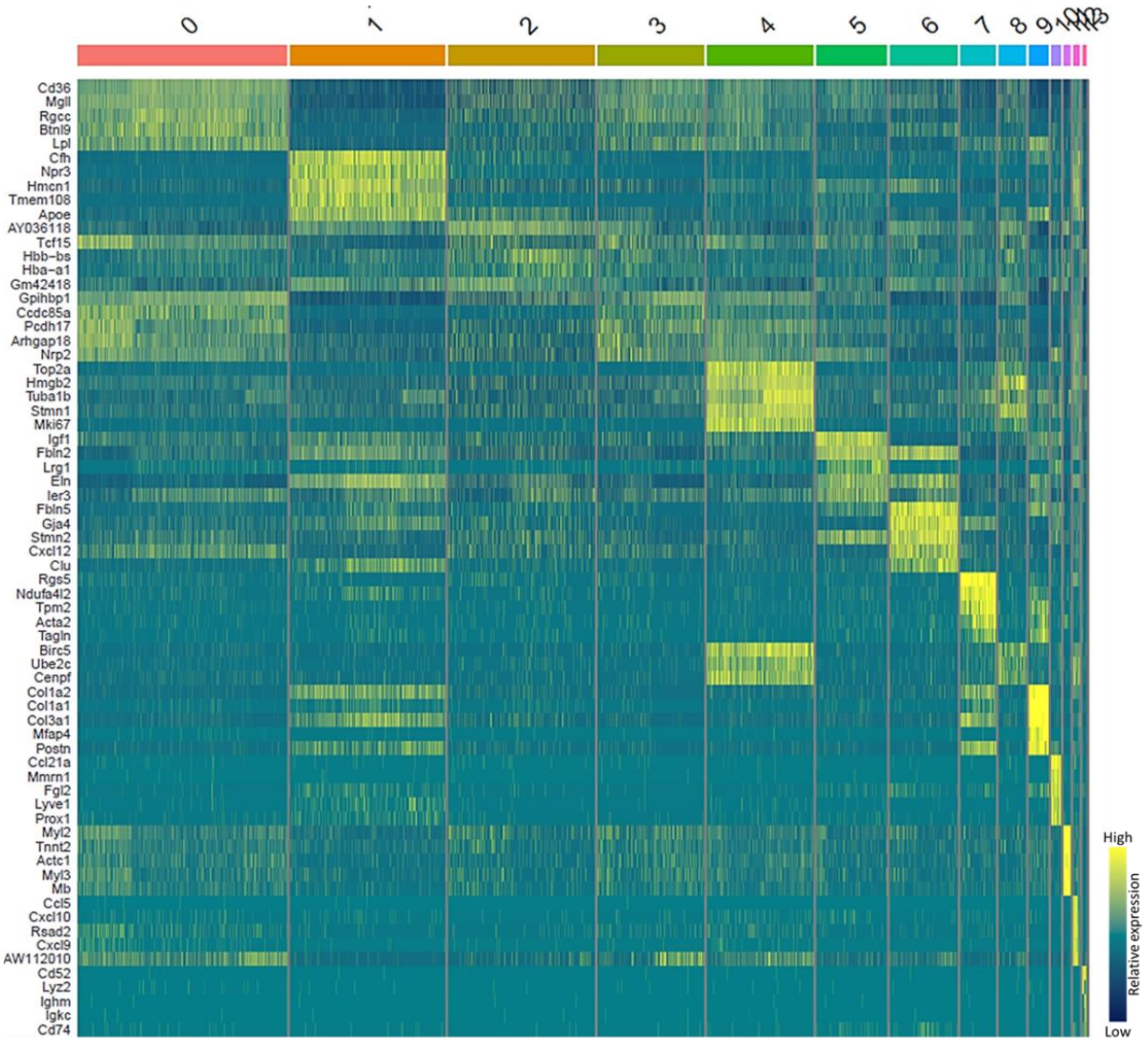

Figure 18 Ventricular endothelial cell heterogeneity in neonatal murine hearts following nTAC.

Heatmap showing expression of top 5 enriched genes for each EC sub-population. A total of 14 distinct clusters were detected with Bimod statistical test following unsupervised clustering of all three conditions combined (10dSham, 10dp1dTAC and 3dp7dTAC). The heatmap in this figure was computed solely by myself.

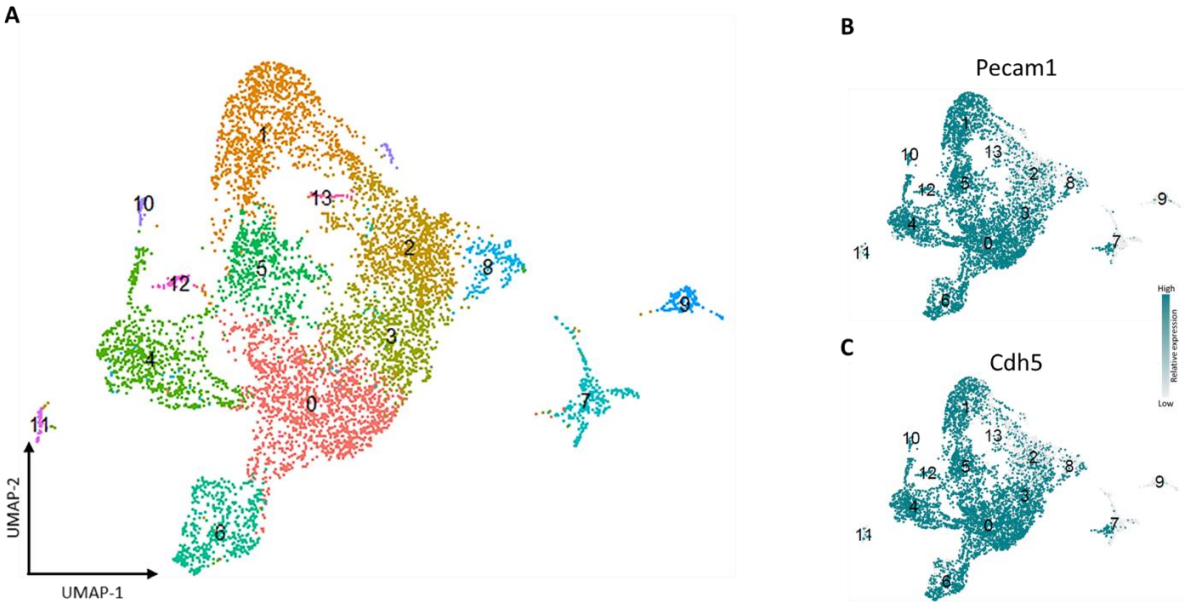

Figure 19 Cardiac endothelial cell heterogeneity revealed by scRNAseq following nTAC.

(**A**) Representative uniform manifold approximation and projection (UMAP) plot of the different endothelial cells (EC) sub-populations obtained from scRNAseq of all three surgical timepoint combined (10dSham, 10dp1dTAC and 3dp7dTAC). A total of 8874 cells were pooled and 14 distinct clusters were identified. Each cluster being assigned its number and color based on the total number of cells located to that specific cluster. (**B and C**) UMAP plots showing the expression of the known EC marker genes Pecam1 (**B**) and Cdh5 (**C**) in the analyzed ECs. The analyzed UMAPs in this figure represent the data analyzed solely by myself.

With the help of online available endothelial cell atlas database (Endotheliomics, KU Leuven, Belgium), I further annotated the nine captured neonatal cardiac EC populations according to their vascular-bed origin into venous EC, arterial EC and capillaries. Besides endothelial cells' specific markers (Pecam1 and Cdh5) expression, EC of venous origin were identified by the expression of Cfh, Cdh11 and H19 genes, while venular capillaries shared Plvap and Vwf genes in addition to Vcam1. I could recognize capillaries mainly based on the expression of Kdr, Rgcc and Cd36 genes. Arteriolar capillaries were marked by expressing Btnl9, Gpihbp1 and Cxcl12, whereas large arteries mainly expressed Sema3g, Fbln5 and Hey1 genes as shown in the dot plot (Figure 10.2.2C). Based on signature marker genes' expression, venous EC were represented in Cluster 1 (C1) and venous capillaries in cluster 5 (C5), arterial EC were grouped in Cluster 6 (C6) and arterial capillaries in cluster 0 (C0) while the majority of the remaining clusters constituted the capillary bed (C2, C3, C4, C8 and C12).

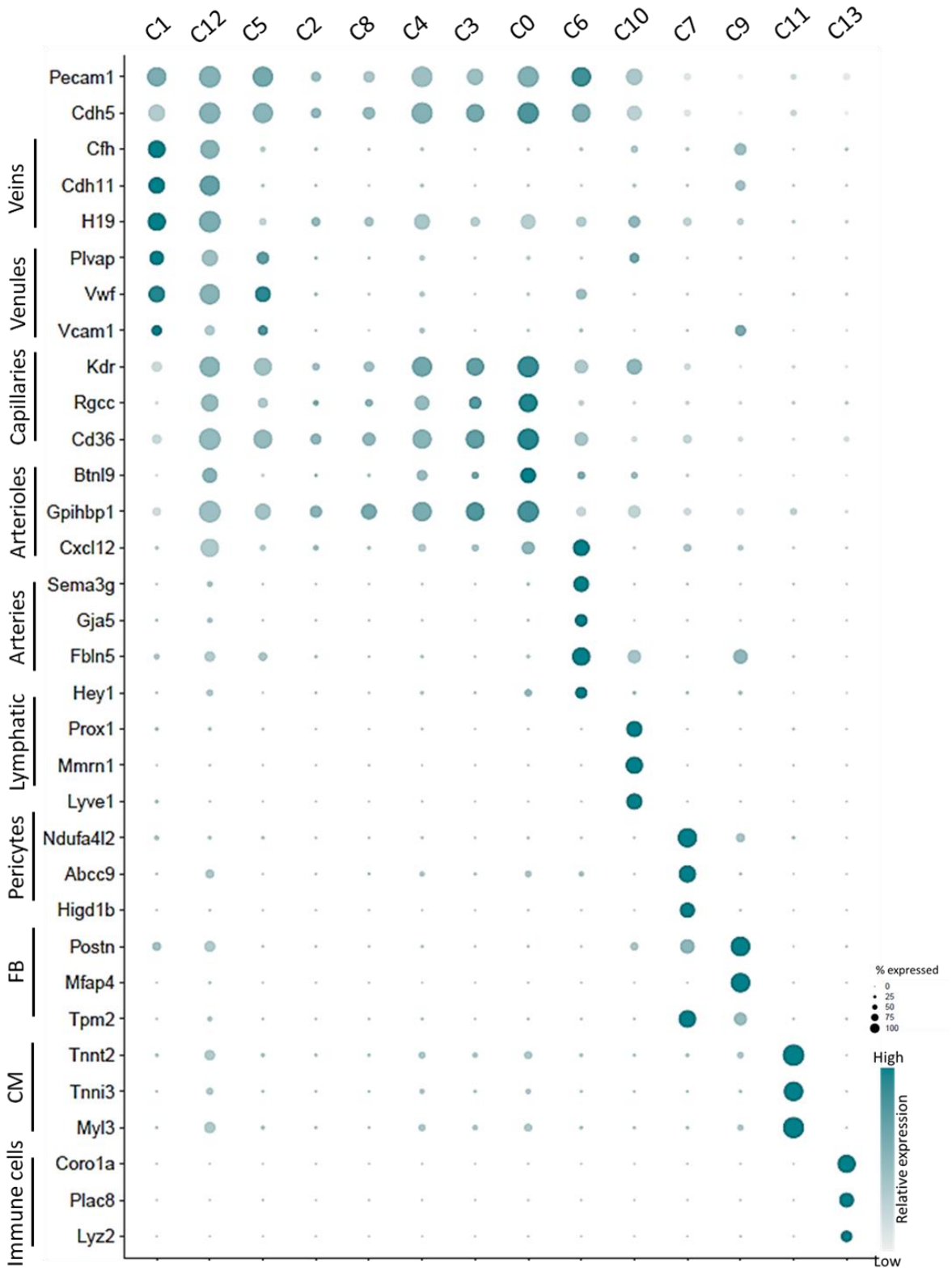

Figure 20 Annotation of cardiac endothelial cells' clusters according to their vascular-bed origin following nTAC.

Dot plot summarizing all cell-type and EC-phenotype specific marker expression for all annotated clusters. Clusters were re-ordered based on their genetic expression profile according to their vascular-bed origin. Color of the dots reflects the relative expression level of the respective gene while its size reflects the percentage of cells expressing that particular gene. The dot plot presented in this figure summarizes the data analyzed solely by myself.

Additionally, I mapped EC heterogeneity in a three-dimensional representation which further confirmed similarities to the known structure of blood vessels starting with arteries and ending with veins at the other pole with the vascular capillary bed in-between. While all EC sub-populations were computed on the same dimensional level, Cluster 5 (C5) as well as Clusters 4 and 8 (C4 and C8) were protruding from the backbone in opposite directions, indicating their distinct genetic profile from the remaining capillaries (Figure 10.2.2D).

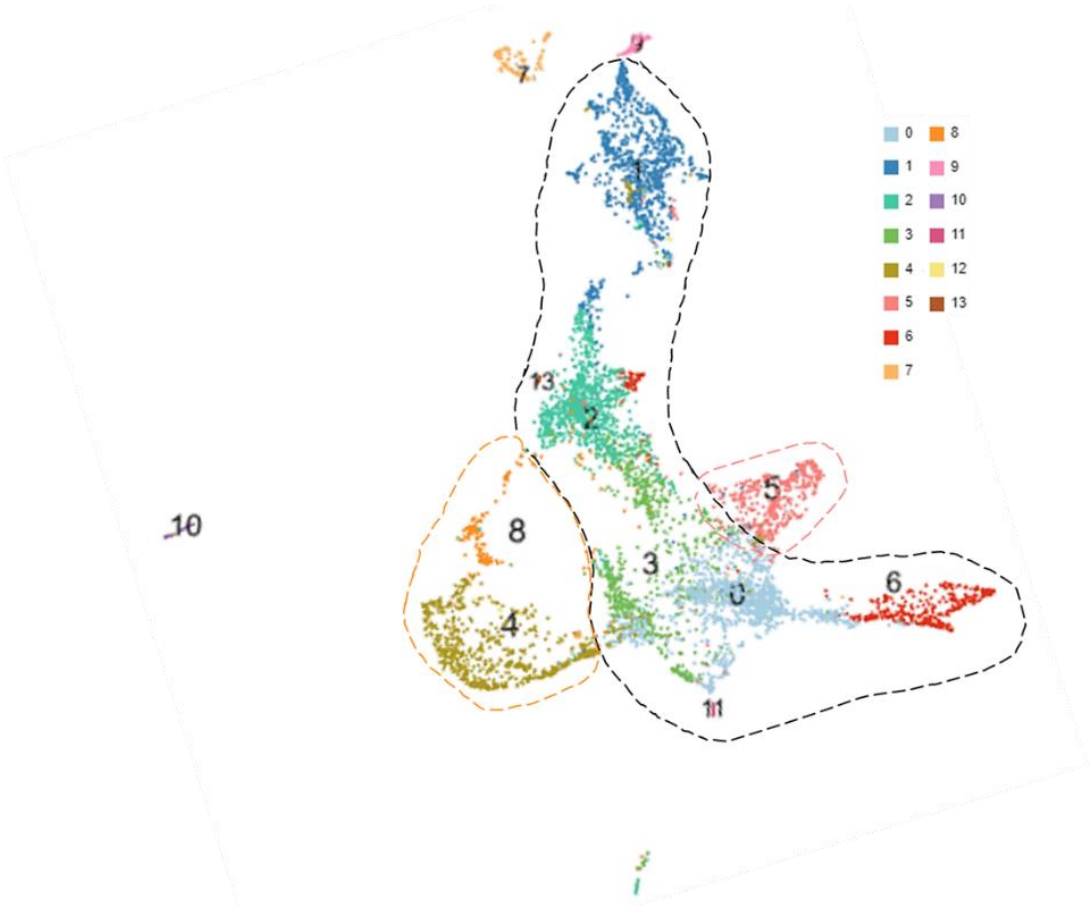

Figure 21 Cardiac endothelial cell heterogeneity confirmed in three-dimensional space.

Three-dimensional uniform manifold approximation and projection (3D-UMAP) plot showing the vascular-bed formed by the different endothelial cells (EC) clusters obtained from scRNAseq. Black dashed line highlights the main endothelial cells backbone starting with the venous C1 (in blue), followed by a capillary-bed (of C2, C3 and C0) ending with the arterial C6 (in red) at the other pole. C5 (pink dashed line) as well as C4 and C8 (orange dashed line) are protruding from the capillary backbone in opposite directions. The analyzed UMAP in this figure summarizes the data analyzed solely by myself.

Nevertheless, less than 10% of the mapped cells were of non-endothelial cells origin. Based on the expression of known marker genes for individual cell types, I assigned pericytes and fibroblasts to clusters 7 and 9 (C7 and C9), respectively. In addition, lymphatic endothelial cells, cardiomyocytes and immune cells were located in clusters 10, 11 and 13 (C10, C11 and C13), in respective order (Figure 10.2.2C).

10.2.3. Neonatal TAC at different postnatal ages in mice induces distinctive differences in cardiac endothelial cells' composition

By analyzing scRNAseq data, I could detect that inducing cardiac pressure overload in neonatal mice at the regenerative (P1) and non-regenerative (P7) age lead to distinct variances in the composition of endothelial cells. Additionally, my analysis showed that 10 days after neonatal TAC performed at the regenerative age (10dp1dTAC) was accompanied with a significant increase in percentage of cluster 0 (C0, 20.2%) and cluster 5 (C5, 8.1%), in comparison to 3dp7dTAC (13.3% C0 and 4.5% C5) and Sham (14.2% C0 and 2.9% C5) (Figure 10.2.3 - A). When I performed gene ontology (GO) analysis for biological processes (BP) of genes belonging to these clusters I could demonstrate that vascular development (C0) and sprouting angiogenesis (C5) related genes were enriched in 10dp1dTAC, which supports their valuable role in the adaptive compensation to nTAC in P1 mice (Figure 10.2.3 - B).

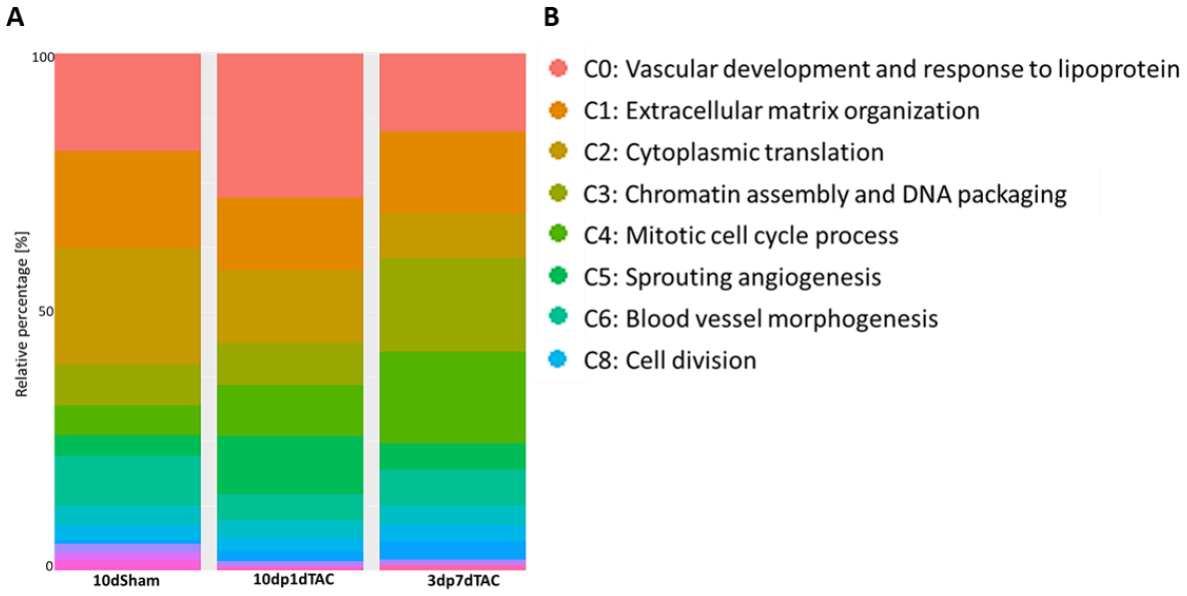

Figure 22 nTAC induction during the regenerative age (P1) mediates sprouting angiogenesis in distinct endothelial subtypes.

(**A**) Stacked bar diagram showing the number of endothelial cells (EC) allocated to each cluster relative to the total number of cells per surgical timepoint. (10dSham n = 2709 cells, 10dp1dTAC n = 3948 cells and 3dp7dTAC n = 2217). (**B**) Representative enriched gene ontology (GO, biological process) term analysis of identified EC clusters. This figure is obtained based on the scRNAseq data analyzed solely by myself.

On the other hand, genes associated with extracellular matrix organization were grouped in Cluster 1 (C1). Interestingly, the percentage of this cluster was meaningfully reduced in regenerative endothelial cells (10.1%) compared to maladaptive 3dp7dTAC (14.4%) and sham (14%). In contrast, mitosis and cellular division related clusters (C4 and C8) showed higher percentage in 3dp7dTAC (15.7% in C4, 2.7% in C8) versus 10dp1dTAC (7.1% C4, 2% C8) and sham (4.4% in C4, 2.2% in C8). The rest of clusters were involved in cytoplasmic translation (C2), chromatin assembly (C3) and blood vessel morphogenesis (C6) (Figure 10.2.3 - A).

10.2.4. Angiogenesis-related transcriptional regulators are downregulated in maladaptive endothelial cells in response to nTAC

A fundamental player to a gene's expression is the regulation of its transcription through transcription factors (TF). The latter are in most cases proteins with the ability to bind to certain DNA sequences, thereby affecting their transcription to mRNA. Accordingly, TFs can both enhance the transcription of certain genes (transcriptional activators) or repress it (transcriptional repressors). Hence, my first aim was to explore whether inducing cardiac pressure overload with nTAC at different postnatal ages in neonatal mice was associated with a differential expression in angiogenesis-related transcriptional regulators. For this purpose, I analyzed clusters-specific as well as universal differentially expressed TFs between conditions and summarized my findings in the dot plot in Figure 10.2.4. In cluster 0 (C0) related to vasculature development, capillaries with a maladaptive phenotype showed a significant downregulation in Tbx3 transcription factor's expression in 3dp7dTAC, which is a TF known to have an impact on cellular development and proliferation. On the other hand, mitotic ECs in cluster 4 (C4) were hallmarked by diminished expression of the chromatin modulator Phf12, which plays a role in senescence prevention, specifically following nTAC in the non-regenerating age (3dp7dTAC). Additionally, I found that the expression of the arterial-specific EC transcription regulator Prdm16 was significantly reduced in the maladaptive TAC in C6, which might contribute to the pathological remodeling due to defective arterial blood flow. Of interest, regardless of their vascular origin, neonatal cardiac EC with a maladaptive phenotype after nTAC were characterized by a general downregulation in the expression of TFs promoting vascular branching and angiogenesis (for example Lmo2 and Gata2), as well as vascular integrity and wound healing (Sox18 and Klf4).

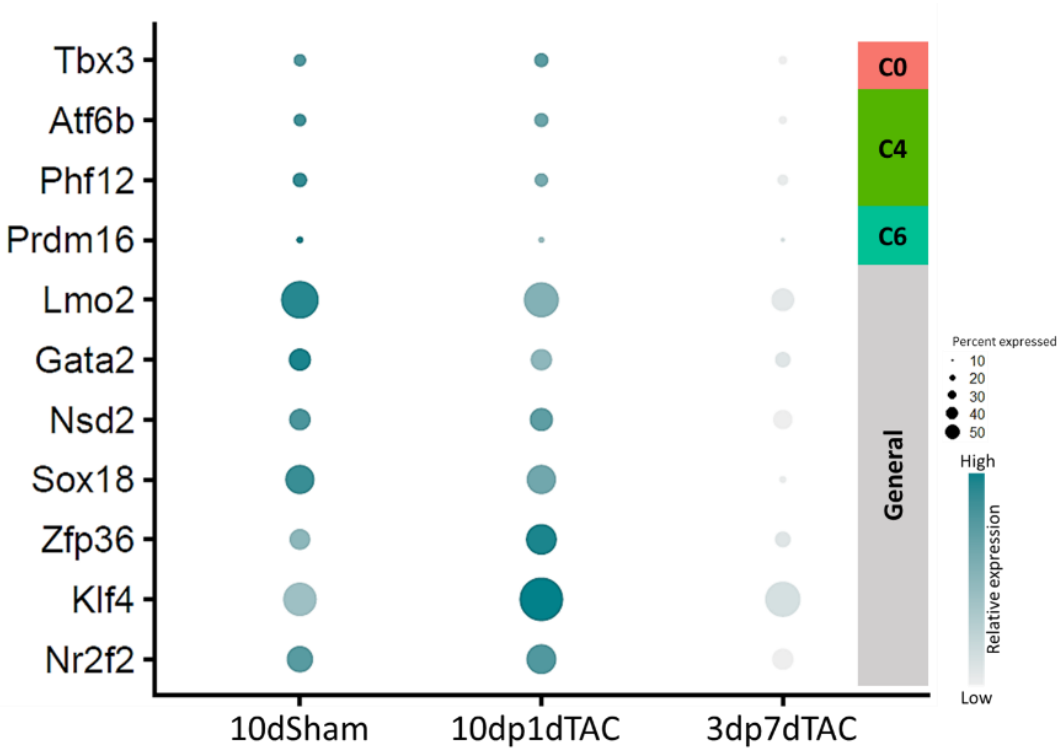

Figure 23 Maladaptive response to nTAC is mediated through downregulation of angiogenesis-related transcriptional regulators.

Dot plot showing cluster-specific as well as universal transcription regulators differentially regulated after TAC induction at different post-natal ages. Respective EC clusters where the transcription factors originate are summarized on the right of the graph. Color of the dots reflects the relative expression level of the respective gene while its size reflects the percentage of cells expressing that particular gene. The data shown in this figure summarize the transcription regulators obtained from my scRNAseq data analyzed solely by myself.

10.2.5. Adaptive cardiac endothelial cells following nTAC were hallmarked by an enhanced revascularization signature

Subsequently, my main analysis focused on cardiac endothelial cells' sub-populations which were enriched solely in EC during an adaptive response to nTAC (10dp1dTAC) in comparison to maladaptive EC (3dp7dTAC) and sham, particularly Clusters 0 and 5 (C0 and C5) (Figure 10.2.3 - A). For this purpose, I could identify cells uniquely allocated to these two clusters on the UMAP and select them separately using the R-based tool SleepWalk [72], while extracting their genes for further downstream analysis (Figure 10.2.5 – A-B). Gene ontology (GO) analysis of the biological processes (BP) of genes exclusively enriched in C0 were related to angiogenesis regulation (including *Col4a2* and *Ets1* genes) as well as blood vessels branching and morphogenesis (like *Col4a1* and *Cxcl12*). In contrast, genes specifically down-regulated in C0 were assigned to extracellular matrix (ECM) organization and production (such as *Fbln2* and *Bgn*), as shown in Figure 10.2.5-C. Similarly, adaptive capillaries in C5 specifically up-regulated genes associated with vasculature development (as *Aplnr*, *Igf1* and *Vegfc*) and regulation of angiogenesis (like *Klf4* and *Flt1*), while explicitly decreasing the expression of genes involved in the negative regulation of angiogenesis (*Dcn* and *Hmgb1*) and cell migration (*Pdgfb* and *Prnp*) Figure 10.2.5-D.

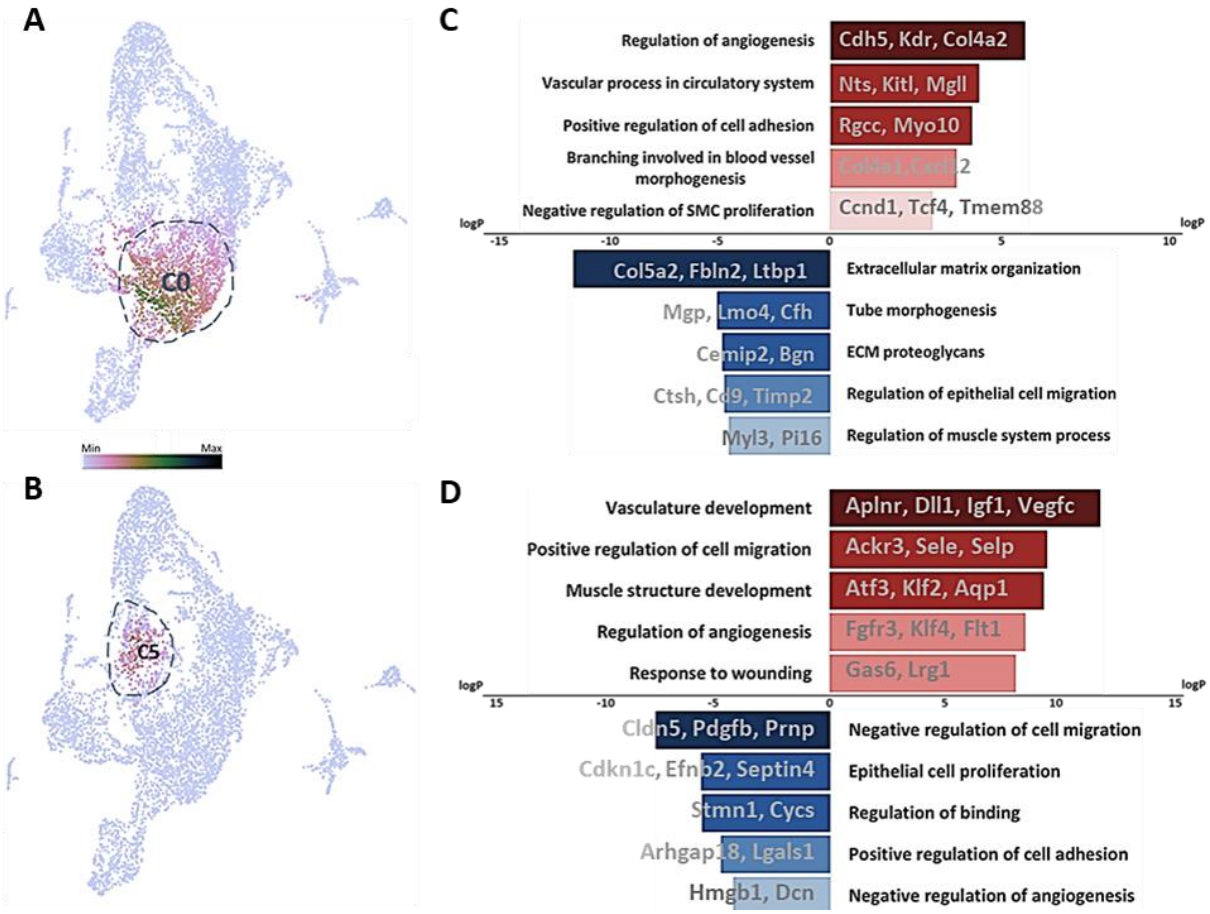

Figure 24 P1 mice adapt to nTAC by inducing angiogenesis-related genes in cardiac endothelial cells.

(**A and B**) UMAP representation with Sleepwalk selection for specific localization and extraction of cells allocated to cluster 0 (A) and cluster 5 (B) from scRNAseq data of all three surgical timepoints combined (10dSham, 10dp1dTAC and 3dp7dTAC). Sleepwalk tool assigns a color to each point (cell) from the UMAP and cells with similar features are grouped together. The darker the color the more these adjacent cells share similar features. (**C and D**) Bar plots summarizing the gene ontology (GO) analysis of biological processes (BP) upregulated (red) and downregulated (blue) in cluster 0 (C) and cluster 5 (D). Exemplary genes were listed for each GO-terms. Genes were filtered with set thresholds fold-change 0.75 ≤ FC and FC > 1.5 and a p-value < 0.05. The analyzed UMAP and bar plots in this figure are analyzed solely by myself.

10.2.6. Regenerating cardiac endothelial cells adapt to neonatal pressure overload by secreting pro-angiogenic factors

To decipher the role of neonatal cardiac endothelial cells (EC) in interacting with their surrounding environment in the heart in response to nTAC injury, I identified EC-specific ligands from the EC-scRNAseq data. In order to deconvolute their respective receptors, I integrated these ligands with bulk RNA-seq from the other main cardiac cell types (cardiomyocytes; CM and fibroblasts; FB) that I previously isolated from murine hearts subjected to nTAC during the regenerative age at P1 (10dp1dTAC) and the non-regenerative P7 age (3dp7dTAC) as well as their sham controls. The ligand-receptor interaction network analysis from the sequencing data revealed that cardiac ECs in the neonatal heart positively adapt to pressure overload following nTAC induction in 1-day old mice (10dp1dTAC) through the expression and secretion of pro-angiogenic ligands in their microenvironment.

More specifically, I was able to identify cluster-specific ligands from the two angiogenesis-promoting clusters enriched in adaptive nTAC (Clusters 0 and 5), as shown in Figure 10.2.3. At 10 days post-nTAC in P1 regenerating hearts (10dp1dTAC), arteriolar endothelial cluster 0 (C0) specifically induced the expression of *Col4a1* (Collagen Type IV Alpha 1 Chain) and *Cxcl12* (C-X-C motif chemokine 12) ligands, and I could compute their interacting receptors in CM (*Itgb1* and *Cxcr4,* respectively). In contrast, the capillary cluster 5 (C5), related to sprouting angiogenesis, upregulated the expression of *Dll1* (Delta Like Canonical Notch Ligand 1) and *Igf1* (Insulin-like growth factor 1), besides their respective receptors (*Notch3* and *Rack1*) were expressed in regenerating CMs. Furthermore, Nts (Neurotensin) was identified as a reoccurring ligand secreted from both endothelial cell populations C0 and C5 (Figure 10.2.6A – A-B).

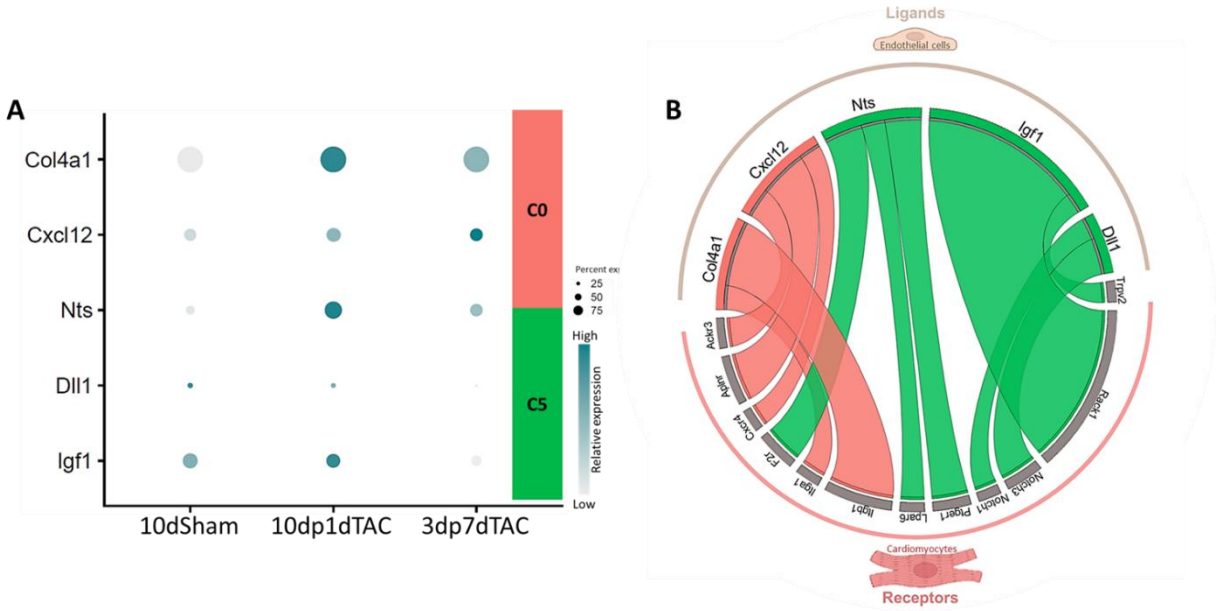

Figure 25 Regenerating cardiac endothelial cells' clusters secret pro-angiogenic factors to adapt to nTAC.

(**A**) Dot plot showing EC-derived cluster-specific (C0 and C5) expressed ligands regulated after TAC induction at different post-natal ages. Respective EC clusters where the transcription factors originate are summarized on the right of the graph. Color of the dots reflects the relative expression level of the respective gene while its size reflects the percentage of cells expressing that particular gene. (**B**) Circos plot summarizing the significantly upregulated ligand-receptor interactions between cardiac endothelial cells (on top, beige) and cardiomyocytes (bottom, red) in 10dp1dTAC. Arrow color indicates the ligand's cluster of origin while the arrow thickness designates the ligand-receptor interaction score. The dot plot and the circos plot in this figure are solely analyzed and computed by myself.

While neonatal mice operated during their first post-natal day (P1) had a total of 10 days to adapt to nTAC (10dp1dTAC) before isolating and sequencing their ECs, pups that I operated at the age of 7-days (P7) were permitted a period of 3 days following nTAC injury (3dp7dTAC) before EC isolation (Figure 10.2.6B-A). To compensate for this unequal time period following injury and to capture the early transcriptional changes to pressure overload in the regenerative age, I performed nTAC on 1-day old mice (P1) and isolated their main cardiac cell types (EC, CM and FB) 3 days following injury (3dp1dTAC) with the same methods. Hence, I named 3dp1dTAC timepoint as early regenerative nTAC, while I recognized 10dp1dTAC as the late regenerative nTAC. For deeper transcriptional sequencing, I sent samples of EC, CM and FB isolated from both conditions for bulk RNA-seq in addition to the early non-regenerative timepoint (3dp7dTAC) as well as sham (Figure 10.2.6B-B). In the Circos plot in Figure 10.2.6B-C, I summarized the ligand-receptor interaction network analysis between ligands upregulated (in

red) and down-regulated (in blue) in early and late regenerative endothelial cells (EC) as well as their identified receptors in CM and FB. My analysis showed that, at 3 days post nTAC in P1 hearts (3dp1dTAC, early regenerative), endothelial cells enhanced the genetic expression of the secreted ligands Bmp7 and Efnb3, while late regenerative EC (10dp1dTAC) adapted to pressure overload by inducing the expression of *Nts*, *Thbs4*, *Apln*, *Inhba*, *Cldn11* and *Fgf11* genes. Both regenerative conditions showed a strong down-regulation of inflammation-associated ligands and decreased their expression, such as *Il6* and *Cxcl11* (in early regenerative EC, 3dp1dTAC) and *Tnf* and *Fgf23* (in late regenerative EC, 10dp1dTAC). Interestingly, the expression of *Ccl21* was decreased early after regenerative nTAC and remained diminished throughout the late timepoint.

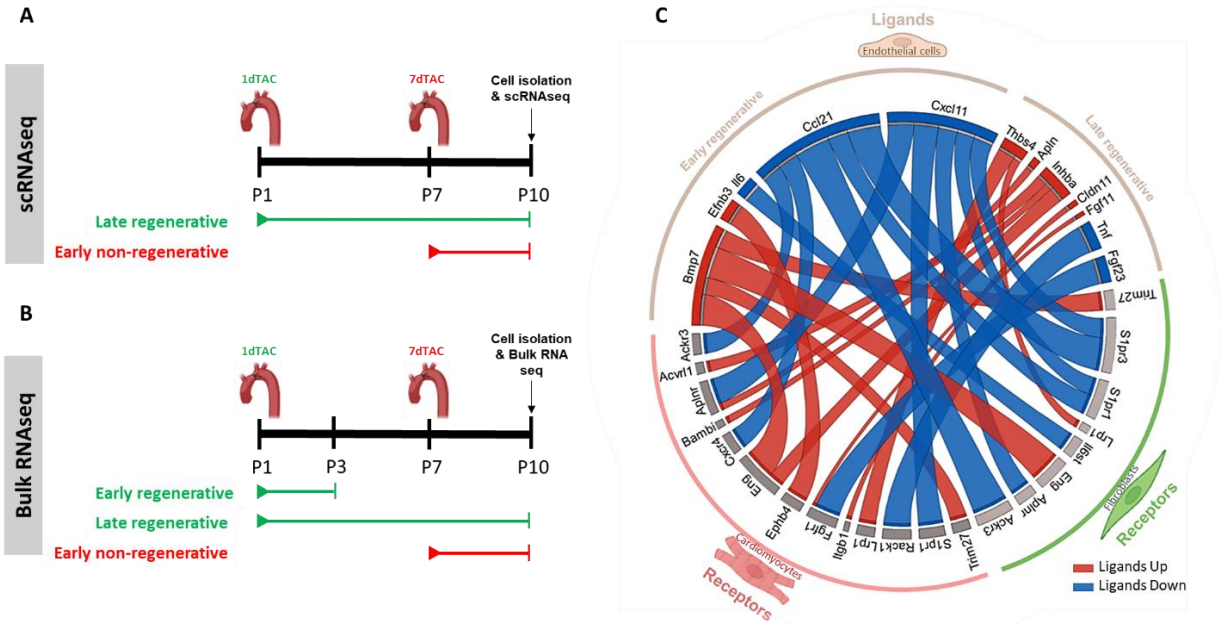

Figure 26 Neonatal endothelial cells upregulate pro-angiogenic ligands during the early and late regenerative stages after nTAC.

(**A**) Schematic representation of experimental design for the single-cell RNA analyses. TAC or sham surgeries were performed on P1 and P7 neonatal pups. Cardiac endothelial cells were isolated on the 10th post-natal day for scRNAseq. (**B**) Schematic representation of experimental setup for the bulk RNA sequencing. TAC or sham surgeries were performed on P1 and P7 neonatal pups. All cardiac cell types (CM, EC and FB) were isolated on the 3rd (early regenerative, 3dp1dTAC) and 10th post-natal day (late regenerative, 10dp1dTAC and non-regenerative; 3dp7dTAC) for bulk RNA sequencing. (**C**) Circos plot showing the differentially regulated ligands secreted from cardiac ECs (on top, beige) interacting with receptors on cardiomyocytes (bottom left, red) and fibroblasts (bottom right, green). Line color specifies whether the ligand is upregulated (in red) or downregulated (in blue) in regenerative EC compared to non-regenerative and control. The arrow thickness indicates the ligand-receptor interaction score. The analyzed circos plot in this figure summarizes the data I analyzed solely by myself.

10.2.7. Establishment of an in-vitro functional screening pipeline to filter the candidates for follow-up

From the ligand-receptor interaction analysis discussed earlier, I detected a total of 18 differentially expressed ligands (13 ligands were upregulated, while 5 were down-regulated in regenerating neonatal cardiac EC (3dp1dTAC and 10dp1dTAC) compared to non-regenerating and sham control), which I summarized in Table 10.2.7.

Table 7 List of candidate ligands differentially regulated in regenerative neonatal cardiac endothelial cells following nTAC

Up in regenerating EC after nTAC		**Down in regenerating EC after nTAC**	
Symbol	**Description**	**Symbol**	**Description**
Col4a1	Collagen Type IV Alpha 1 Chain	*Il6*	Interleukin 6
Cxcl12	C-X-C Motif Chemokine Ligand 12	*Cxcl11*	C-X-C Motif Chemokine Ligand 11
Nts	Neurotensin	*Ccl21*	C-C Motif Chemokine Ligand 21
Dll1	Delta Like Canonical Notch Ligand 1	*Tnf*	Tumor Necrosis Factor
Igf1	Insulin Like Growth Factor 1	*Fgf23*	Fibroblast Growth Factor 23
Bmp7	Bone Morphogenetic Protein 7		
Efnb3	Ephrin B3		
Thbs4	Thrombospondin 4		
Apln	Apelin		
Inhba	Inhibin Subunit Beta A		
Cldn11	Claudin 11		
Fgf11	Fibroblast Growth Factor 11		
Tnfsf13	TNF Superfamily Member 13		

My next aim was to establish an in-vitro model to study the paracrine effect of these EC-derived ligands on neighboring CM as well as their autocrine action on the vasculature. For this purpose, I used Human umbilical vein endothelial cells (HUVECs) to overexpress or downregulate these angiocrine factors by lentiviral infection. Also, I confirmed adequate genetic overexpression and down-regulation of the candidates by qPCR (as in Figure 10.2.7-A).

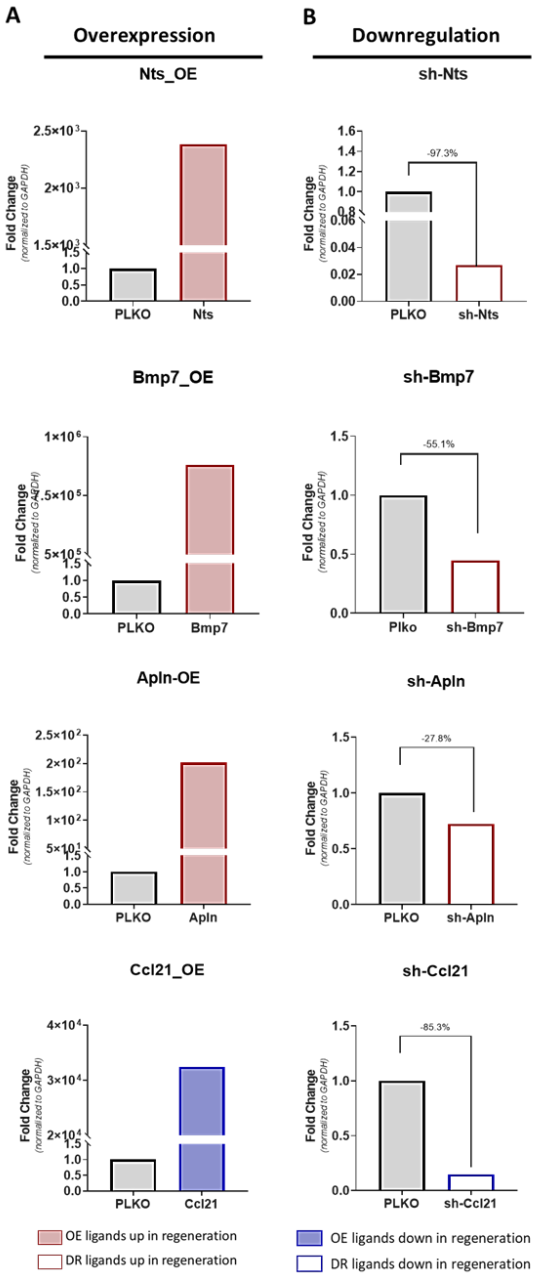

Figure 27 Validation of ligands' overexpression and downregulation in HUVECs by qPCR.

(**A and B**) Relative mRNA expression following ligands' lentiviral overexpression (A) and sh-RNA mediated downregulation (B) in HUVECs as detected by qPCR. Bar's color indicates ligands upregulated (red) or downregulated (blue) in regenerating endothelial cells (3dp1dTAC and 10dp1dTAC) compared to non-regenerating and sham. As a control, the backbone vector for lentivirus PLKO (in black) was used. OE = Overexpression, DR = Downregulation. The data in this figure summarize the qPCR findings analyzed solely by myself.

Subsequently, I co-cultured neonatal rat cardiomyocytes (NRCM) on top of the lentivirus-transfected HUVECs and I analyzed the paracrine effect of these factors on CM proliferation and contractility. Additionally, I studied the autocrine outcome of these candidates on HUVECs' proliferation as well as their angiogenic function (Figure 10.2.7-B). As an experimental control, I transfected HUVECs with an empty lentivirus carrying the backbone vector (PLKO). Using this experimental pipeline developed by myself, four angiocrines showed promising effect on cardiac regeneration, filtering out fifteen candidates from the main observed regulated ligands.

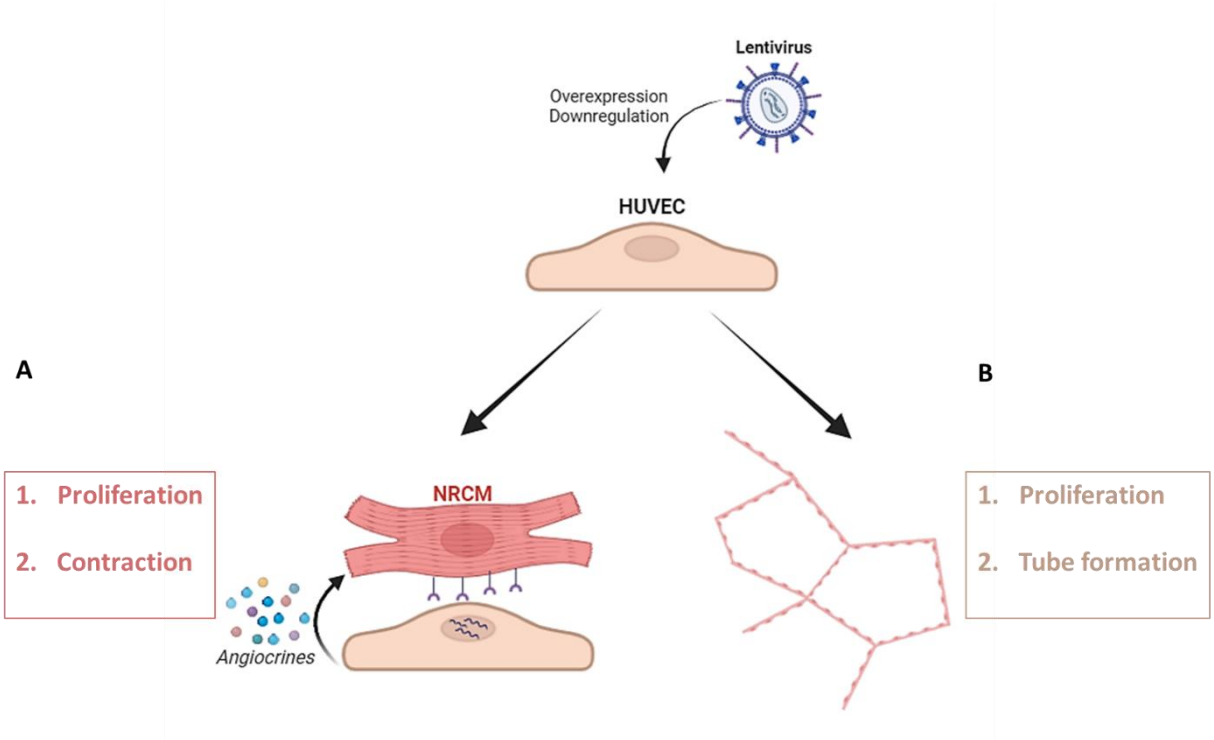

Figure 28 In-vitro screening pipeline for testing candidate ligands' effect on cardiomyocytes and endothelial cells with lentivirus.

Schematic representation of experimental setup for in-vitro screening of EC-derived ligands: HUVECs were initially transfected with lentivirus particles produced by overexpression or shRNA-mediated downregulation of lentiviral plasmids from genome-wide libraries. (**A**) HUVECs overexpressing or downregulating the selected candidates were co-cultured with wildtype neonatal rat cardiomyocytes (NRCM) to test their paracrine effect on CM proliferation and contraction. (**B**) Autocrine effect of overexpressing or downregulating the selected factors in HUVECs was tested though EC proliferation and tube formation assays. *Illustration created by using www.biorender.com.*

10.2.8. Endothelial Bmp7, Apln and Nts promote cardiomyocytes' proliferation

Aiming to study the effect of manipulating the expression of the candidate genes in endothelial cells on the functional behavior of cardiomyocytes, I applied a direct cell-cell contact co-culture method. For this purpose, I used a heterotypic co-culture system in which I directly co-cultured P1-P3 wildtype neonatal rat cardiomyocytes (NRCM) onto a monolayer of HUVECs pre-transfected with lentivirus particles (overexpressing or downregulating the gene of interest). After 48 hours of co-culture, I quantified NRCM proliferation and cytokinesis by immunofluorescent staining of the cell proliferation marker Ki67 and the cytokinesis marker Aurora B kinase along with cardiac troponin T (cTnT) as a CM marker.

At the outset, comprehensive bulk RNA sequencing data across all surgical timepoints of nTAC showed a marked increase in Bone morphogenetic protein 7 (Bmp7) expression during the initial adaptive phase of nTAC in P1 mice (3dp1dTAC). This upregulation was observed not only in endothelial cells (Figure 10.2.8A- A) but predominantly also in cardiomyocytes (Figure 10.2.8A- B).

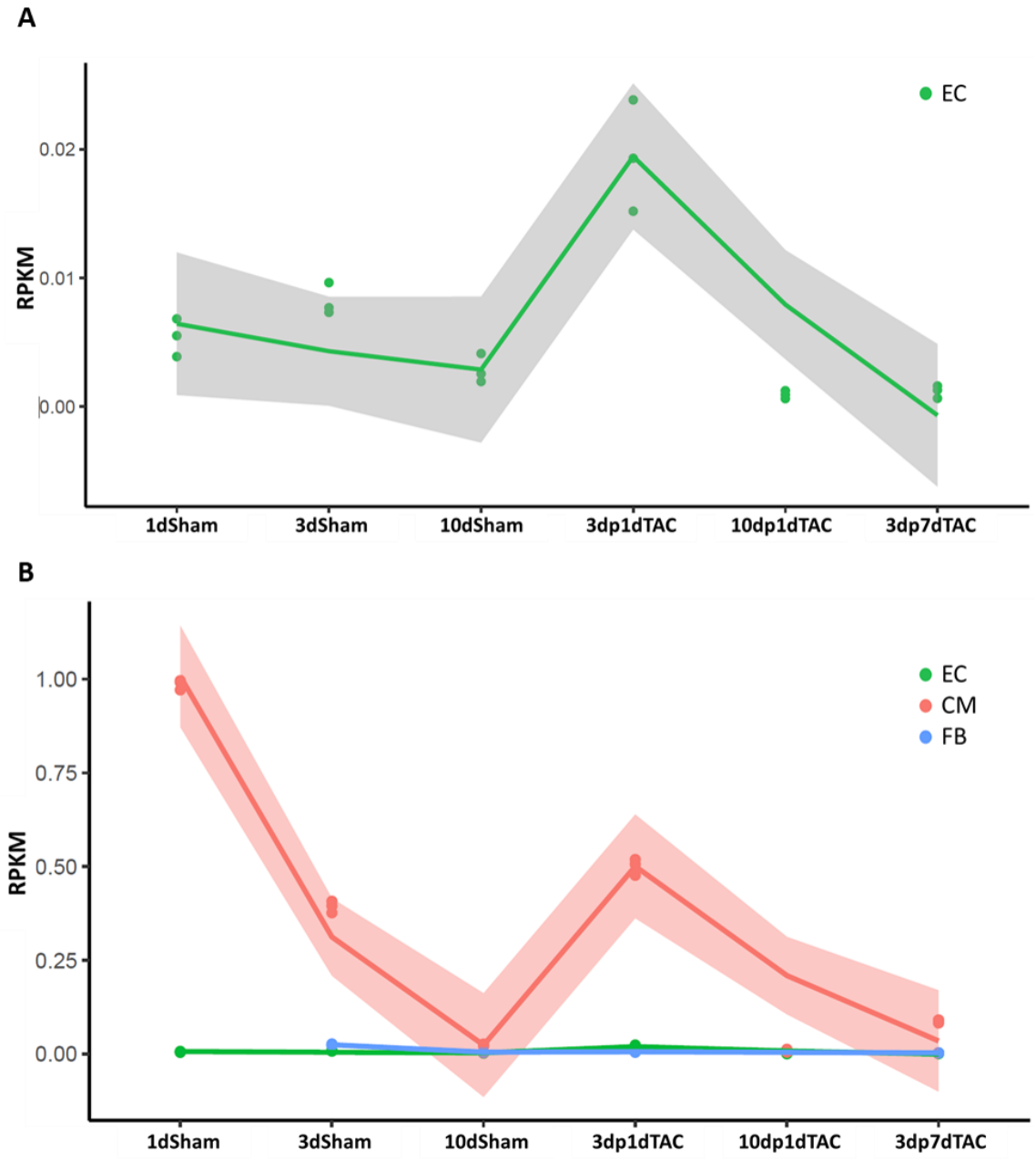

Figure 29 Bone morphogenetic protein 7 (Bmp7) is upregulated during the early regenerative phase after nTAC.

(**A**) Scatter plot showing the expression of *Bmp7* in cardiac endothelial cells (EC) from bulk RNA sequencing data of all nTAC timepoints. (**B**) Scatter plot summarizing the expression of *Bmp7* in the three main cardiac cell types (CM, EC and FB) from bulk RNA sequencing data of all surgical timepoints. The line represents the trend of expression for each cell type while the confidence interval is represented in shaded area around the line. The data presented in this figure are based on the surgeries and analyses performed solely by myself.

Interestingly, I could observe that the exclusive overexpression of the early regenerative angiocrine Bmp7 in HUVECs notably boosted NRCM mitotic activity nearly threefold in a paracrine manner (5.5% compared to 2.2% in the control), as illustrated in Figure 10.2.8B – A-B. I could further validate this increase in NRCM proliferation by the higher total count of NRCMs per high power field (HPF) following endothelial cell-specific overexpression of Bmp7 (160 NRCM/HPF in Bmp7-OE compared to 127 NRCM/HPF in control) (Figure 10.2.8B – C).

Conversely, my findings showed that the reduction of Bmp7 expression using short-hairpin RNA (shRNA) delivered via lentivirus in HUVECs led to a substantial six-fold decrease in NRCM proliferation (10.2.8B – A-B), resulting in a noticeable decline in the total count of NRCMs per high power field (HPF) (81 in sh-Bmp7 versus 127 in the control), as depicted in Figure 10.2.8B-C.

In mice during the initial stages after birth, the majority of cardiomyocytes undergo DNA synthesis and nuclear division (karyokinesis) without progressing to cytoplasm division (cytokinesis), leading to the formation of binucleated cells. Likewise, in humans, the majority of cardiomyocytes experience DNA synthesis without undergoing karyokinesis, leading to polyploidization. For evaluating the influence of the selected candidates on neonatal rat cardiomyocytes' division, I stained the cells with Aurora B kinase in addition to cardiac troponin to label NRCM. This kinase is observed to localize at the equatorial region of the central spindle during late anaphase and at the midbody during cytokinesis. I could find that inducing Bmp7 overexpression exclusively in HUVECs through lentiviral methods notably increased NRCM cytokinesis to 2.7%, compared to 0.5% in the control. Contrarywise, reducing Bmp7 levels in HUVECs completely halted cardiomyocyte cytokinesis (10.2.8B – E).

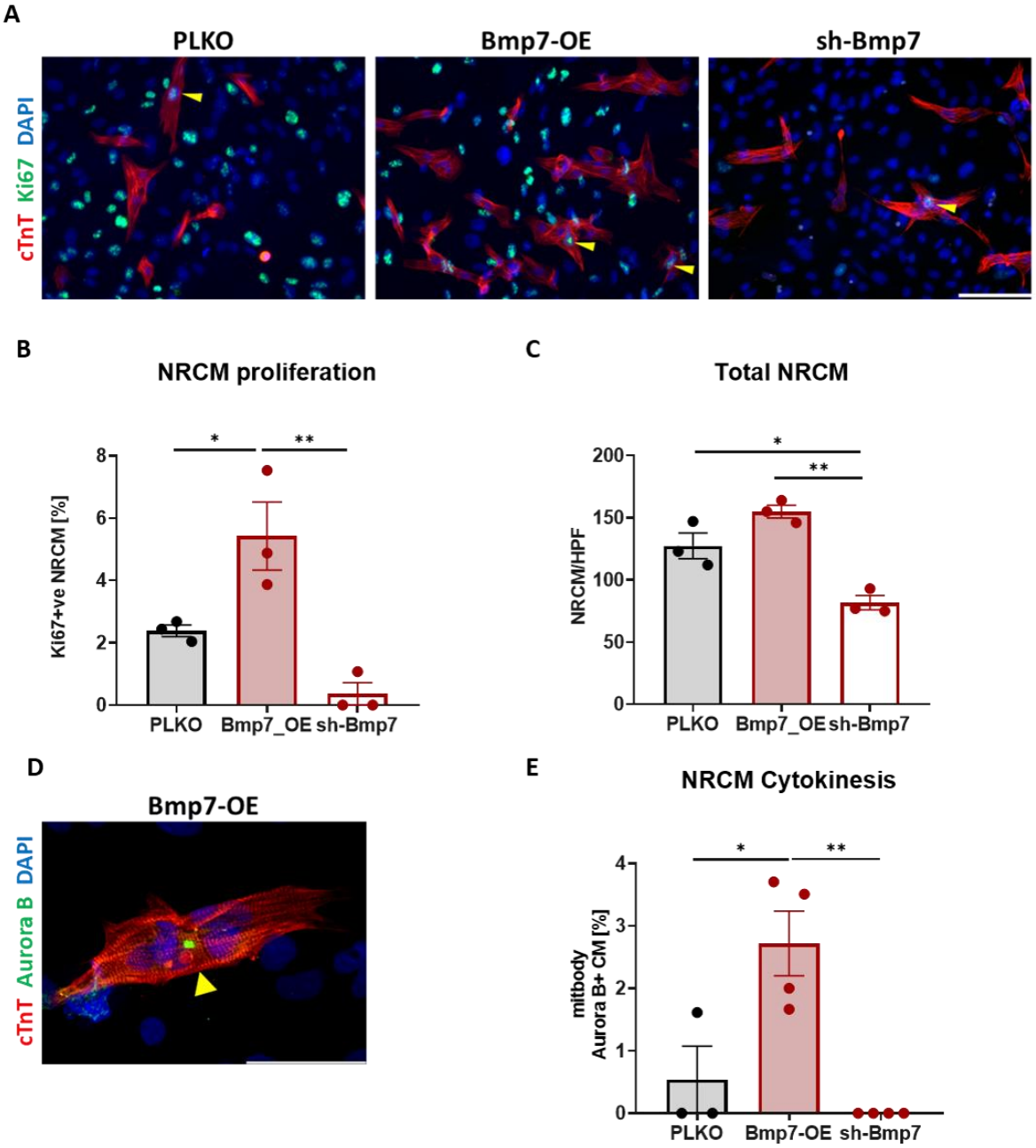

Figure 30 Cardiomyocytes' proliferation is enhanced through Bmp7 overexpression in endothelial cells with lentivirus.

(**A**) Representative immunofluorescent images of the pan proliferation marker (Ki67, green) and the cardiomyocytes' marker cardiac troponin T (cTnT, in red). Isolated neonatal rat cardiomyocytes (NRCM) co-cultured on lentivirus-transfected HUVECs (OE) or downregulating (sh) Bmp7. PLKO is the control (infected with control lentivirus). Yellow arrow pointing at Ki67 positive NRCM. Scale bar, 100µm. (**B**) Quantification of NRCM proliferation (Ki67 positive NRCM) plated on lentivirus-transduced HUVECs. (**C**) Quantification of total number of NRCM per high-power field (HPF). (**D**) Representative immunofluorescent image of the cytokinesis marker Aurora B Kinase (green) and the cardiomyocytes' marker cardiac troponin T (cTnT, in red). Yellow arrow pointing at midbody Aurora B kinase between two NRCM co-cultured on lentivirus-transfected HUVECs overexpressing Bmp7. Scale bar, 50µm. (**E**) Quantification of NRCM cytokinesis (midbody Aurora B kinase positive NRCM) plated on lentivirus-transduced HUVECs. Data presented as mean ±SEM (n=3-4 per condition). *p<0.05, **p<0.01 (one-way ANOVA/Sidak's multiple-comparisons test). The images and graphs in this figure were acquired and analyzed solely by myself.

Unlike Bmp7, the angiocrine Apelin (Apln) showed predominant upregulation during the late adaptive phase of nTAC in P1 mice (10dp1dTAC), although it is already (but to a smaller degree) upregulated also early after nTAC as revealed by bulk RNA sequencing data (Figure 10.2.8C- A). Notably, the upregulation of Apln induced by nTAC was primarily attributed to endothelial cells (Figure 10.2.8C- B).

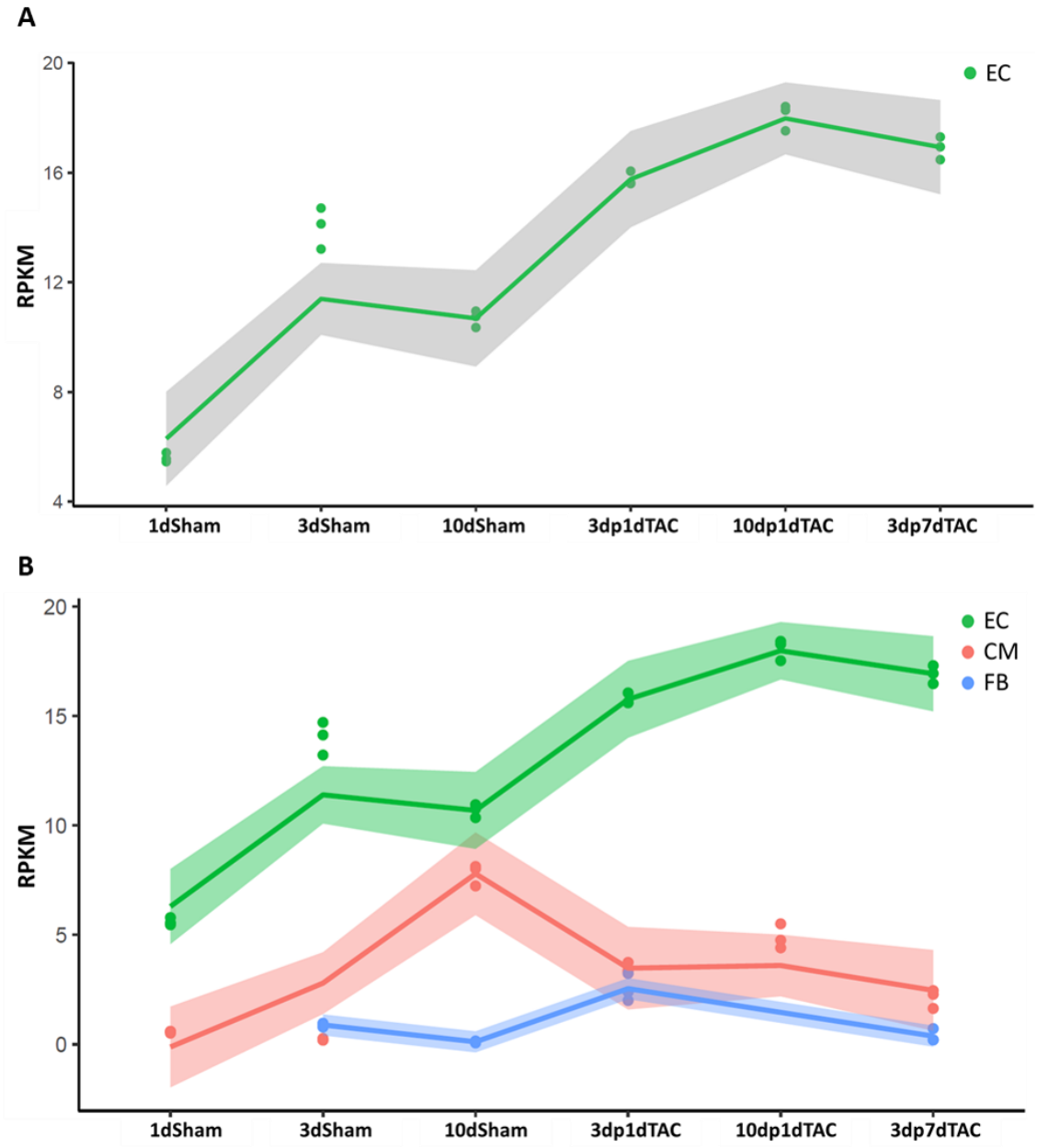

Figure 31 Apelin (Apln) is upregulated in endothelial cells during the early and late regenerative phase after nTAC.

(**A**) The scatter plot illustrates the expression levels of *Apln* in cardiac endothelial cells (EC), derived from bulk RNA sequencing data collected across all surgical timepoints. (**B**) Scatter plot providing a summary of *Apln* expression across the three primary cardiac cell types (CM, EC, and FB), based on bulk RNA sequencing data collected throughout all surgical timepoints. Each cell type is depicted by a trend line, with the shaded area around it representing the confidence interval. The data presented in this figure are based on the surgeries and analyses performed solely by myself.

I could also verify that lentiviral-induced overexpression of the early/late regenerative factor Apelin (Apln) exclusively in HUVECs significantly amplified NRCM proliferation fourfold (rising from 2.2% in the control to 8.2% Ki67-positive NRCM post-Apln overexpression), as illustrated in Figure 10.2.8D – A-B. This endothelial-driven enhancement of NRCM mitotic activity by apelin resulted in a nearly 1.5-fold rise in the total number of NRCM per high-power field (HPF) (183 NRCM/HPF following Apln-OE compared to 127 NRCM/HPF in the control virus), as depicted in Figure 10.2.8D – C. I provided further validation of this effect through Aurora B kinase staining, revealing that endothelial-specific overexpression of Apln in HUVECs increased NRCM cytokinesis by 2.6%, as depicted in Figure 10.2.8D – D-E.

On the contrary, diminishing Apln expression in endothelial cells (HUVECs) resulted in NRCM proliferation rates similar to the control (2.2%) (Figure 10.2.8D – A-B). However, it markedly decreased the total count of NRCM per high-power field (HPF) to one-third with shRNA-Apln (41 NRCM/HPF compared to 127 in PLKO-control), as indicated in Figure 10.2.8D – C. I hypothesized that the notable decrease in total NRCM number could be attributed to the significant reduction in NRCM cytokinesis observed through Aurora B kinase staining (Figure 10.2.8D-E).

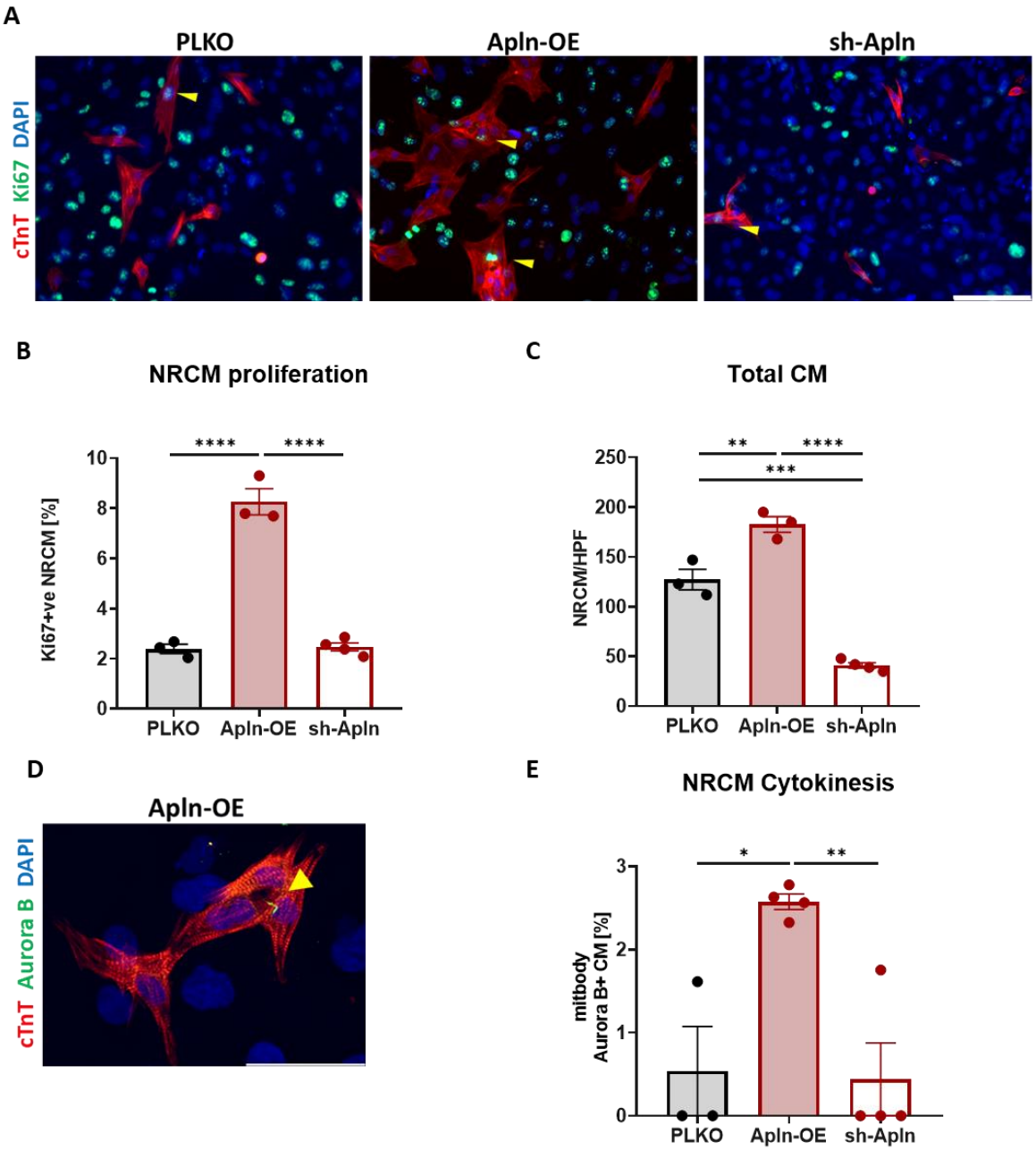

Figure 32 Enhanced proliferation of cardiomyocytes occurs via lentivirus-mediated overexpression of Apln in endothelial cells.

(**A**) Exemplary immunofluorescent images depicting the pan-proliferation marker (Ki67, green) alongside the cardiomyocyte marker cardiac troponin T (cTnT, in red). Neonatal rat cardiomyocytes (NRCM) were isolated and co-cultured on HUVECs transfected with lentivirus, either overexpressing (OE) or downregulating (sh) Apln. PLKO is the control (infected with control lentivirus). Yellow arrow indicates Ki67-positive NRCM. Scale bar: 100µm. (**B**) Measurement of neonatal rat cardiomyocyte (NRCM) proliferation (Ki67-positive NRCM) on lentivirus-transfected HUVECs. (**C**) Quantification of total number of NRCM per high-power field (HPF). (**D**) Representative immunofluorescent image of the cytokinesis marker Aurora B Kinase (green) and the cardiomyocytes' marker cardiac troponin T (cTnT, in red). Yellow arrow pointing at midbody Aurora B kinase between two NRCM co-cultured on lentivirus-transfected HUVECs overexpressing Apln. (**E**) Quantification of neonatal rat cardiomyocyte (NRCM) cytokinesis (NRCM positive for midbody Aurora B kinase) on HUVECs transduced with lentivirus. Data presented as mean ± SEM (n=3-4 per condition). *p<0.05, **p<0.01, ***p<0.001, ****p<0.0001 (one-way ANOVA/Sidak's multiple-comparisons test). The images and graphs in this figure were acquired and analyzed solely by myself.

Consistent with the single-cell RNA sequencing data I previously presented in Figure 10.2.6-A, the increased release of the angiocrine Neurotensin (Nts) was specifically triggered during the late regenerative stage of nTAC in P1 mice (10dp1dTAC), as depicted in Figure 10.2.8E- A. Interestingly, the increase in Apln expression prompted by nTAC primarily stemmed from cardiac endothelial cells (Figure 10.2.8E- B).

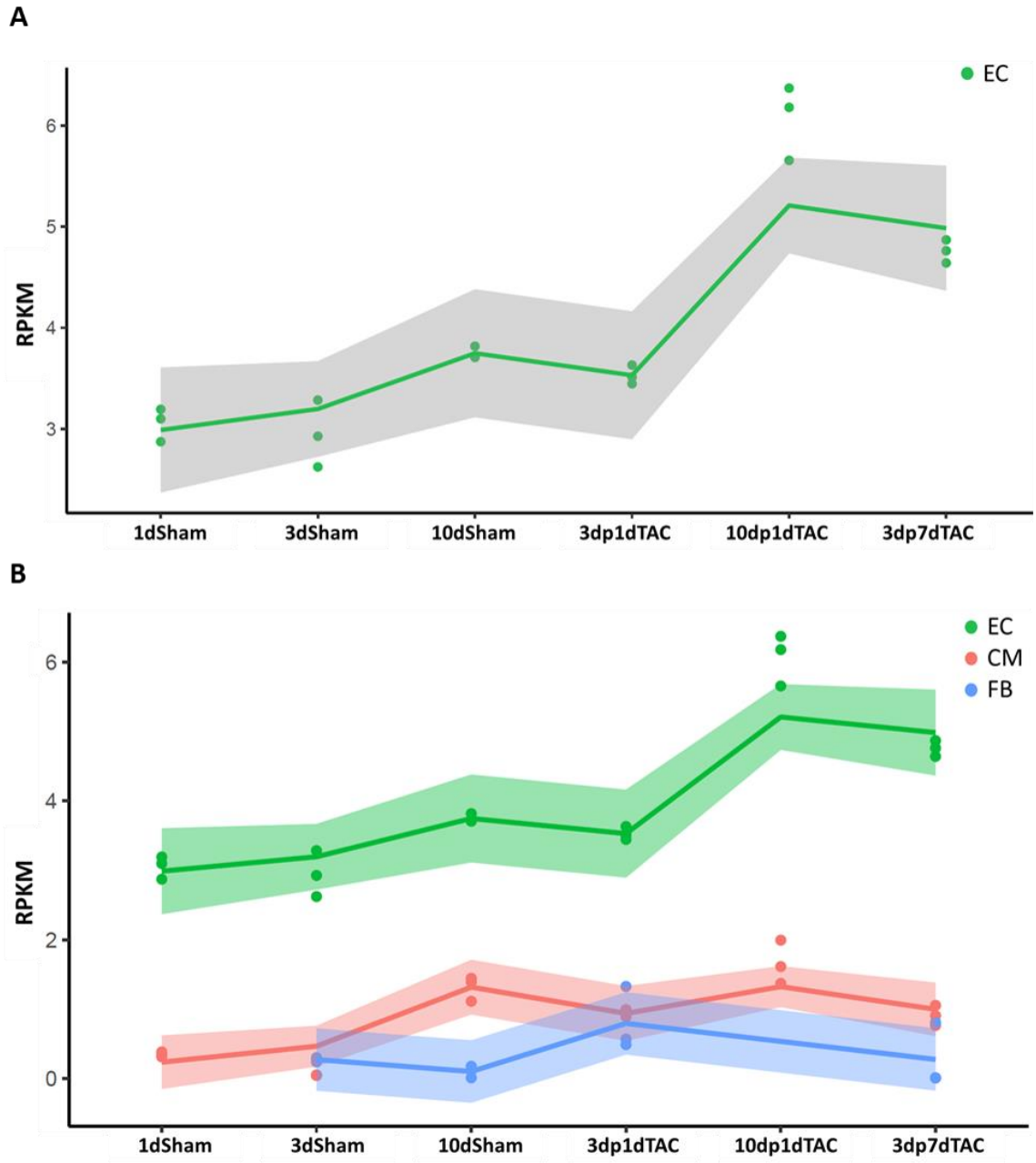

Figure 33 During the late regenerative phase following nTAC, there is a selective upregulation of Neurotensin (Nts) in endothelial cells.

(**A**) Scatter plot illustrating the expression pattern of *Nts* in cardiac endothelial cells (EC) derived from bulk RNA sequencing data spanning all surgical timepoints. (**B**) Scatter plot summarizing the expression levels of *Nts* across the three primary cardiac cell types (CM, EC, and FB), derived from bulk RNA sequencing data collected at all surgical timepoints. The line indicates the expression trend for each cell type, with the shaded area surrounding it representing the confidence interval. The data presented in this figure are based on the surgeries and analyses performed solely by myself.

By the same approach, I modulated the genetic expression of the angiocrine Neurotensin (Nts) using lentivirus in HUVECs. Specifically, endothelial cell-specific overexpression of Neurotensin almost doubled NRCM proliferation in the direct co-culture system (increasing from 2.2% in PLKO-control to 4% after Nts overexpression). This enhancement was accompanied by an approximate 1.5-fold increase in the number of NRCMs per high-power field (HPF) (183 after Nts-OE compared to 127 NRCM/HPF in control), as depicted in Figure 10.2.8F – A-C. Aurora B kinase staining provided additional validation, indicating that the HUVECs-specific overexpression of Nts was associated with a trend towards increased NRCM cytokinesis to 2% (Figure 10.2.8F – D-E).

Conversely, the downregulation of Nts through shRNA-lentivirus in HUVECs resulted in a notable one-third reduction in NRCM proliferation (Figure 10.2.8F – A-B), which subsequently led to decreased NRCM cytokinesis and a lower total count of NRCM per high-power field (98 in sh-Nts compared to 127 in control), as shown in Figure 10.2.8F – C-E.

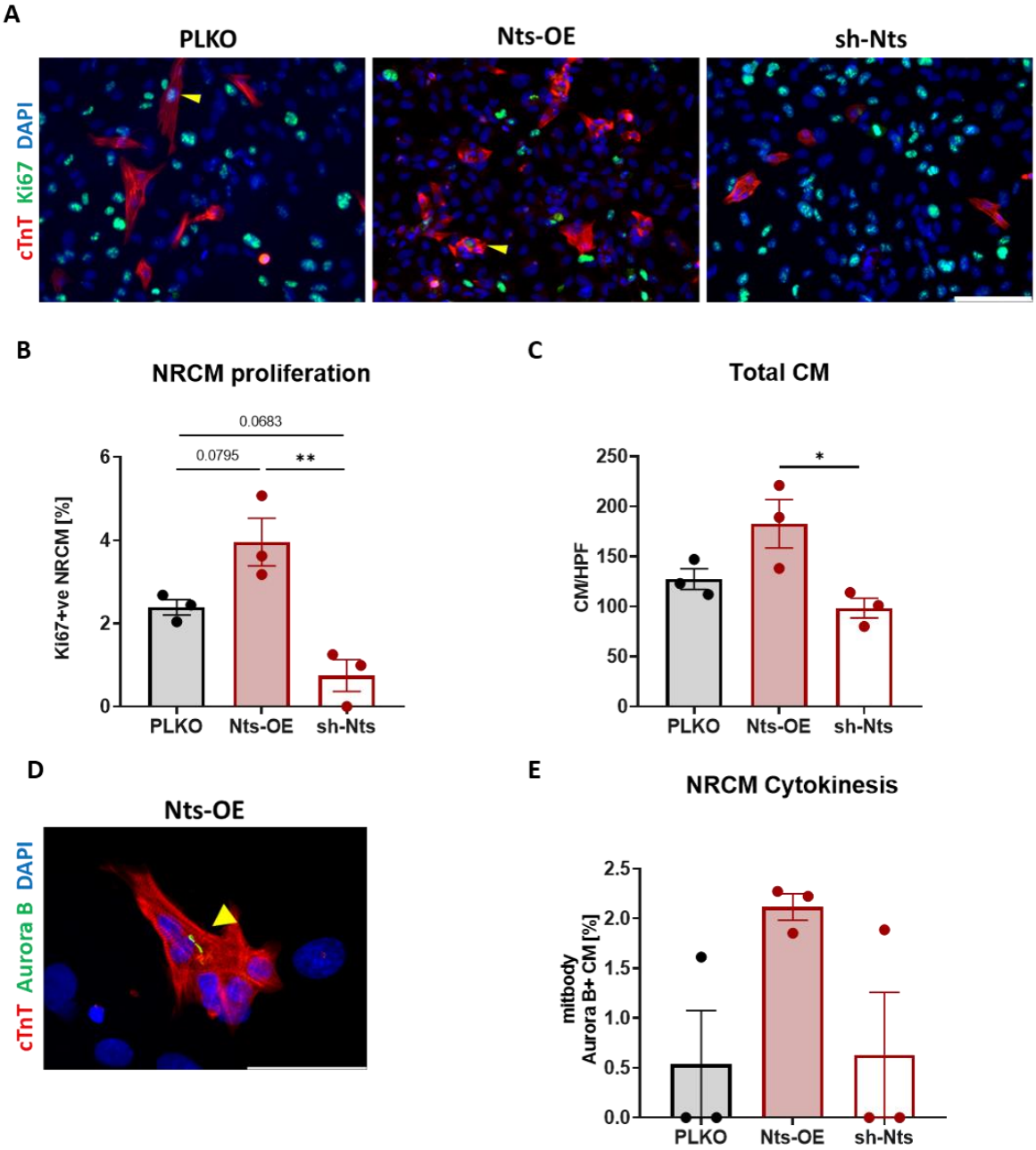

Figure 34 Increased proliferation of cardiomyocytes is facilitated through the lentivirus-mediated overexpression of Nts in endothelial cells.

(**A**) Illustrative immunofluorescent images portraying the pan-proliferation marker (Ki67, green) alongside the cardiomyocyte marker cardiac troponin T (cTnT, in red). Neonatal rat cardiomyocytes (NRCM) were isolated and co-cultured on HUVECs transfected with lentivirus, which either overexpressed (OE) or downregulating (sh) Nts. PLKO is the control (infected with control lentivirus). Yellow arrow indicates Ki67-positive NRCM. Scale bar: 100µm. (**B**) Quantitative evaluation of neonatal rat cardiomyocyte (NRCM) proliferation (Ki67-positive NRCM) on lentivirus-transfected HUVECs. (**C**) Quantification of the total number of NRCM per high-power field (HPF). (**D**) Representative immunofluorescent image displaying the cytokinesis marker Aurora B Kinase (green) and the cardiomyocytes' marker cardiac troponin T (cTnT, in red). A yellow arrow points at midbody Aurora B kinase between two NRCM co-cultured on lentivirus-transfected HUVECs overexpressing *Nts*. (**E**) Quantitative assessment of neonatal rat cardiomyocyte (NRCM) cytokinesis (NRCM positive for midbody Aurora B kinase) on HUVECs transduced with lentivirus. Data presented as mean ± SEM (n=3-4 per condition). *p<0.05, **p<0.01 (one-way ANOVA/Sidak's multiple-comparisons test). The images and graphs in this figure were acquired and analyzed solely by myself.

On the other hand, bulk RNA sequencing data I collected across all surgical timepoints of nTAC revealed a notable increase in endothelial-specific expression of C-C Motif Chemokine Ligand 21 (Ccl21) only after I performed nTAC during the non-regenerative age (3dp7dTAC), as depicted in Figure 10.2.8G- A, despite the expression of this ligand not being limited to endothelial cells (Figure 10.2.8G- B).

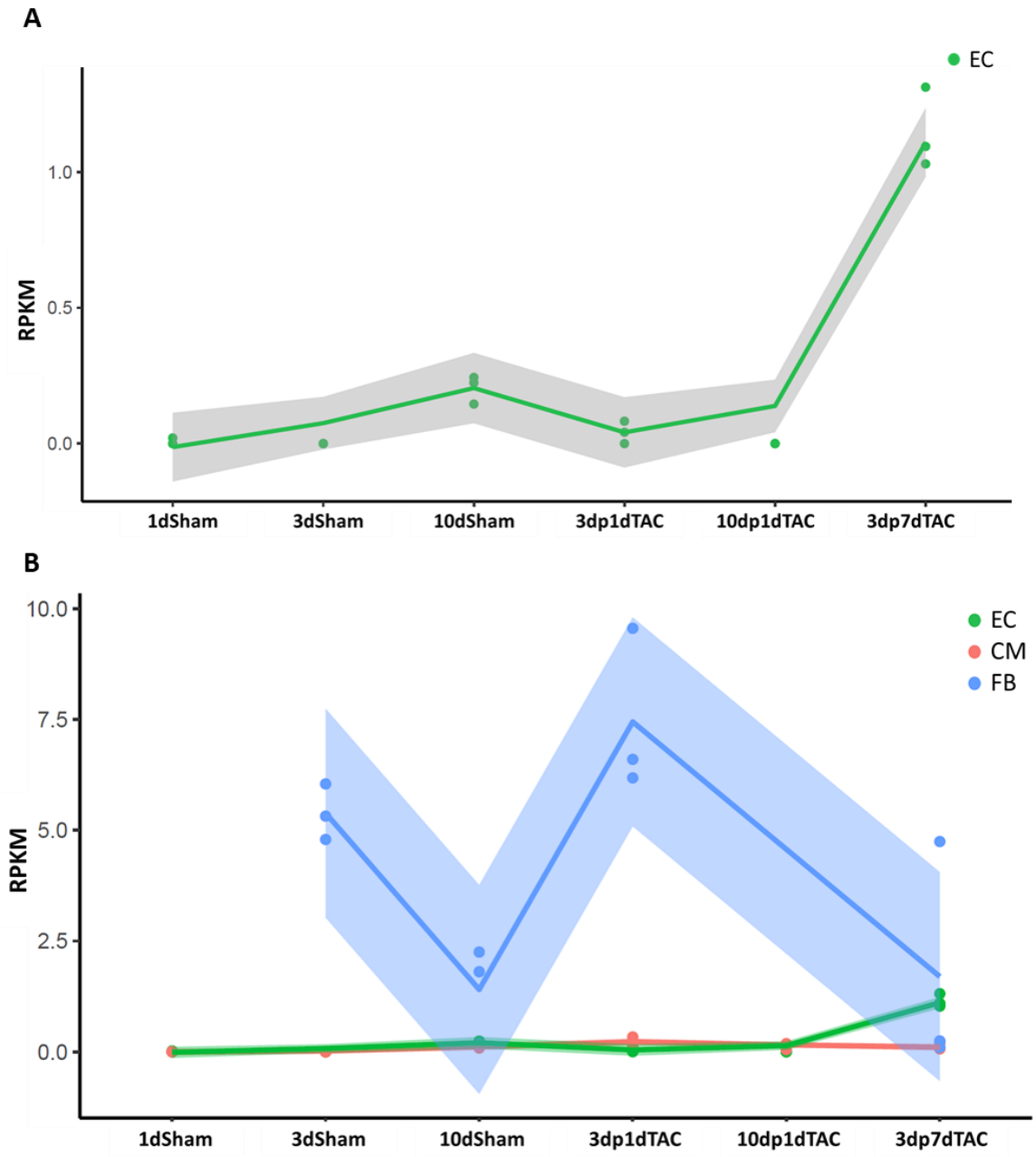

Figure 35 During the non-regenerative age, nTAC prompts selective induction of the inflammatory ligand Ccl21 specifically in endothelial cells.

(**A**) Scatter plot showcasing the expression profile of *Ccl21* in cardiac endothelial cells (EC) obtained from bulk RNA sequencing data encompassing all surgical timepoints. (**B**) Scatter plot providing a summary of the expression levels of *Ccl21* across the three primary cardiac cell types (CM, EC, and FB), derived from bulk RNA sequencing data collected at all surgical timepoints. Each cell type is represented by a trend line, and the shaded area surrounding it represents the confidence interval. The data presented in this figure are based on the surgeries and analyses performed solely by myself.

In contrast to the aforementioned pro-regenerative angiocrine factors, when I targeted the overexpression of Ccl21 specifically in HUVECs, it nearly halted NRCM proliferative activity and markedly reduced the number of NRCM detected per high-power field (HPF) (Figure 10.2.8H – A-C).

However, endothelial cell-specific genetic downregulation of Ccl21 using shRNA lentivirus restored and doubled NRCM mitosis (up to 4%) (Figure 10.2.8H – A-B), as well as increased the total number of NRCM (227 NRCM/HPF compared to 127 in PLKO-control), as depicted in Figure 10.2.8H – C.

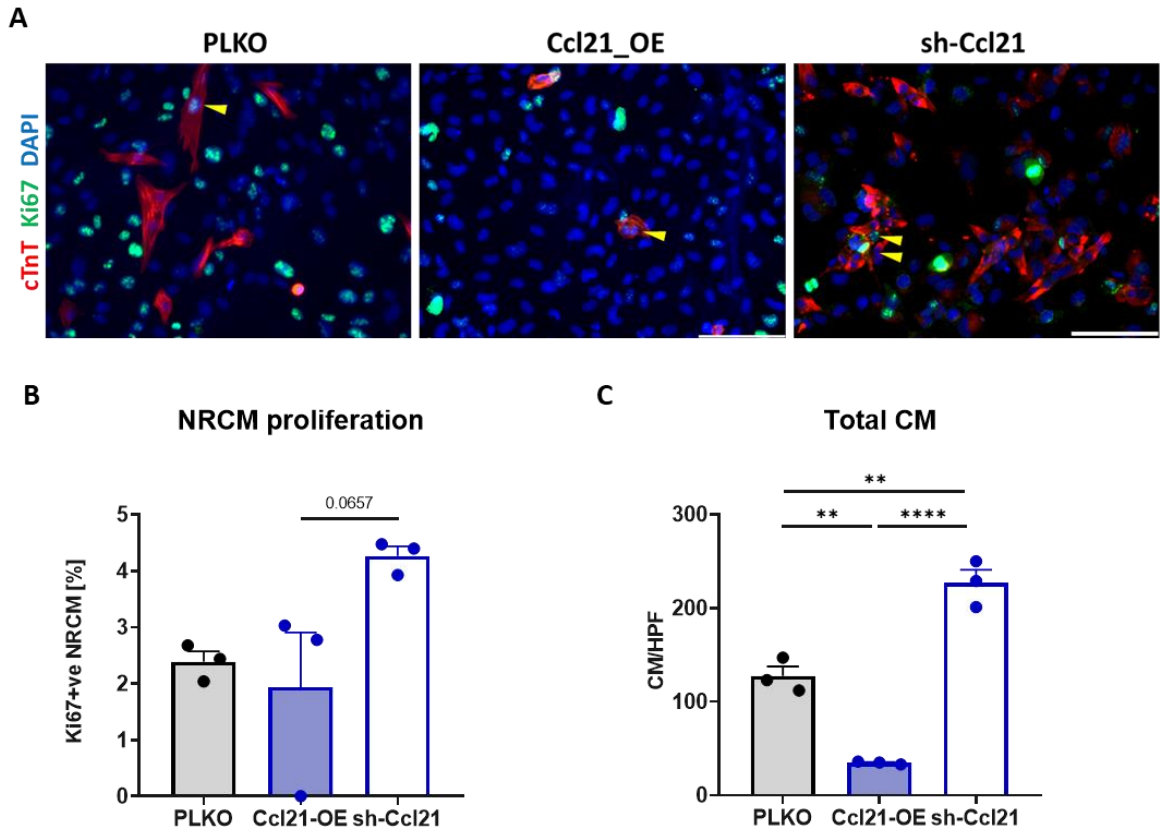

Figure 36 Endothelial-specific overexpression of the inflammatory cytokine Ccl21 induced by lentivirus reduces NRCM proliferation.

(**A**) Exemplary immunofluorescent images displaying the pan-proliferation marker (Ki67, green) alongside the cardiomyocyte marker cardiac troponin T (cTnT, in red). Neonatal rat cardiomyocytes (NRCM) were co-cultured on HUVECs transfected with lentivirus, either overexpressing (OE) or downregulating (sh) Ccl21. PLKO is the control (infected with control lentivirus). Yellow arrow indicates Ki67-positive NRCM. Scale bar: 100µm. (**B**) Measurement of neonatal rat cardiomyocyte (NRCM) proliferation (Ki67-positive NRCM) on lentivirus-transfected HUVECs. (**C**) Quantification of the total number of NRCM per high-power field (HPF). Data presented as mean ± SEM (n=3-4 per condition). **p<0.01, ****p<0.0001 (one-way ANOVA/Sidak's multiple-comparisons test). The images and graphs in this figure were acquired and analyzed solely by myself.

10.2.9. Endothelial cell-derived Ccl21 induces cardiomyocytes' arrhythmia

Given the necessity of assessing the impact of endothelial-secreted angiocrines on cardiomyocyte functionality, I evaluated the beating rate and contraction amplitude of neonatal rat cardiomyocytes (NRCM) directly co-cultured on a monolayer of HUVECs pre-transfected with lentivirus particles (either overexpressing or downregulating the gene of interest) in vitro. Following a 48-hour co-culture period, I observed the spontaneous beating of NRCM and recorded it for 30-60 seconds using a light microscope. Subsequently, using the ImageJ macro MYOCYTER, I quantified the contraction rhythm and amplitude, serving as functional indicators of cardiomyocyte health and viability.

Notably, I could observe that lentivirus-mediated endothelial-specific overexpression of the inflammatory cytokine Ccl21 was characterized by a pronounced arrhythmic phenotype in directly co-cultured NRCM, as depicted in Figure 10.2.9-A. Consequently, there was a marked reduction in the beating rate of NRCM (Figure 10.2.9-B), with the arrhythmia evidenced by the observed strong alterations in the contraction amplitude (Figure 10.2.9-C).

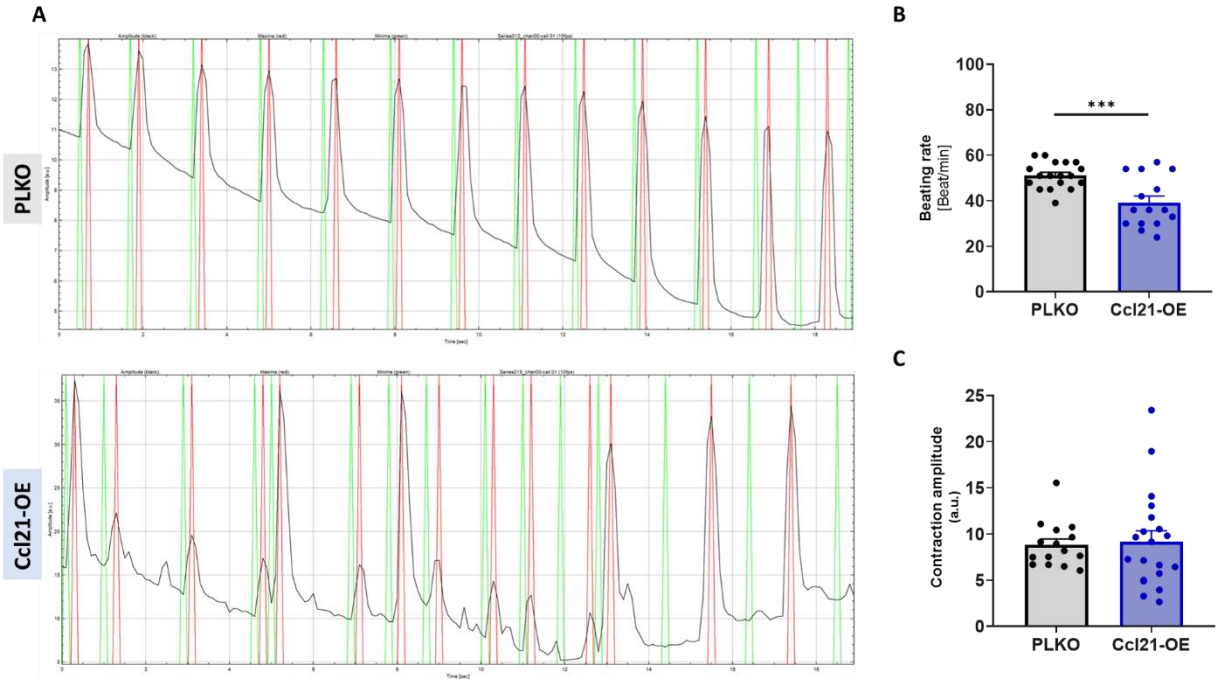

Figure 37 Lentivirus-mediated endothelial-specific overexpression of the inflammatory cytokine Ccl21 leads to arrhythmia in NRCM.

(**A**) Graph depicting the amplitude and velocity of contraction in spontaneously beating neonatal rat cardiomyocytes (NRCM), derived from video sequences and analyzed using MYOCYTER. P1-P3 rat CMs were co-cultured with HUVECs overexpressing Ccl21 for a duration of 2 days. (**B**) The cardiac beating rate and contraction amplitude (**C**) of NRCM co-cultured with HUVECs overexpressing Ccl21. The beating rate and amplitude was determined from video sequences using MYOCYTER. Data presented as mean ± SEM. ***p<0.001 (two-tailed unpaired t-test). The data and graphs in this figure were acquired and analyzed solely by myself.

10.2.10. Endothelial Bmp7, Apln, and Nts promote angiogenesis, while Ccl21 exhibits antiangiogenic properties

To evaluate the angiogenic properties of candidate ligands I identified from bulk and single-cell RNA sequencing, I investigated the formation of tubular structures by vascular endothelial cells in vitro. Following lentiviral transduction, I cultured HUVECs with either overexpression or suppression of the candidate ligands on Matrigel-coated wells. I monitored the tube formation over time, and after 24 hours, I quantified the number of closed (intact) loops and the length of the tubes.

Notably, I could detect that HUVECs overexpressing the early-phase regenerative angiocrine *Bmp7* exhibited significantly longer (Figure 10.2.10A-C) and more closed loops with intact lumens (58%) compared to HUVECs transduced with the control backbone vector PLKO (25.6%), as depicted in Figure 10.2.10A- A-B. Conversely, downregulation of *Bmp7* in HUVECs using shRNA lentivirus markedly diminished the formation of closed loops to 8.7% in these cells, resulting in shorter default lengths (Figure 10.2.10A- A-C).

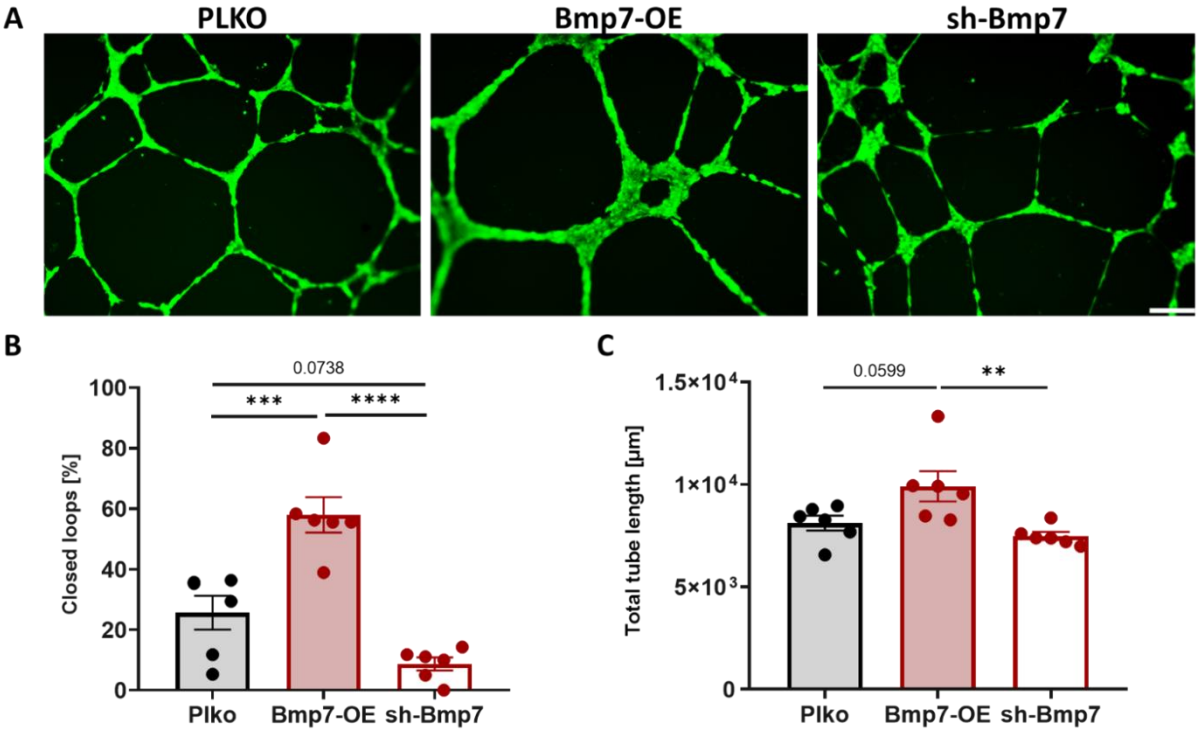

Figure 38 Endothelial-specific overexpression of the early regenerative cytokine Bmp7 enhances angiogenesic activity of endothelial cells.

(**A**) Exemplary immunofluorescent images demonstrating the impact of Bmp7 overexpression and downregulation in endothelial cells using lentivirus on tubule formation. Lentiviral-transfected HUVECs were cultured on a Matrigel matrix for 24 hours, with BCECF added, and tubule formation was then assessed by fluorescent microscopy. Scale bar: 200µm. (**B and C**) Quantifications represent the number of complete loops (**B**) and total tubule length (**C**) per visible field. Data presented as mean ± SEM (n=6 per condition). **p<0.01, ***p<0.001, ****p<0.0001 (one-way ANOVA/Sidak's multiple-comparisons test). The images and graphs in this figure were acquired and analyzed solely by myself.

Likewise, after lentiviral overexpression of the late regenerative factor Apln in HUVECs, the number of closed loops more than doubled (58% after Apln-OE compared to 25.6% in control), as illustrated in Figure 10.2.10B- A and C. However, there was no significant change detected in the length of the formed tubes (Figure 10.2.10B- D). Conversely, I could see that shRNA-induced downregulation of Apln in HUVECs resulted in the formation of more porous loops with incomplete lumens (Figure 10.2.10B- A and C), without affecting the length of the tubes (Figure 10.2.10B- D).

Similarly, overexpression of Nts in HUVECs increased the percentage of closed-loop formation to 51.6% compared to control (25.6%), as depicted in Figure 10.2.10B- B and E, with no impact on the overall length of the tubes (Figure 10.2.10B- F). In contrast, HUVECs with suppressed Nts expression due to shRNA lentiviral transfection were unable to form loops and were characterized by the emergence of only small and short tubes, as shown in Figure 10.2.10B- B and F.

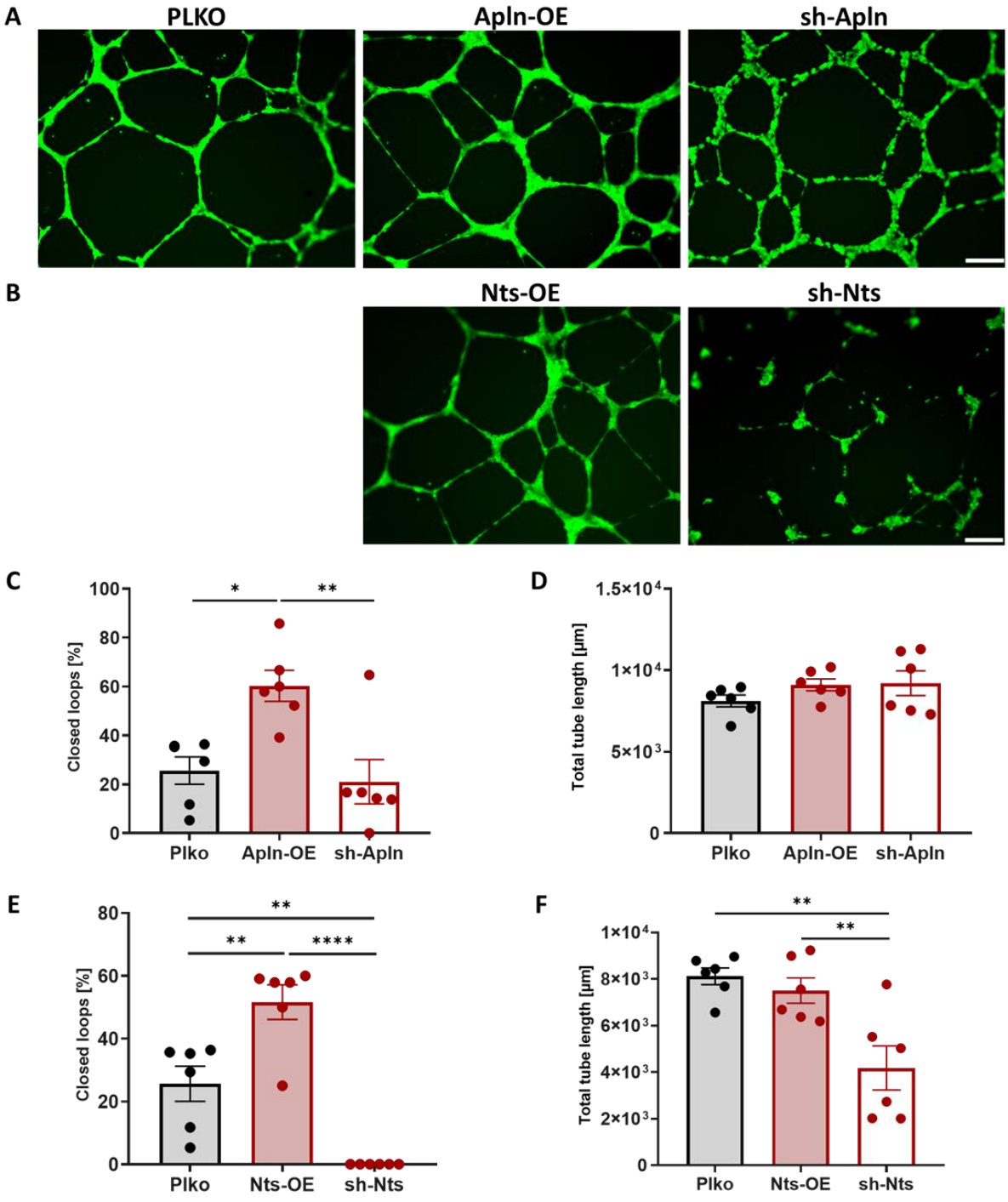

Figure 39 Endothelial-specific overexpression of the late regenerative cytokines Apln and Nts promotes tubule formation as readout for angiogenic activity in vitro.

(**A and B**) Exemplary immunofluorescent images illustrate the impact of *Apln* (**A**) and *Nts* (**B**) overexpression and downregulation in endothelial cells via lentivirus on tubule formation. Lentiviral-transfected HUVECs were cultured on a Matrigel matrix for 24 hours, with BCECF added, and tubule formation was subsequently assessed using fluorescent microscopy. Scale bar: 200µm. (**C-F**) Quantifications indicating the number of complete loops (**C and E**) and total tubule length (**D and F**) per visible field. Data presented as mean ± SEM (n=6 per condition). *p<0.05, **p<0.01, ****p<0.0001 (one-way ANOVA/Sidak's multiple-comparisons test). The images and graphs in this figure were acquired and analyzed solely by myself.

Just as I observed with Nts downregulation, the overexpression of the non-regenerative ligand *Ccl21* in HUVECs markedly decreased both the length and the number of closed loops in vitro. However, lentiviral-mediated downregulation of *Ccl21* did not reverse this phenotype, as shown in Figure 10.2.10-C.

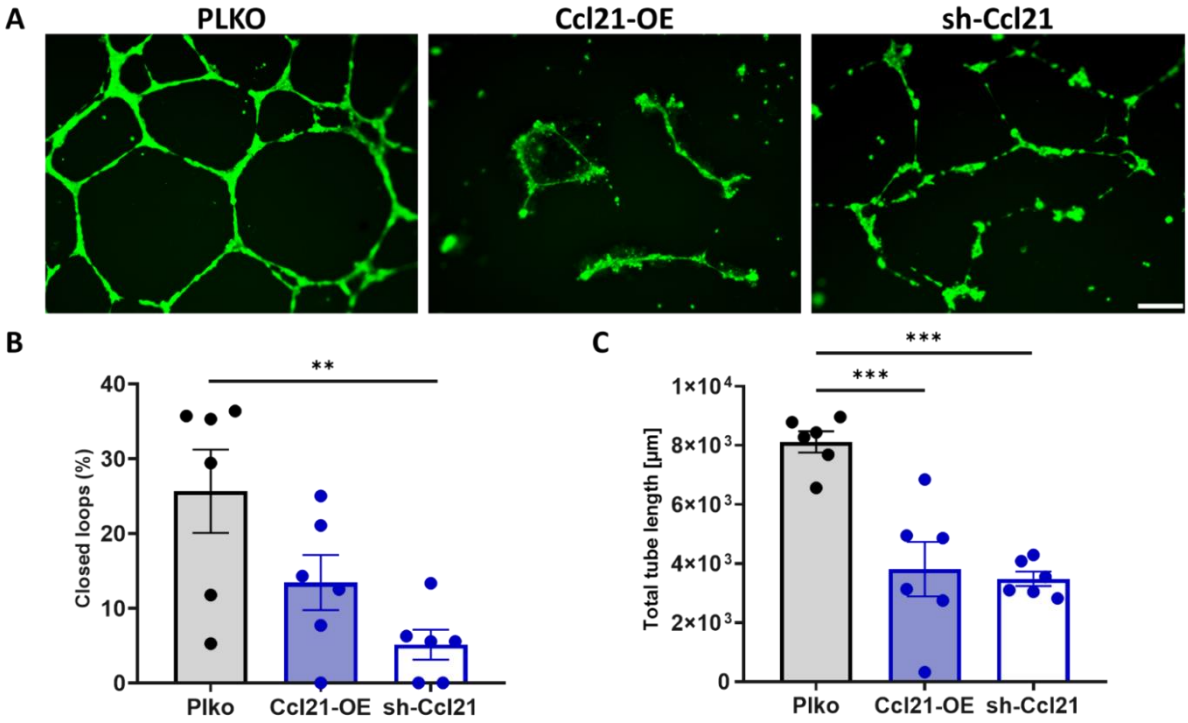

Figure 40 Endothelial-specific overexpression of the inflammatory cytokine Ccl21 via lentivirus disrupts the ability to form tubes.

(**A**) Illustrative immunofluorescent images depicting the influence of lentivirus-mediated Ccl21 overexpression and downregulation in endothelial cells on tubule formation. HUVECs transfected with lentivirus were cultured on a Matrigel matrix for 24 hours, with BCECF added, followed by the assessment of tubule formation using fluorescent microscopy. Scale bar: 200µm. (**B and C**) Quantifications indicate the count of complete loops (**B**) and the total length of tubules (**C**) per visible field. Data presented as mean ± SEM (n=6 per condition). **p<0.01, ***p<0.001 (one-way ANOVA/Sidak's multiple-comparisons test). The images and graphs in this figure were acquired and analyzed solely by myself.

10.3. Section 3: *Harnessing Cardiac Organoids to Test the Regenerative Effects of Identified Angiocrine Factors*

Cardiac organoids have emerged as an invaluable tool in cardiovascular research due to their ability to closely mimic the structure and function of the mammalian heart. These three-dimensional, multicellular constructs provide a more physiologically relevant model compared to traditional 2D cultures. [75] By incorporating various cardiac cell types, organoids facilitate the investigation of complex interactions within the heart. This relevance is crucial for accurately studying heart development, disease mechanisms, and potential treatments. Additionally, these 3D-organoids serve as a platform for testing the regenerative effects of various factors, such as growth factors and angiocrines, which are crucial for developing novel therapies for heart repair and regeneration.[75]

Therefore, my primary objective of the third part of my thesis was to utilize cardiac organoids as a versatile and powerful tool to investigate the impact of the previously identified angiocrine factors on heart regeneration.

10.3.1. Establishment of a three-dimensional, multicellular cardiac organoid model

To recapitulate the intercellular cross-talk between the three primary cardiac cell types— cardiomyocytes (CM), endothelial cells (EC), and fibroblasts (FB)— the three-dimensional triculture method developed by Wagner et al., 2019 was employed. [70]

To accomplish this, I cultured ventricular CM and FB isolated from P1-P3 wildtype neonatal rat hearts in hanging drops to promote the formation of spheroids. Following a 5-day incubation period, I collected the cardiac spheroids and subsequently seeded human umbilical vein endothelial cells (HUVECs) transduced with lentivirus, either overexpressing or downregulating the candidate genes, onto them. I cultured the cardiospheres with 200 µM phenylephrine (PE) for a duration of 10 days.

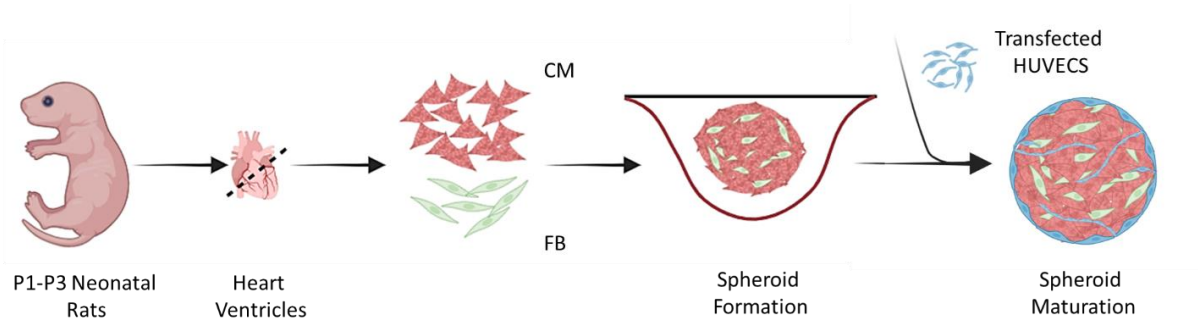

Figure 41 Establishment of a three-dimensional vascularized cardiac organoid.

Schematic presentation of cardiosphere formation. Cardiomyocytes (CM) and fibroblasts (FB) were extracted from neonatal rat hearts and cultivated in hanging drops to permit spheroid formation. After incubating for 5 days, the cardiac spheroids were harvested, and human umbilical vein endothelial cells (HUVECs) transduced with lentivirus, either overexpressing or downregulating the candidate genes, were then seeded onto the cardiac spheroids. Cardiospheres were cultured for additional 10 days and subsequently collected for further analysis. *Illustration created by using www.biorender.com.*

10.3.2. Lentiviral-induced overexpression of *Bmp7*, *Apln* and *Nts* in endothelial cells boosts angiogenesis and vasculature formation in 3D-cardiac organoids

As an essential step in the formation of 3D-cardiac organoids, I added endothelial cells and then allowed the organoids to mature for 10 days. Thus, this model could be utilized to evaluate the impact of lentivirus-mediated modulation of candidate gene expression on the ability of endothelial cells to form functional tubules, a critical function of endothelial cells. Hence, to evaluate the impact of various genetic modifications using lentivirus on the EC phenotype, I performed immunofluorescent staining with the endothelial cell marker VE-cadherin. I measured the extent of vascular network coverage as the overall area covered by ECs within each cardiosphere.

Similar to my findings observed in the 2D-tubule formation test, the upregulation of the potential early adaptive factor *Bmp7* in HUVECs resulted in increased formation of capillaries within 3D-cardiospheres. This was characterized by a doubling in vascular network coverage, extending to 4% of the total area of the cardiosphere (Figure 10.3.2A - A-B). Further I could observe that the overexpression of *Bmp7* encourages the initiation of the vascular bed, along with elongation of tubules and their infiltration between cardiomyocytes, as depicted in Figure 10.2.2B-A. However, HUVECs with downregulation of *Bmp7* did not successfully form

functional tubules (Figure 10.2.2B-A), which was associated with a reduction in vascular coverage of the cardiosphere, as illustrated in Figure 10.3.2A - A-B.

Likewise, lentiviral overexpression of the regenerative factor *Apln* in HUVECs significantly enhanced the capillaries coverage in 3D-cardiac, leading to a substantial rise in the total area covered by EC within each cardiosphere, as illustrated in Figure 10.3.2A – C-D. Interestingly, the newly formed tubules were arranged in a vascular mesh-like structure that originated at the periphery of the organoid and extended into longer tubules penetrating between cardiomyocytes, as depicted in Figure 10.2.2B-B. However, this ability was entirely lost with shRNA-induced downregulation of *Apln*, leading to the accumulation and compaction of fenestrated HUVECs on one side of the cardiosphere. Consequently, they were unable to extend and form proper functional tubules, as evident in Figure 10.3.2A – C-D and Figure 10.2.2B-B.

Comparable to *Apln*, overexpression of the late angiocrine factor *Nts* in HUVECs via lentivirus significantly increased vascular network formation and coverage in cardiac organoids, as shown in Figure 10.3.2A – E-F. Surprisingly, EC-specific overexpression of *Nts* enhanced the phenotype of the formed vessels, leading to the development of long, intact vessel-like structures within the cardiospheres. I could notice that these structures extended from the capillaries at the periphery to form large vessels penetrating between the cardiomyocytes, as shown in Figure 10.2.2B-C. On the other hand, HUVECs with downregulated *Nts* lost their endothelial phenotype and were unable to initiate vessel formation (Figure 10.3.2A – E-F and Figure 10.2.2B-C).

Impressively, simultaneous overexpression of all three angiocrine factors (referred to as Mix-OE, comprising *Bmp7*, *Apln*, and *Nts*) in HUVECs increased the total area covered by endothelial cells per cardiosphere by 3.6-fold, as illustrated in Figure 10.3.2A – G-H. Indeed, the newly formed vasculature was characterized by thick, large vessels that extended through the center of the cardiosphere and reached the periphery between the cardiomyocytes, as shown in Figure 10.2.2B-D.

In summary, my findings show a potential autocrine role of the angiocrine factors *Bmp7*, *Apln*, and *Nts* in endothelial cell function, enhancing the formation of new vasculature and the elongation of tubules.

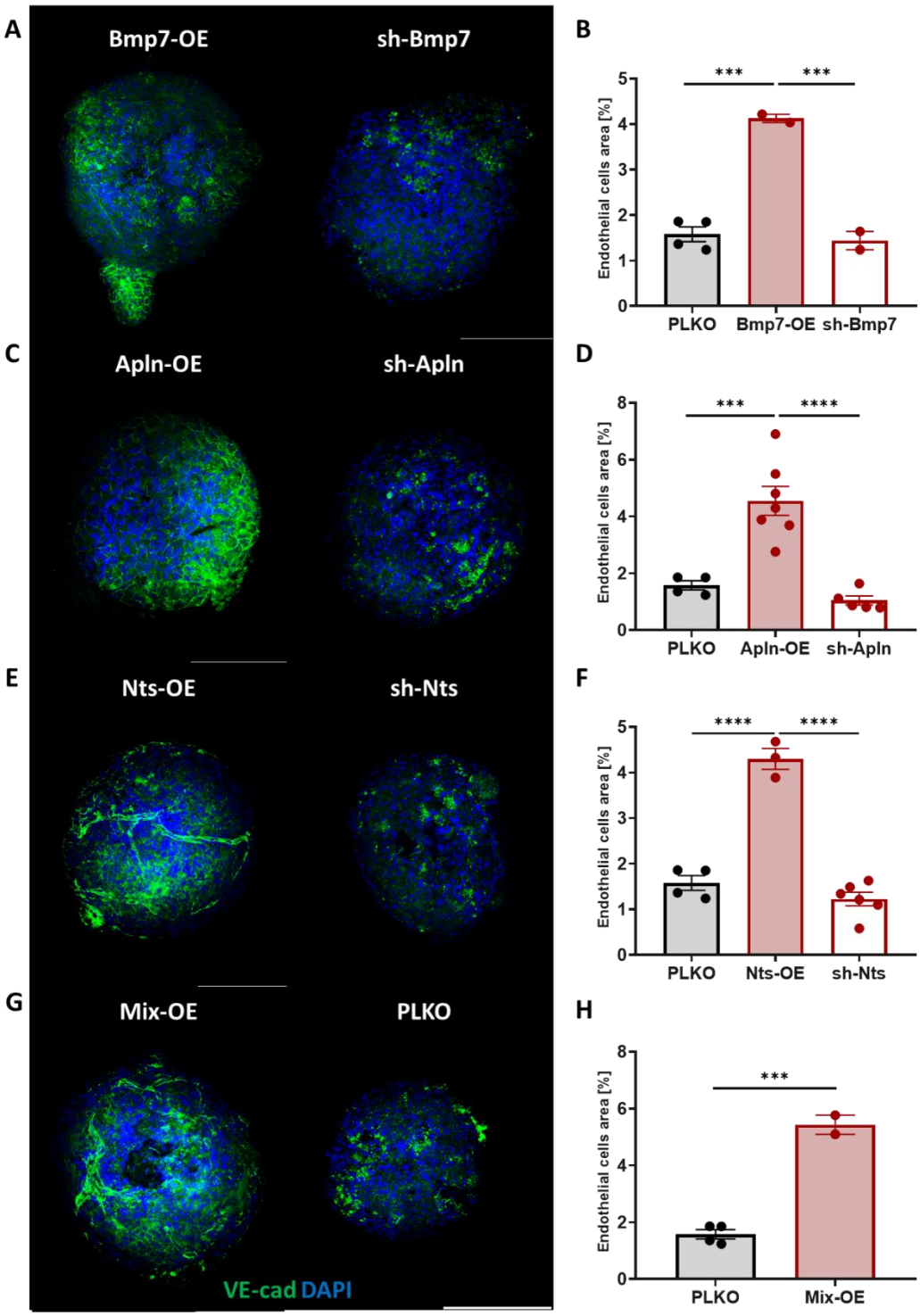

Figure 42 In 3D-cardiac organoids, the endothelial-specific overexpression of Bmp7, Apln, and Nts enhances tubule formation and vascular network coverage.

(**A-G**) Immunofluorescent images illustrating the effects of lentivirus-mediated overexpression and downregulation of Bmp7 (**A**), Apln (**C**), Nts (**E**), and Mix (**G**) in endothelial cells on vascular network coverage in 3D-cardiospheres. Lentivirus-transfected HUVECs were seeded onto a combination of CM and FB and incubated for a period of 10 days. After harvesting, the cardiospheres were stained with the EC marker VE-cadherin (VE-cad, in green) and the nuclear stain DAPI. Mix-OE involves the simultaneous overexpression of all three candidate genes (Bmp7, Apln, and Nts) in HUVECs. Scale bar: 200µm. (**B-H**) Quantification of the overall area covered by ECs within each cardiosphere. Data presented as mean ± SEM (n=2-7 per condition). ***p<0.001, ****p<0.0001 (one-way ANOVA/Sidak's multiple-comparisons test and two-tailed unpaired t-test). The images and graphs in this figure were acquired and analyzed solely by myself.

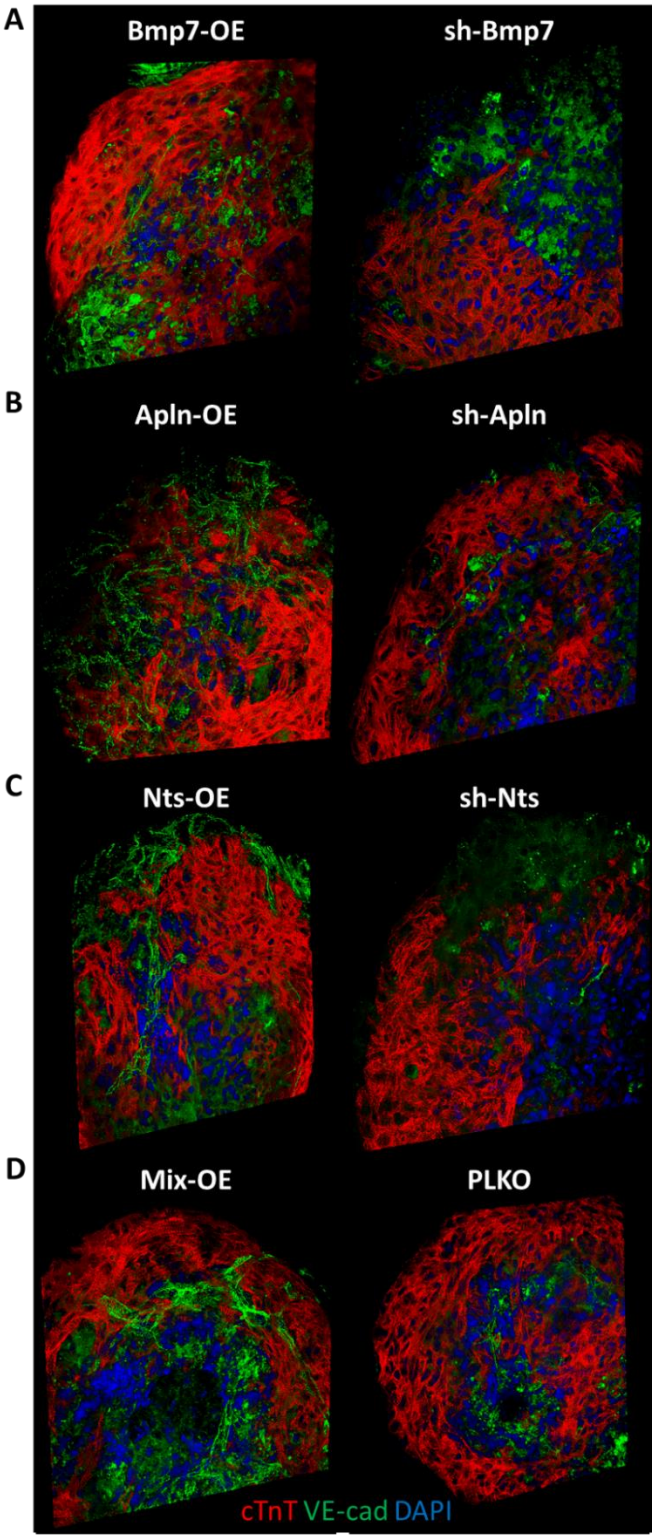

Figure 43 Enhanced vasculature formation in 3D-cardiac organoids observed following the overexpression of Bmp7, Apln, and Nts in endothelial cells.

(**A-D**) Illustrative immunofluorescent images depicting the influence of lentivirus-mediated *Bmp7* (**A**), *Apln* (**B**), *Nts* (**C**) and Mix (**D**) overexpression and downregulation in endothelial cells on vasculature formation in 3D-cardiospheres. Lentivirus-transfected HUVECs were seeded onto a mixture of CM and FB and incubated for a 10 days period. Following harvesting, cardiospheres were stained with the CM marker cardiac troponin T (cTnT, in red) and the EC marker VE-cadherin (VE-cad, in green) along with the nuclear stain DAPI. Formed vascular tubes could be visualized infiltrating through CM. The images and graphs in this figure were acquired and analyzed solely by myself.

10.3.3. Endothelial cell-derived Bmp7, Apln, and Nts enhance the contractility of cardiac organoids, whereas Ccl21 induces an arrhythmogenic phenotype.

As with the previously discussed 2D co-culture system, I evaluated the spontaneous contraction for each 3D-cardiac organoid 10 days after the addition of lentiviral-transfected HUVECs, which were either overexpressing or downregulating the angiocrine factors of interest. For this purpose, I singularized cardiospheres in a round-bottom 96-well plate, and recorded videos of their spontaneous beating for 60 seconds. Subsequently, I quantified the contraction rhythm and amplitude, serving as functional indicators of the cardiospheres' health and performance, using the ImageJ macro MYOCYTER.

Notably, individual overexpression of *Bmp7, Apln* and *Nts* exclusively in HUVECs resulted in a substantial increase in the beating rate of cardiospheres by 2 to 3 folds (Figure 10.3.3A – A-F). Moreover, EC-specific overexpression of these factors individually not only augmented the beating rate, but also significantly boosted the contraction force of cardiac organoids, as evidenced by the quantification of the contraction amplitude I show in Figure 10.3.3A – G-I. Nevertheless, downregulation of these angiocrines in HUVECs using shRNA not only reduced the number of beats and contraction amplitude, but also was associated with an arrhythmic phenotype in 3D-cardiospheres (Figure 10.3.3A).

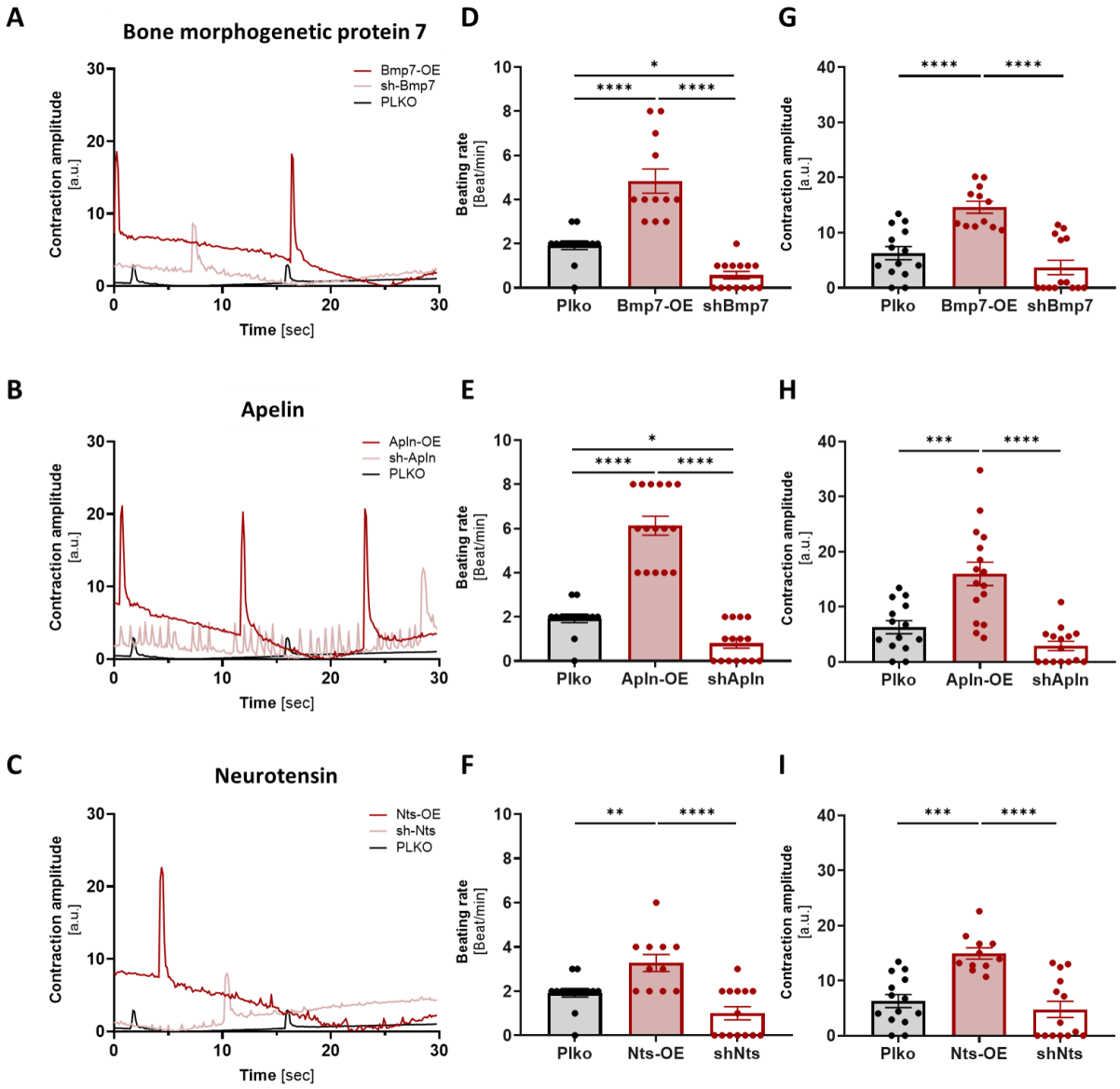

Figure 44 Lentiviral-induced overexpression of Bmp7, Apln and Nts individually in HUVECs enhances 3D-cardiac organoids contractility.

(**A-C**) Plot depicting the amplitude and velocity of contraction in spontaneously beating 3D-cardiac organoids, derived from video sequences and analyzed using MYOCYTER. The graph shows the influence of lentivirus-mediated *Bmp7* (**A**), *Apln* (**B**) and *Nts* (**C**)) overexpression (dark red) and downregulation (faint red) in endothelial cells on 3D-cardiospheres contraction, compared to PLKO control (in black). Lentivirus-transfected HUVECs were transferred to a mixture of CM and FB and incubated for a 10 days period. (**D-F**) Quantitative measurements of the cardiac beating rate and contraction amplitude (**G-I**) of cardiac organoids. The beating rate and amplitude were determined from video sequences using MYOCYTER. Data presented as mean ± SEM (n=11-16 per condition). *p<0.05, **p<0.01, ***p<0.001, ****p<0.0001 (one-way ANOVA/Sidak's multiple-comparisons test). The graphs in this figure were acquired and analyzed solely by myself.

Interestingly, simultaneous overexpression of all three regenerative factors (*Bmp7*, *Apln*, and *Nts*, collectively referred to as Mix-OE) in HUVECs significantly increased the contraction amplitude of 3D-cardiospheres more than the overexpression of each angiocrine individually, as shown in Figure 10.3.3B.

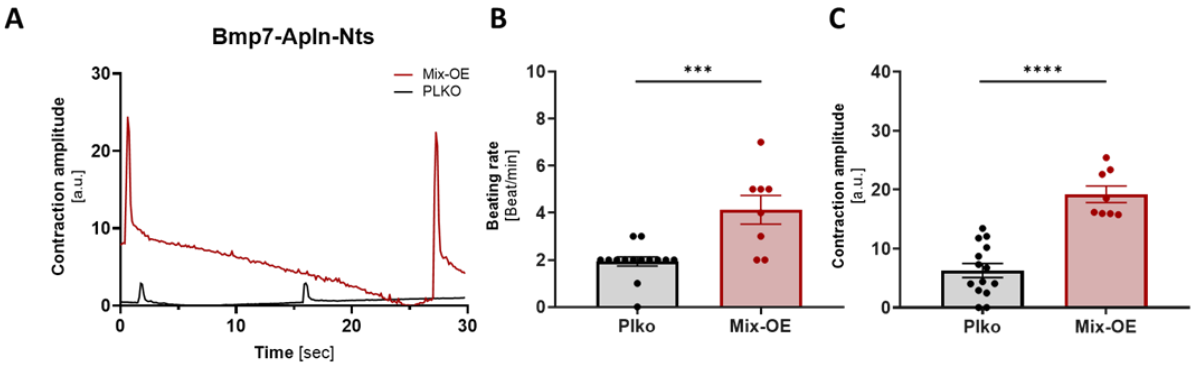

Figure 45 Combined overexpression of Bmp7, Apln and Nts in HUVECs using lentivirus promotes 3D-cardiac organoids contraction force.

(**A**) Graph depicting the amplitude and velocity of contraction in spontaneously beating 3D-cardiac organoids, derived from video sequences and analyzed using MYOCYTER. The plot shows the influence of lentivirus-mediated combined overexpression of *Bmp7*, *Apln* and *Nts* (in dark red) in endothelial cells on 3D-cardiospheres contraction, compared to PLKO control (in black). Lentivirus-transfected HUVECs were transferred to a mixture of CM and FB and incubated for a 10 days period. (**B**) Quantitative measurements of the cardiac beating rate and contraction amplitude (**C**) of cardipspheres. The beating rate and amplitude were determined from video sequences using MYOCYTER. Data presented as mean ± SEM (n=8-14 per condition). ***p<0.001, ****p<0.0001 (two-tailed unpaired t-test). The graphs in this figure were recorded and analyzed solely by myself.

Conversely, similar to my observations in the 2D co-culture model, overexpression of the inflammatory angiocrine *Ccl21* in HUVECs induced remarkable arrhythmia in 3D-cardiospheres. However, this arrhythmic phenotype was partially improved by downregulating *Ccl21* with shRNA lentivirus in HUVECs. This intervention was also associated with improved contraction amplitude and beating rate (Figure 10.3.3C).

Therefore, I could hypothesize a paracrine cross-talk between endothelial cells secreting Bmp7, Apln, and Nts and cardiomyocytes, enhancing the contractile rhythm and amplitude of cardiac organoids. This provides insight into the possible mechanisms involved in the cardiac adaptation of P1 mice to nTAC.

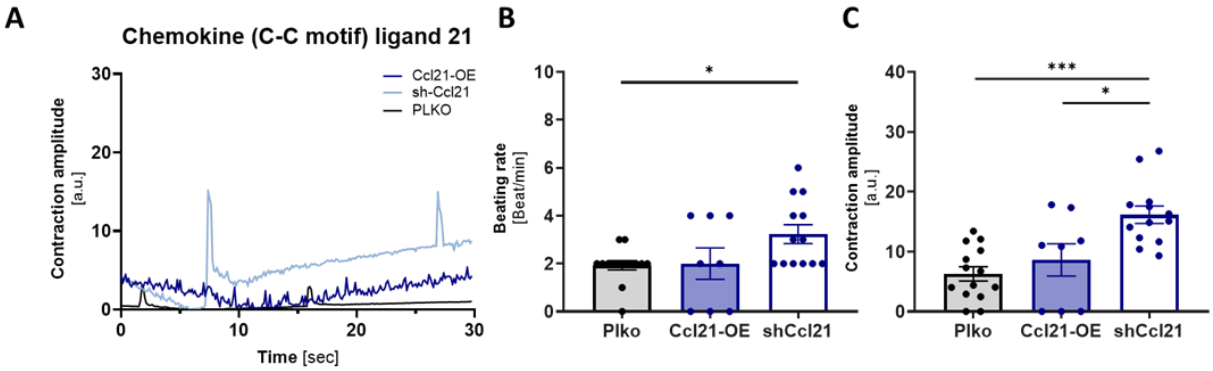

Figure 46 Lentivirus-mediated endothelial-specific overexpression of the inflammatory cytokine Ccl21 leads to arrhythmia in 3D-cardiac organoids.

(**A**) Graph depicting the amplitude and velocity of contraction in spontaneously beating 3D-cardiac organoids, derived from video sequences and analyzed using MYOCYTER. The plot shows the influence of lentivirus-mediated *Ccl21* overexpression (in dark blue) and downregulation (in light blue) in endothelial cells on 3D-cardiospheres contraction, compared to PLKO control (in black). Lentivirus-transfected HUVECs were transferred to a mixture of CM and FB and incubated for a 10 days period. (**B**) Quantitative measurements of the cardiac beating rate and contraction amplitude (**C**) of cardipspheres. The beating rate and amplitude were determined from video sequences using MYOCYTER. Data presented as mean ± SEM (n=8-14 per condition). ***p<0.001, ****p<0.0001 (one-way ANOVA/Sidak's multiple-comparisons test). The graphs in this figure were acquired and analyzed solely by myself.

10.3.4. Endothelial-derived Bmp7, Apln, and Nts play a crucial role in stimulating the proliferation of cardiomyocytes in 3D-cardiac organoids.

In adult mammalian hearts, the regenerative capacity in response to injuries is significantly hindered, primarily due to their limited ability of cardiomyocyte proliferation. However, effective proliferation and cytokinesis of CMs are potentially crucial drivers for enhancing cardiac repair, particularly through the formation of new, healthy cardiac muscle cells. Believing in the importance of cardiomyocyte division for proper healing following cardiac injury, I studied the effect of the identified angiocrines on CM proliferation in 3D-cardiac organoids. With this approach, I aimed to simulate the complex heart structure and explore the potential cross-talk mechanisms between endothelial cells and cardiomyocytes, in presence of fibroblasts. For this purpose, I co-cultured lentiviral-transfected HUVECs, either overexpressing or downregulating the angiocrine factors of interest, with CM and FB as 3D-organoids for 10 days. Subsequently, I quantified CM proliferation by immunofluorescent staining of the proliferation marker Ki67 along with cardiac troponin T (cTnT) as a CM marker. Additionally, I measured the extent of cardiac muscles coverage as the overall area covered by CMs within each cardiosphere.

Interestingly, I observed that lentiviral-induced overexpression of the early angiocrine factor *Bmp7* in HUVECs significantly boosted CM proliferation (measured by assessing the rate of KI76 positive cardiomyocytes) by 3.3 folds in comparison to the control PLKO, as illustrated in Figure 10.3.4A – A-B. The increase in CM division observed following endothelial *Bmp7* overexpression was accompanied by a significant rise in CM abundance in 3D-cardiac organoids. I could quantify this by the increase in the total red area covered by CM within each cardiosphere, as depicted in Figure 10.3.4B – A-B. However, this boosted proliferative capacity was significantly reduced after downregulating *Bmp7* in HUVECs with shRNA lentivirus, resulting in decreased cardiomyocyte coverage within each organoid, as shown in Figure 10.3.4A – A-B and Figure 10.3.4B – A-B.

Notably, the increased cardiomyocyte proliferation I observed with endothelial-derived Bmp7 was also achieved following the overexpression of the regenerative factors *Apln* and *Nts*. In 3D-cardiac organoids, overexpression of *Apln* and *Nts* separately in HUVECs using lentivirus led to a significant increase in CM division, up to threefold (Figure 10.3.4A – C-F). I further noticed

that the enhanced cardiomyocytes' proliferation was marked by the doubling of the total area covered by CM within each cardiosphere, as illustrated in Figure 10.3.4B – C-F. On the contrary, downregulation of *Apln* and *Nts* individually in HUVECs with shRNA lentivirus turned off the CM proliferation machinery back to the control level (Figure 10.3.4A – C-F and Figure 10.3.4B – C-F).

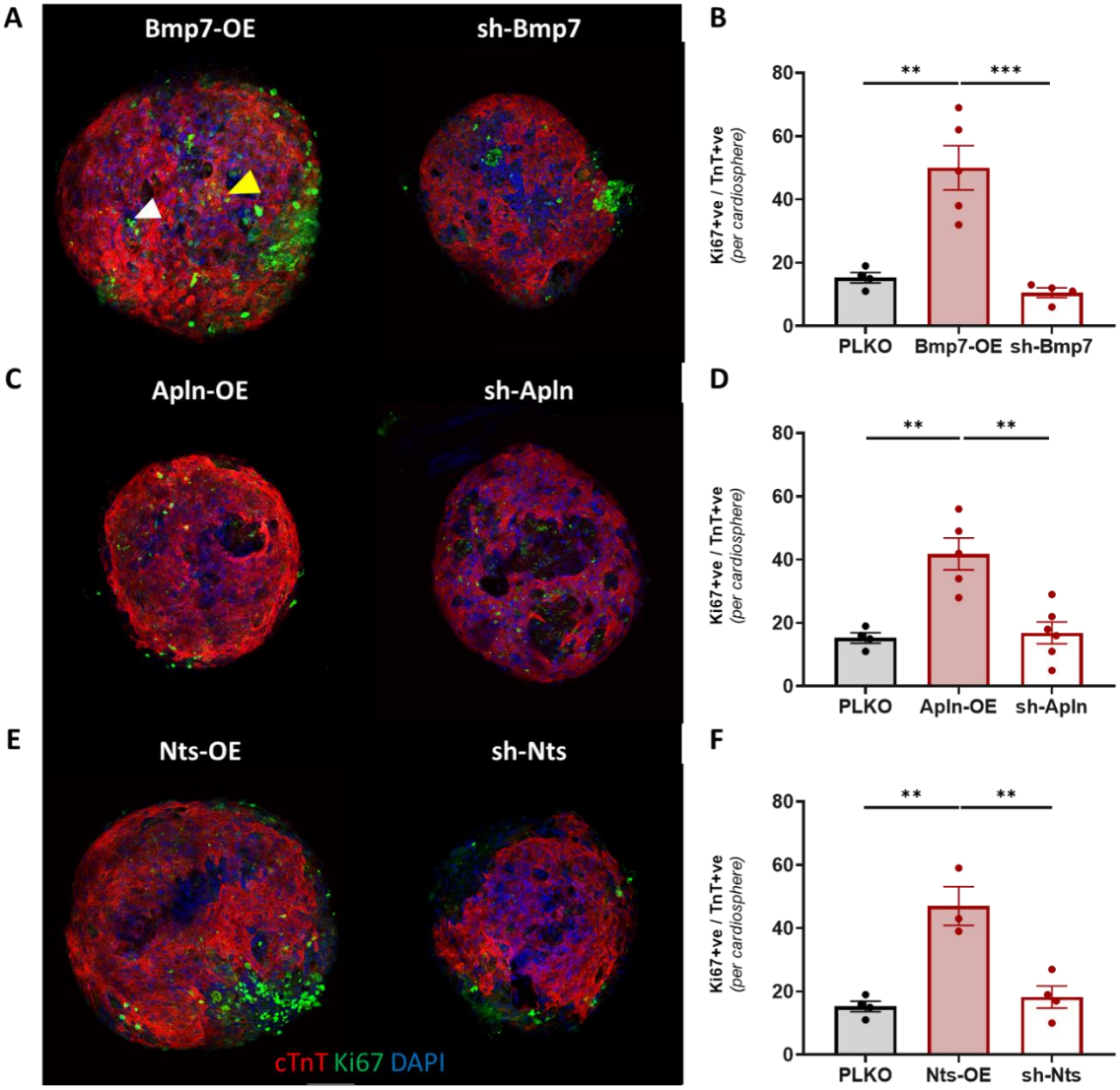

Figure 47 Lentiviral-induced overexpression of Bmp7, Apln and Nts individually in HUVECs promotes cardiomyoctes proliferation in 3D-cardiac organoids.

(**A-E**) Immunofluorescent images illustrating the effects of lentivirus-mediated overexpression and downregulation of *Bmp7* (**A**), *Apln* (**C**) and *Nts* (**E**) in endothelial cells on CM proliferation in 3D-cardiospheres. Lentivirus-transfected HUVECs were seeded onto a combination of CM and FB and incubated for a period of 10 days. After harvesting, the cardiospheres were stained with the pan proliferation marker (Ki67, green) along with the cardiomyocytes' marker cardiac troponin T (cTnT, in red). Yellow arrow pointing at an exemplary Ki67+ve cardiomyocyte. White arrow pointing at Ki67+ve non-cardiomyocyte (not included in the couting) (**B-F**) Quantification of CM proliferation (Ki67 positive NRCM) per 3D-cardiosphere with lentivirus-transduced HUVECs. Data presented as mean ± SEM (n=3-6 per condition). **p<0.01, ***p<0.001 (one-way ANOVA/Sidak's multiple-comparisons test). The images and graphs in this figure were acquired and analyzed solely by myself.

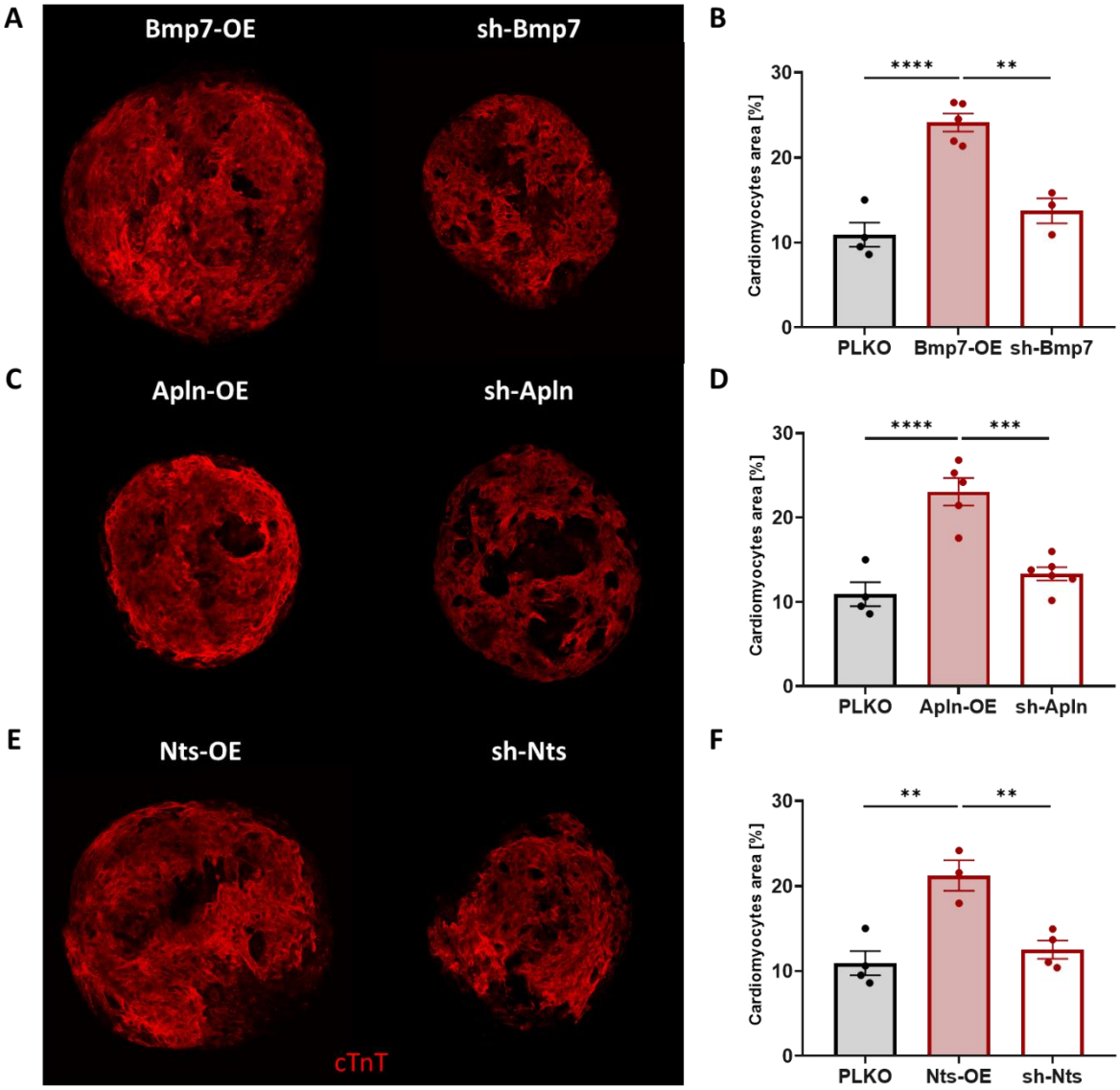

Figure 48 Individual overexpression of Bmp7, Apln and Nts with lentivirus in HUVECs increases cardiomyoctes' coverage in 3D-cardiac organoids.

(**A-E**) Immunofluorescent images illustrating the effects of lentivirus-mediated overexpression and downregulation of *Bmp7* (**A**), *Apln* (**C**) and *Nts* (**E**) in endothelial cells on CM coverage in 3D-cardiospheres. Lentivirus-transfected HUVECs were seeded onto a combination of CM and FB and incubated for a period of 10 days. After harvesting, the cardiospheres were stained with the cardiomyocytes' marker cardiac troponin T (cTnT, in red). (**B-F**) Quantification of the overall area covered by CMs within each cardiosphere. Data presented as mean ± SEM (n=3-6 per condition). **p<0.01, ***p<0.001, ****p<0.0001 (one-way ANOVA/Sidak's multiple-comparisons test). The images and graphs in this figure were acquired and analyzed solely by myself.

On the other hand, similar to my observations in the 2D co-culture system, endothelial *Ccl21* overexpression reduced CM proliferation by half compared to PLKO in 3D-cardiac organoids. Nevertheless, downregulating *Ccl21* in HUVECs with shRNA partially restored CM proliferation in cardiospheres to a level 1.6 times higher than the PLKO control, as seen in Figure 10.3.4-C. This enhanced cardiomyocytes' proliferation was correspondingly associated with a notable increase in the total area covered by CM within each organoid, as depicted in Figure 10.3.4-D.

Taken together, I hypothesize that the potential role of the angiocrines Bmp7, Apln, and Nts, secreted by endothelial cells during cardiac adaptation following nTAC surgery in P1 mice, may be attributed to enhanced cardiomyocytes' proliferation and abundance, as observed in 3D-cardiac organoids.

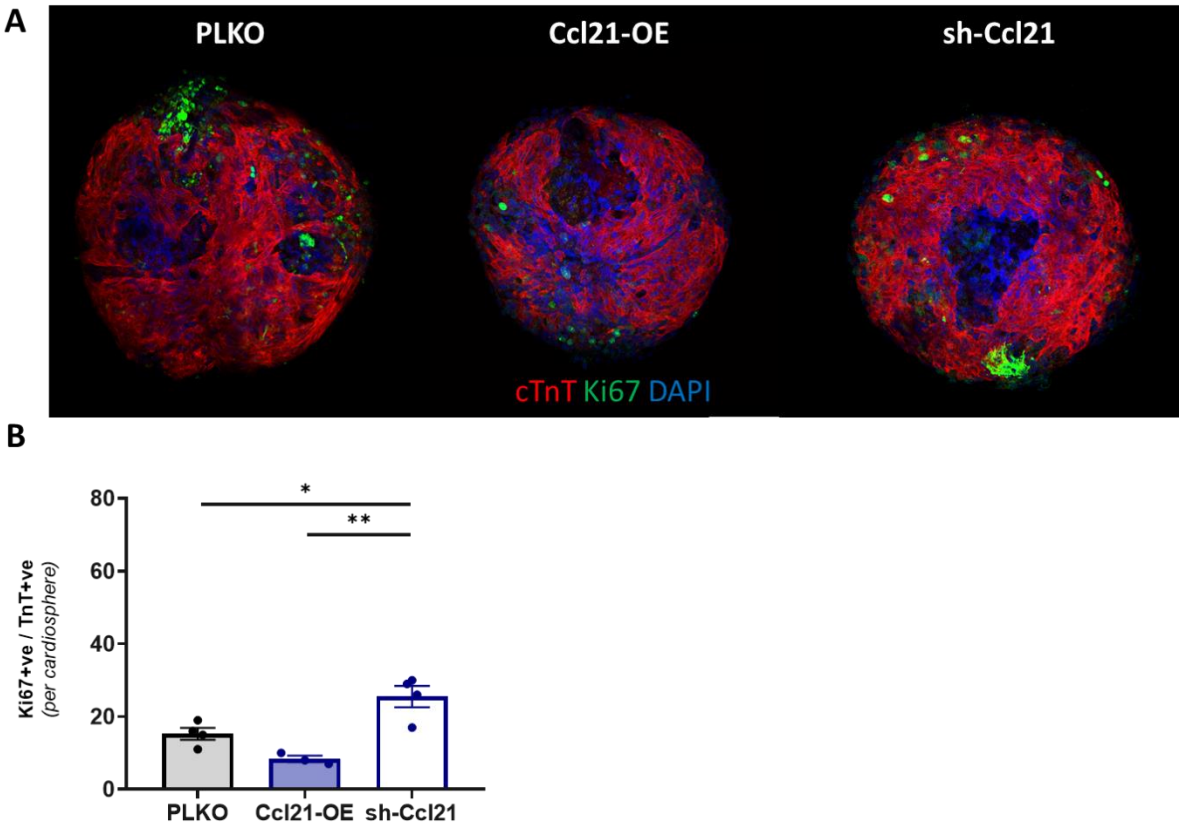

Figure 49 Lentiviral-induced downregulation of the inflammatory angiocrine Ccl21 in HUVECs restores cardiomyoctes' proliferation in 3D-cardiac organoids.

(**A**) Immunofluorescent images illustrating the effects of lentivirus-mediated overexpression and downregulation of *Ccl21* in endothelial cells on CM proliferation in 3D-cardiospheres. Lentivirus-transfected HUVECs were seeded onto a combination of CM and FB and incubated for a period of 10 days. After harvesting, the cardiospheres were stained with the pan proliferation marker (Ki67, green) along with the cardiomyocytes' marker cardiac troponin T (cTnT, in red). (**B**) Quantification of CM proliferation (Ki67 positive NRCM) per 3D-cardiosphere with lentivirus-transduced HUVECs. Data presented as mean ± SEM (n=3-4 per condition). *p<0.05, **p<0.01 (one-way ANOVA/Sidak's multiple-comparisons test). The images and graphs in this figure were acquired and analyzed solely by myself.

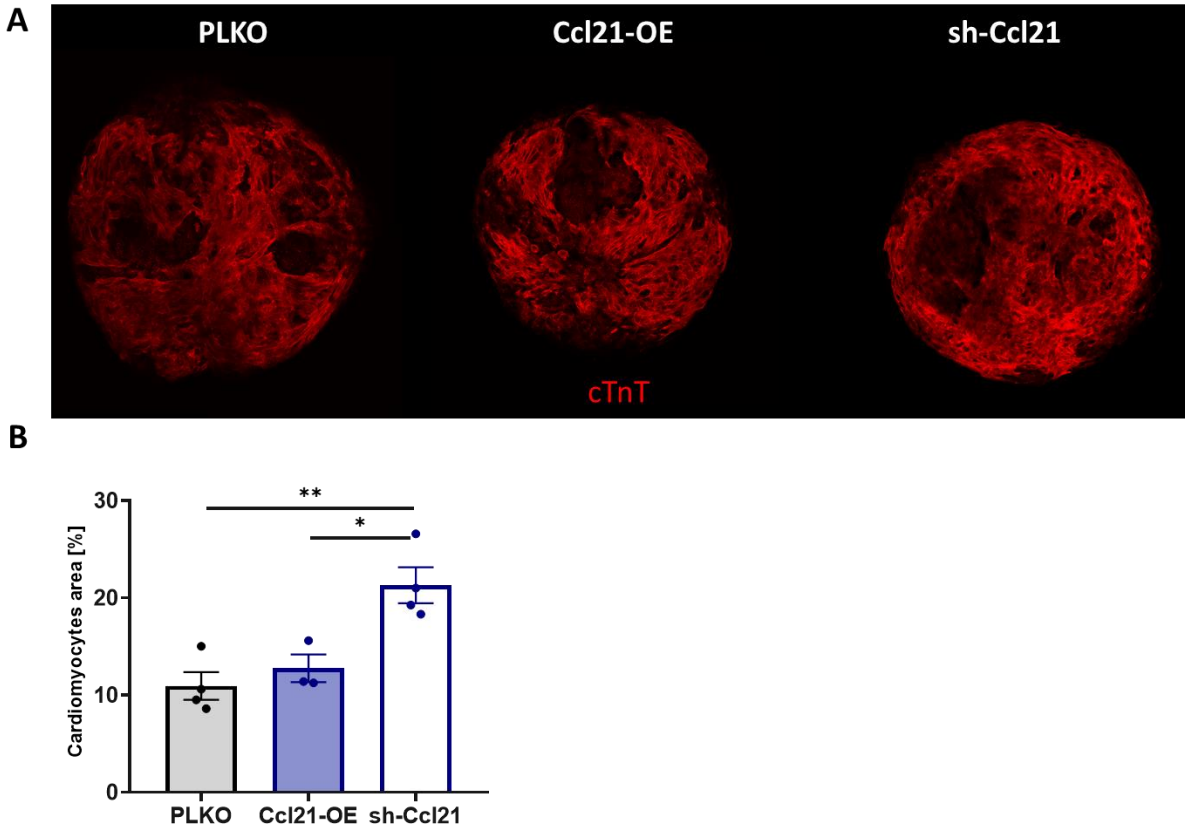

Figure 50 Lentiviral-induced downregulation of the inflammatory angiocrine Ccl21 in HUVECs enhances cardiomyoctes' coverage in 3D-cardiac organoids.

(**A**) Immunofluorescent images illustrating the effects of lentivirus-mediated overexpression and downregulation of *Ccl21* in endothelial cells on CM coverage in 3D-cardiospheres. Lentivirus-transfected HUVECs were seeded onto a combination of CM and FB and incubated for a period of 10 days. After harvesting, the cardiospheres were stained with the cardiomyocytes' marker cardiac troponin T (cTnT, in red). (**B**) Quantification of the overall area covered by CMs within each cardiosphere. Data presented as mean ± SEM (n=3-4 per condition). *p<0.05, **p<0.01 (one-way ANOVA/Sidak's multiple-comparisons test). The images and graphs in this figure were acquired and analyzed solely by myself.

11. Chapter 4: Discussion

11.1. Adult Endothelial Cells Exhibit a Dynamic Phenotype Driving a Maladaptive Remodeling to Pressure Overload

TAC, first described by Rockmann et al., is a well-established in-vivo method for inducing pressure overload and cardiac hypertrophy in adult mice.[67] The initial part of my study focused on investigating the contribution of cardiac endothelial cells to the maladaptive cardiac remodeling during the acute and chronic phases of TAC. These findings have been published in iScience under the title *'Analysis of myocardial cellular gene expression during pressure overload reveals matrix based functional intercellular communication'* (Froese, N*, Cordero, J* and Abouissa, A* et al., 2022). [74] *All the figures shown in the first section of my results part were adapted from the published article and represent the part I completed entirely on my own and reflect my individual contribution to the paper. Below, I discuss only the results related to my part.*

(*equally contributing first authors)

11.1.1. Highest Transcriptional Dynamicity in Endothelial Cells was Observed During the Acute Phase of TAC

Perks of the new advances in cell isolation technologies as well as next generating sequencing and analysis is the expanded view on cellular and subcellular changes in heart failure. In the last ten years, multiple studies addressed the alterations in myocytes and non-myocytes under homeostatic as well as pathological conditions.[76-79] However, pressure-overload associated response in EC was not extensively studied.

Analysis of bulk RNA sequencing data I presented in my results showed that the most dynamic transcriptional changes in ECs occur during the acute phase after TAC (one week after surgery). Notably, I observed that cell cycle-related, ECM and inflammatory genes were transiently upregulated in these ECs. The initially enhanced angiogenesis by ECs is crucial during the primary response to pressure overload-induced cardiac hypertrophy. This serves as a preliminary adaptation to compensate for the increased oxygen and nutrients demand by CMs following PO.[80] However, sustained overload leads to impaired cardiac angiogenesis and

capillary rarefaction. This phenomenon exacerbates CMs apoptosis, which get replaced by a non-contractile scar tissue leading to contractile dysfunction.[20,49,50,81] In concordance with these data, during the chronic phase after TAC (eight weeks), I could present that the transcription machinery of ECs returns to the basic level. This drove my suggestions to that the imbalance between CM growth and angiogenesis drives the transition from adaptive to pathological hypertrophy, leading to the progression of heart failure.

11.1.2. Enhanced Extracellular Matrix Secretion from Endothelial Cells is Detected During the Acute Phase of TAC

Among the transiently upregulated genes specifically in ECs one week after TAC are genes related to ECM organization, such as *Fn1*, *Col1a1*, *Col3a1* and others. This upregulation was concomitant with the normal expression of EC-markers in these cardiac ECs during the acute phase of PO. In the past, it was believed that a complete endothelial to mesenchymal transition (EndMT) occurs, by which ECs completely change their phenotype and transit to the fibroblast lineage, and this was believed to be a strong driver of cardiac fibrosis in response to injury. [53,82,83] However, this hypothesis has been recently challenged and a definitive transdifferentiation of cardiac ECs into FBs was questioned. In concordance with the findings reported here, Stefanie Dimmeler´s group also recently suggested that a transient EndoMT-like process might rather occur after MI. During this process, EC upregulate mesenchymal genes while maintaining their original cellular identity.[84] Hence, a new terminology has been assigned to describe this phenomenon, named as endothelial to mesenchymal activation (EndMA).[55] Notably, this study, and particularly the immunofluorescent staining and analyses performed by myself showing the co-localization of ECs and EMC markers, was the first time to report about EndMA in pressure overload. [74]

From the computational interaction analysis, my data show the TAC-induced ligands in ECs as well as their respective receptors on EC, CM and FB. I could observe that the highest EC-derived cross-talk with the other cells happened mainly during the acute phase after TAC. This enriched inter-cellular communication significantly diminished during the chronic phase after TAC.

Interestingly, the main drivers involved in this EC-derived cross-talk were ECM proteins, for instance, fibronectin and collagens.

One week after TAC, I could notice that fibronectin expression was mainly localized in ECs, however, later on during the chronic phase of TAC, its expression shifted to other cell types. This finding was further evidenced by our group, where we found that ECs contribute to organ fibrosis by initially secreting matrix proteins and inflammatory mediators that recruit FBs, which then take over this role and increase ECM proteins even further. This leads then to an amplified fibrotic response during the disease progression.[54]

Since the vascular basement membrane is considered a critical regulator of angiogenesis by forming a cellular scaffold, I could detect that fibronectin enhanced ECs proliferation and migration. [85,86] However, it also promoted FB migration and CM hypertrophy. These effects, indeed, could be a major player in disease progression and maladaptive cardiac remodeling after PO.[87,88]

Conclusively, given the dynamic plasticity of ECs reported in my findings and their major contributions to CVDs progression, new therapeutic approaches are highly needed to shift this EC-derived maladaptive role in adult pressure overload to a more adaptive compensatory phenotype.

11.2. Neonatal endothelial cells play a crucial role in cardiac adaptation to pressure overload

As noted in section 1, TAC induction in adult mice exacerbates pathological remodeling and triggers extensive cardiac fibrosis, resembling HFrEF caused by chronic arterial hypertension or aortic stenosis. This cardiac remodeling is hallmarked by a dynamic genetic signature in ECs that varies at different time points following TAC (see above). On the contrary, performing nTAC in neonatal P1 mice was associated with an adaptive response. This compensation was primarily attributed to increased myocardial angiogenesis and enhanced proliferation of cardiomyocytes. [35,66]

In this thesis, my comprehensive studies elucidate the role of four key angiocrine factors— Bmp7, Apln, Nts, and Ccl21— secreted from neonatal cardiac ECs in response to adaptive nTAC in P1 mice. My findings extensively document the autocrine effects of these mediators, as well

as their paracrine impact on adjacent cardiomyocytes, underscoring their significant potential contribution to cardiac adaptation after nTAC.

11.2.1. Comparative Single-Cell Transcriptomics Reveal Distinct Features of Adaptive Cardiac Endothelial Cells to nTAC

Previously, to investigate the complex cellular signaling networks activated in response to cardiac injury, most mechanistic studies employed RNA sequencing from bulk tissue or flow cytometry-sorted (FACS) major cell types. These studies applied various genomic and proteomic approaches to address differential genetic and epigenetic expression, as well as protein abundance, in all cardiac cell types following myocardial infarction (MI) in neonatal mice. [89-92] Similarly, our group examined the changes in the heart's genetic landscape between regenerating P1 and non-regenerating P7 mice upon exposure to nTAC: our innovative model of neonatal cardiac pressure overload in mice. For this purpose, bulk RNA sequencing from whole heart of operated mice was used. The analysis revealed a distinct upregulation of genes directly involved in angiogenesis and CM proliferation after nTAC in P1 mice. When angiogenesis was pharmacologically inhibited, P1 adaptation to nTAC failed, and cardiomyocyte proliferation ceased. [35,66] This underscored the crucial role of endothelial cells in cardiac compensation following nTAC, raising questions about the specific contributions of this cell to neonatal adaptation to nTAC.

Droplet-based scRNAseq offers a powerful, high-throughput method for analyzing cellular heterogeneity and gene expression dynamics. This method has been widely used in cardiovascular research in both adult and neonatal contexts, across animal models and human studies. Previous investigations have utilized this method to gain insights into cellular subpopulations experiencing significant changes in response to different treatments. In 2020, Wang, Cui and colleagues [93,94] conducted scRNAseq on non-cardiomyocytes isolated at various timepoints from neonatal murine hearts following MI. However, the specific contribution of the ECs populations was obscured by the presence of other cell types in the analysis. At the end of 2023, Long et al. performed scRNAseq on enriched ECs following MI in regenerating (P1) and non-regenerating (P8) mice. [95] In contrast, EC heterogeneity following cardiac pressure overload in neonatal mice has not been studied to date.

In this study, I performed nTAC in the beginning and at the end of the regenerative window in neonatal mice. Following enzymatic digestion, I enriched cardiac EC to reach 98% purity. Differential gene expression of EC from neonatal hearts undergoing adaptive and maladaptive response to nTAC was profiled at the single-cell level. My scRNAseq analysis revealed that ventricular ECs in the neonatal murine heart are transcriptionally heterogenous in response to nTAC at various timepoints. In contrast to Wang et al. [93], I could identify nine ECs subpopulations with distinct genetic profile following nTAC induction during the regenerative and the non-regenerative ages in mice. In concordance with the single-cell data from Long et al. following MI [95], most of the ECs heterogeneity I observed was among the capillary subpopulations. In response to nTAC in P1 mice, adaptive ECs notably increased the number of two major capillaries populations. Gene ontology enrichment analysis of these two clusters revealed a strong enrichment of genes related to vasculature development and sprouting angiogenesis. In comparison, the percentage of these two subpopulations was meaningfully reduced among ECs from mice with a maladaptive phenotype after nTAC at P7. As reported in earlier studies, sprouting angiogenesis, along with the capacity of pre-existing endothelial cells to form new blood vessels by activating the transcription machinery for relevant genes in response to cardiac injury, is crucial for supporting the heart's ability to regenerate and repair damaged myocardium. [96-98] Using scRNAseq, this concept has been proven mainly in in-vivo models inducing direct damage of the myocardium through MI, in zebrafish as well as mice. In the context of cardiac pressure overload, our group have previously demonstrated the importance of angiogenesis in supporting the heart adaptation to nTAC by providing a scaffold supporting CMs proliferation. [35,66] However, the exact contribution of specific ECs subpopulation as well as the phenotypic origin was unknown. Hence, my study provides a detailed response about the origin as well as the localization of these angiogenesis-driving clusters in response to nTAC. Additionally, it highlights the significance of both the diversity as well as the dynamic nature of capillary ECs in response to nTAC at different postnatal ages.

11.2.2. Regulatory Landscape of Single Endothelial Cells in Adaptive and Maladaptive Neonatal Hearts after nTAC

Among various signaling molecules, transcription factors (TFs) are vital for the development and maintenance of the cardiovascular system. They play crucial roles in angiogenesis and

heart regeneration by regulating the expression of genes involved in endothelial cell function, vessel formation, and tissue repair. The primary role of TFs is to recruit transcriptional regulatory components to specific genomic loci, modulating the expression of cardiovascular genes and thereby controlling crucial morphogenetic steps. [99] These TFs orchestrate the complex processes required for new blood vessel growth and the restoration of cardiac tissue after injury. [100] The role of TFs in cardiovascular remodeling has become a significant research focus, uncovering novel therapeutic approaches for CVDs. [35,101-103]

Inducing neonatal TAC during the non-regenerative stage (at P7) in mice resulted in a significant downregulation of various transcription factors directly involved in angiogenesis. Among these transcription regulators is the LIM-only protein LMO2 that plays a crucial role in embryonic angiogenesis and sprouting. [104] As a multimeric protein complex, LMO2 play a key role in its assembly and can directly bind to TAL1 and GATA2. This complex acts synergistically to regulate the expression of multiple angiogenesis-related downstream genes. [104-107] It has been reported that binding of LMO2 to TAL1 triggers vascular sprouting initiation. [106,108] Indeed, this complex plays a major role for angiogenic remodeling into mature vasculature and enhancing the expression of its direct targets *Cdh5*, *Angpt2*, *Kdr* and *Dll4*. [109-112] Interestingly, the mRNA expression *Lmo2* and *Gata2* was significantly downregulated in ECs isolated from mice showing a maladaptive phenotype after nTAC at P7.

One of the transcription factors notably increased in endothelial cells showing an adaptive response to nTAC in P1 mice is Krüppel-like factor 4 (KLF4). Its transcriptional expression is elevated in over half of all endothelial cell populations. KLF4 is a zinc finger transcription factor that plays a significant role in various cellular processes, including proliferation, differentiation, and apoptosis. [113] In the context of angiogenesis and heart regeneration, KLF4 is emerging as a critical regulator. It enhances the angiogenic response to vascular endothelial growth factor (VEGF), a principal driver of angiogenesis, through upregulation of VEGFR2 and AKT pathway activation. [114,115] In addition to its pro-angiogenic properties, KLF4 has been reported to exhibit an anti-inflammatory action by suppressing the expression of pro-inflammatory cytokines, thereby has a protective role on the endothelium. [116,117]

Additionally, from my scRNAseq data, I identified SRY (Sex Determining Region Y)-Box 18 (SOX18) as a transcription factor significantly downregulated in ECs with a maladaptive phenotype following nTAC in P7 mice. SOX18 was initially reported as a major player in

lymphangiogenesis through the upregulation of PROX1. [118,119] Moreover, it has been identified to be transiently expressed during angiogenesis and to promote skin wound healing. [120] Since then, SOX18 showed promising involvement on postnatal angiogenesis in mice. [121] However, the exact role of SOX18 in heart regeneration and its contribution to cardiac compensation are still undetermined.

In addition to the aforementioned TFs, my analysis revealed cluster-specific regulators that are directly involved in vasculature development and integrity as well as heart morphogenesis. Among these TFs are TBX3, PHF12 and PRDM16. [122-125] These TFs exhibited significant downregulation in maladaptive ECs in response to nTAC at P7.

11.2.3. Endothelial Cells-Derived Cross-Talk with its Microenvironment after nTAC

The heart is a complex multicellular organ composed mainly of ECs, CMs and FBs along with stromal and immune cells. These cells interact with each other under both physiological and pathological conditions, either to maintain normal cardiac homeostasis or to drive maladaptive remodeling in response to injury. Paracrine signaling from ECs plays a crucial role in heart regeneration. Endothelial cells release a variety of signaling molecules that influence the behavior of neighboring cells, including CMs, FBs and immune cells. These signals are essential for coordinating the complex processes of tissue repair and regeneration. [126]

Vasculature is considered the largest “endocrine organ” in the body. In response to physiological or pathological stimuli, endothelial cells secrete proteins that have been termed “angiocrines”. These proteins influence neighboring cell types by forming a vascular niche that supports normal organ growth and multi-organ regeneration. [127-129] However, the cardiac ECs secretome in response to injurious stimuli is still emerging in cardiovascular research. While some of the EC-derived angiocrines have been shown to exert a beneficial effect on their microenvironment, other factors are secreted in pathological conditions.

My ligand-receptor network analysis from scRNAseq data identified various EC-derived ligands, some of them already reported to exert either a favorable or a detrimental effect in cardiac regeneration. Among these known angiocrines is the Insulin-like growth factor 1 (Igf1). This ligand is significantly upregulated in sprouting capillaries with an adaptive response to nTAC in

P1 mice, while its transcription is significantly reduced following nTAC in P7 mice. Studies over the past decade have uncovered the significant role of Igf1 in regulating postnatal cardiac growth. [130,131] Its signaling pathways are mainly involved in cardiac proliferation and contractility as well as angiogenesis. [131,132]

On the other hand, my findings identified the inflammatory mediators Il6 and Tnf among the ligands strongly downregulated in adaptive ECs following nTAC in P1 mice, during the early and late regenerative stage, respectively. Since decades, the effect of these ligands has been extensively studied in cardiovascular research. [133] Among the demonstrated effects, Il6 promoted CMs hypertrophy and apoptosis leading to impaired contractile function. [134,135] Even though initial Il6 overstimulation has been proven to stimulate angiogenesis [136,137], abnormal Il6 elevation induced pathological remodeling and exacerbated inflammatory response. [138,139]

Similarly, overexpression of Tnf in HUVECs via lentivirus reduced CMs proliferation and disturbed their contractility as well as exhibited pro-angiogenic properties (data not shown). These data come in concordance with the published data about the deleterious effect of Tnf on the myocardium and its contribution to pathological fibrosis following MI.[140,141]

11.2.4. Endothelial-Derived Bmp7 Regulates Angiogenesis and CM Function and Cytokinesis during the Early Adaptive Phase following nTAC

Bone morphogenetic protein-7 is (BMP7) belongs to the Transforming Growth Factor Beta (TGF-β) superfamily of cytokines. [142] They are a group of evolutionarily conserved secretory proteins that play crucial roles in growth and development.[143]

Bmp7 protein is expressed in the majority of tissues throughout the body. [144] Originally, it is synthesized within the cells as a pro-protein composed of 431 amino acids, that is hydrolyzed by furin-like proteinase into the mature peptide of 139 amino acid residues. [145] During bone formation, Bmp7 can function as both homodimers and heterodimers with Bmp2 and Bmp7; however, the heterodimers exert a more potent action. [146]

Bmp7 is a pleiotropic secreted growth factor playing a major role in organ development and cellular differentiation under physiological conditions. It exerts its action through binding to

type I BMP receptors, commonly known as activing-like kinases (ALKs), and type II BMP receptors on the cell surface. [147] These receptors contain a serine/threonine kinase domain responsible for the downstream biological effects. [148] Bmp7 binding to its receptors leads to the activation of two major signaling pathways in the cell cytoplasm. In endothelial cells, Bmp7 activates ALK1 and BMPR2, triggering the canonical Smad-dependent pathway. In this pathway, regulatory Smads (Smad-1, 5, and 8) are phosphorylated in the cytoplasm and then form a complex with the co-stimulatory molecule Smad-4, which translocates to the nucleus. This process leads to increased endothelial cell proliferation and migration. [144,149]

On the other hand, Bmp7 plays a crucial role in maintaining an anti-inflammatory milieu. This action is primarily attributed to a Bmp7-activated non-canonical signaling pathway. In this case, Bmp7-receptor binding leads to phosphorylation and activation of Phosphotidylinositol 3 kinase (PI3K) downstream signaling. This pathway is specifically involved in the inhibition of pro-inflammatory cytokines' secretion (including Tnf-α and Il6, mentioned above) while enhancing anti-inflammatory cytokines. This immune response mitigation is principally responsible for shifting the pro-inflammatory action in M1 macrophages to enhanced M2 macrophages polarization. [150-152] This micro-environmental anti-inflammatory shift has been shown to have a major cardioprotective role in MI and atherosclerotic diseases. [153,154]

In cardiovascular diseases, recent studies proved that Bmp7 facilitates functional recovery of the heart following MI by enhancing CMs proliferation and regeneration as well as attenuating cardiac fibrosis. [155-157] Earlier this year, Bongiovanni and colleagues demonstrated the role of Bmp7 in promoting CM regeneration in zebrafish and mice, following cryoinjury and MI, respectively. Intraperitoneal/intravenous administration of Bmp7 to adult mice following MI was associated with a cardioprotective effect, mainly by reducing the infarct size leading to enhanced cardiac function. Bmp7 administration increased cell-cycle re-entry and proliferation in CMs. [158,159]

In concordance with Bongiovanni et al., the scRNAseq data in my study showed a significant upregulation of *Bmp7* in ECs during the early adaptive phase to nTAC in P1 mice. Nevertheless, I could see that Bmp7 ligand expression was also enhanced in CMs, predominantly three days following nTAC in P1 mice. Interestingly, restricted overexpression of Bmp7 in ECs per se could increase CMs proliferation and cytokinesis by 2-3 folds, as demonstrated in 2D and 3D co-culture systems I reported above. On the other hand, Bmp7 downregulation specifically in ECs

significantly reduced CMs proliferation and entirely halted CM cytokinesis. Hence, my findings could further confirm the mitogenic impact of Bmp7 reported earlier.

Furthermore, my findings show that EC-derived Bmp7 significantly improved the contractile function of 3D cardiospheres, as evidenced by an increased beating rate and enhanced contraction amplitude. Therefore, my study represents the first evidence of the novel role of Bmp7 on enhancing contractility.

In addition to its proliferative effect on CMs, my data demonstrate that Bmp7 remarkably enhanced tubule formation and vasculature coverage in 3D cardiac organoids. The angiogenic role of Bmp7 has been reported in the field of endocrinology where its action through VEGFa enhanced osteoblasts differentiation. [160-162] However, its pro-angiogenic role in cardiovascular diseases has not been yet investigated in details.

Taken together, my findings represent the first comprehensive study of the multifactorial cardioprotective effects of Bmp7 in neonatal cardiac pressure overload model.

11.2.5. Endothelial-Derived Apelin Pro-angiogenic and Cardio-proliferative Effects are maintained during the Early and Late Adaptive Phase following nTAC

Apelin (Apln) is originally synthesized as 77 amino acids containing pre-pro-peptide. It is subsequently cleaved into smaller fragments of different lengths by proteolysis. These fragments bind to the orphan G-protein-coupled apelin receptor (expressed by *Aplnr* gene). [163,164] Pyr-apelin 13 is the predominant isoform in human heart, exhibiting the greatest affinity to the apelin receptor [165], despite having a short plasma half-life. The predominant source of Apln is primarily located in the endothelium and in adipocytes.[166, 167] Interestingly, pyr-apelin 13 is a substrate of angiotensin converting enzyme 2 (ACE2), which potentiates its degradation. Hence, it is considered the principal negative regulator of apelin in cardiac vasculature. [168]

In the vasculature, apelin exerts a major role as a vasodilator as well as pro-angiogenic factor. These actions are mainly achieved via nitric-oxide (NO)-dependent signaling and adenosine monophosphate activated protein kinase (AMPK) and Akt signaling, respectively. [169-171]

My scRNAseq and bulk RNAseq data demonstrated that the expression of the angiocrine Apln as well as its receptor, Aplnr, are significantly upregulated in cardiac ECs showing an adaptive compensatory response to nTAC induced in P1 mice. The elevated specific expression of Apln in ECs started during the early adaptive phase after nTAC, and further peaked during the late adaptive phase. EC-specific overexpression of Apln using lentivirus significantly boosted tubule formation as well as vasculature coverage, in monoculture and 3D cardiac organoids models. My observations come in concordance with the investigations from Liu and colleagues, showing the importance of Apln in mediating VEGF-dependent vascular sprouting, which was also shown by Marín-Juez et al. in zebrafish model. [97,172] Additionally, a recent study by Helker et al. highlighted Apln/Aplnr requirement for endothelial tip cell morphology and hypersprouting via Notch signaling involvement. [171]

In addition, Apln overexpression solely in ECs induced a positive inotropic as well as chronotropic effect on 3D cardiac organoids. My findings are consistent with the reported Apln direct effect on CM contractility and electrophysiology, which is secondary to enhanced myofilament sensitivity to Ca^{2+}. [164,173,174] My results, indeed, further confirm the applied pipeline to screen the potential cardiovascular effects of the EC-secreted ligands detected in my analysis.

Interestingly, in the 2D and 3D co-culture systems, I could show a novel role of Apln on CM regeneration. Overexpression of Apln specifically in ECs was associated with a remarkable enhancement in CMs proliferation as well as cytokinesis. I could prove this by the increased Ki67 and Aurora B detection in CM, in the 2D direct co-culture model as well as in 3D cardiac organoids. To date, the effect of EC-derived Apln on the neighboring CM proliferative machinery has not been reported. Hence, my findings might provide a novel insight into Apln-induced cardioprotective action.

11.2.6. A Novel Role of Endothelial-Secreted Neurotensin in Cardiac Adaptation following nTAC

Neurotensin (NT), encoded by the gene *Nts*, is a small peptide consisting of 13 amino acids, originally found in the bovine hypothalamus. Despite its small size, it is considered to produce pleiotropic functions. It is produced intracellularly after the proteolytic cleavage of its larger

precursor as pro-neurotensin (pro-NT). The active mini-peptide is subsequently stored in vesicles until being released in a calcium-dependent manner. [175] Neurotensin exerts its biological action upon binding to three neurotensin receptors (NTSR1, NTSR2 and NTSR3). [176]

Apart from its action in the central nervous system, increased NT secretion has been merely linked to acute rise in plasma triglyceride levels. Since then, it has been associated with detrimental effects on atherosclerosis, obesity as well as diabetes [177,178,179,180]. However, the impact of NT on heart regeneration has not yet been studied.

From the scRNAseq data as well as bulk sequencing of ECs, my analysis showed that *Nts* expression was significantly elevated in more than half of sprouting capillaries following nTAC in P1 mice. Interestingly, this upregulation was highly EC specific and was a hallmark of the late adaptive phase of ECs to nTAC.

Lentivirus-mediated overexpression of Nts in EC clearly enhanced the formation of intact tubes. I could confirm this finding additionally in 3D cardiac organoids, where EC-specific *Nts*-overexpression significantly improved the phenotype of the formed vessels extending the capillary network from the periphery of the cardiosphere towards the intra-myocardial space. The extension of these long and intact vessel-like structures in-between the CMs could play a crucial role in forming a scaffold to strengthen their function. Nevertheless, this ameliorated angiogenic property was completely abolished by EC-specific deletion of *Nts*. These data are in concordance with the increased intestinal and endometrial angiogenesis via NT-VEGFa signaling, as reported in the literature. [181,182] Yet, my observations might provide the first evidence for Nts involvement in cardiac vascularization.

In addition to its pro-angiogenic properties, EC-specific overexpression of Nts remarkably exerted a positive inotropic effect on 3D cardiac organoids. This effect on cardiac contraction has been reported and could be mediated via the stimulation of substance P release from cardiac neurons. The positive inotropic effect of NT has also been attributed to enhanced histamine release by mast cells upon stress. [183] Interestingly, NT has been reported to be four times more potent inotrope than noradrenaline. [184]

Despite extensive and decades-old research involving NT, its role in cardiac regeneration has been largely understudied. From my 2D co-culture experiments as well as 3D cardiac organoids, Nts overexpression solely in ECs has significantly boosted CM proliferative machinery. This was

notably associated with a remarkable increase in CM cytokinesis as well. To date, this is the first time to report a potential pivotal role for NT in cardiac adaptation to pressure overload as well as heart regeneration.

11.2.7. Combined Expression of Bmp7, Apln, and Nts from EC has a Synergistic Effect on Angiogenesis and Cardiomyocytes Function

In addition to their individual contributions on EC and CM behavior as discussed earlier, simultaneous overexpression of these three angiocrines (Bmp7-Apln-Nts) in ECs further enhanced vasculature coverage in 3D cardiac organoids. The synergistic effect of the three angiocrines led to the formation of large vessel-like structures, characterized by their thick and strong lumen. My results show that these formed vessels extended throughout the whole cardiosphere, with deeper penetration as a scaffold between individual CMs.

Furthermore, combined expression of this “Mix” of angiocrines specifically in ECs had a strong positive chronotropic effect on 3D cardiospheres. The chronotropic effect of this Mix is more potent than individual angiocrines.

Collectively, my findings highlight a novel EC-derived cross-talk with CM through Bmp7, Apln and Nts expression, which might drive the main adaptive phenotype of ECs in response to nTAC. Moreover, these observations might shed the light on the potential important role of these angiocrines in driving a compensatory mechanism to cardiac pressure overload.

11.2.8. Endothelial-Derived Ccl21 causes a Detrimental Effect on Cardiomyocytes

Ccl21 is a homeostatic chemokine and a powerful regulator that facilitates T-cell migration into non-lymphoid tissue via its canonical receptor Ccr7. [185] Both the ligand and its receptor are expressed in ECs [186] as well as FBs [187]. Ccl21 has primeval role in immune cells homing and mediating a strong inflammatory response by recruiting T-cells, macrophages and dendritic cells. [95,188,189]

In cardiovascular research, increased Ccl21 production and circulation has been initially linked to atherosclerosis and plaque destabilization due to its pro-inflammatory role. [186,188] In 2014, Finsen and colleagues first identified a strong correlation between raised serum level of Ccl21 in patients with symptomatic AS. Higher serum Ccl21 levels were directly associated with all-cause mortality in these patients. [190] Subsequently, Jiang et al. found a significant increase in circulating levels of Ccl21 during the first week following MI in mice. [191]

Interestingly, *Ccl21* transcriptional expression was specifically upregulated in ECs when nTAC is performed in P7 mice, as detected in my analysis. Notably, these EC significantly contributed to the maladaptive remodeling observed in response to nTAC induction during the non-regenerative age in mice. My findings harmonize with the data from Jiang and colleagues where Ccl21 levels positively correlated with cardiac maladaptive remodeling following MI. [191] However, a detailed study of Ccl21 involvement in maladaptation to pressure overload as well as its role in cardiac regeneration following MI are still lacking.

Interestingly, *Ccl21* overexpression solely in ECs using lentivirus severely affected CMs contractile function, in 2D co-culture and 3D cardiac organoid models. This paracrine effect of EC-derived Ccl21 caused a strong arrhythmic phenotype in individual CMs as well as the whole cardiosphere. Indeed, the cardiac arrhythmia I observed could be partially reversed, and normal cardiac beating could be partially restored with the specific downregulation of Ccl21 in endothelial cells.

Additionally, EC-derived Ccl21 significantly reduced CMs proliferation in the 2D direct co-culture model. Surprisingly, downregulation of Ccl21 in ECs restored and even increased CMs proliferation in a paracrine manner. To date, my findings reported in this study provide the first evidence of Ccl21 effects on cardiac arrhythmia as well as CM proliferative ability. Hence, these observations provide a new insight on possible emerging roles of Ccl21 in cardiac maladaptive remodeling in pathological pressure overload as well as impaired heart regeneration following MI.

On top of its effect on CM proliferation and contraction, Ccl21 overexpression in EC significantly impaired tube formation. However, Ccl21 downregulation in EC did not improve this anti-angiogenic effect. This might suggest that a minimal level of Ccl21 expression is required for proper ECs function. This observation needs to be further studied in detail.

11.3. Clinical Relevance and Future Plans: Targeted Overexpression of *Bmp7*, *Apln* and *Nts* in Endothelial Cells

Despite modern scientific advances, CVDs remain to cause a high global burden and continue to be the leading cause of mortality worldwide. Recent studies provide new insights aimed at developing novel therapies to prevent or reverse left ventricular remodeling observed in pressure overload- induced cardiomyopathy.

During the recent decade, novel therapeutic approaches for CVDs have emerged. Part of these therapeutic strategies relied on the improved delivery of certain growth factors to the heart. For instance, Báez-Díaz and colleagues recently applied microencapsulated IGF-1 in a swine model of acute MI via intracoronary infusion. [192]

Other approaches involved the use of recombinant proteins, protein analogues as well as organ-targeted gene therapy. For example, recombinant Bmp7 administration and cardio-selective overexpression of Bmp7 using AAV6 significantly improved LV remodeling after TAC and in diabetic cardiomyopathy, respectively. [159,193] Similarly, Bmp7-based peptides exerted a cardioprotective role in pressure overload by reducing TGF-β-induced fibrosis and myocardial remodeling. [194]

Based on my studies described here, EC-derived Bmp7, Apln and Nts exert novel functional effects on angiogenesis and CM proliferation, respectively. Hence, my next approach aims to overexpress these identified angiocrines specifically in cardiac ECs using $G2^{CNN}$ AAV9, recently developed by Bozoglu and colleagues. [195] This method relies on targeting AAVs toward cardiac ECs via coating with second-generation polyamidoamine dendrimers (G2) linked to endothelial-affine peptides (CNN).

These vascular EC-targeted AAV9 overexpressing Bmp7, Apln and Nts will be delivered via intraperitoneal injection to P7 mice during their non-regenerative stage. Subsequently, these neonatal pups will be subjected to nTAC and the cardiac function will be monitored overtime. Additionally, the cross-talk effect of these angiocrines on CMs proliferation and cytokinesis will be studies in depth.

The angiocrines with promising effects will be delivered with the same technique to adult mice. These mice will be subjected to TAC and the effect of these factors on the prevention of PO-induced cardiac remodeling will be analyzed.

In parallel, more mechanistic studies will be conducted in vitro to help understanding the downstream effects of these EC-derived angiocrines on the three main cell types. Bulk RNA sequencing as well as phosphoproteomics will be applied to ECs, CMs and FBs to further characterize downstream effectors responsible for the potential cardioprotective roles of these angiocrines.

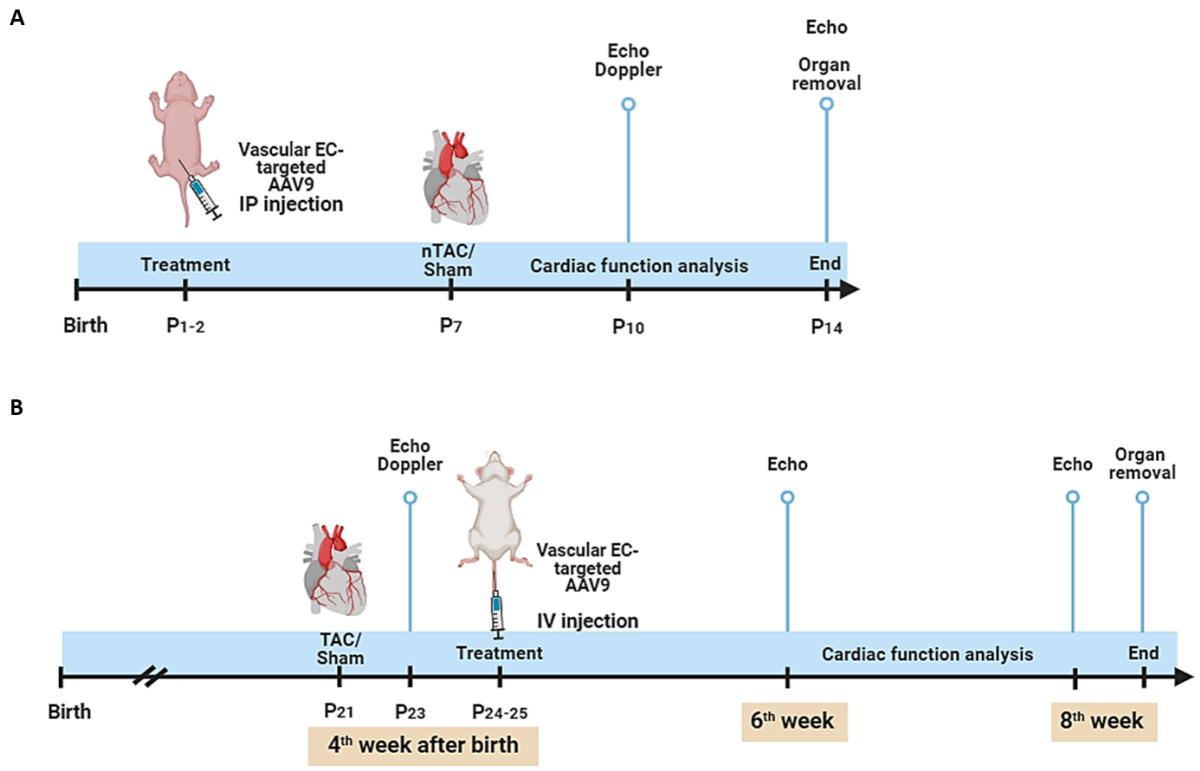

Figure 51 Future Plans: Schematic representation for in-vivo testing of pro-regenerative ligands.

(A) 1-2 days old mice will be treated with vascular EC- targeted AAV9 containing Bmp7, Apln or Nts via IP injection. nTAC will be performed in P7 mice (non-regenerating age). Cardiac functions will be followed-up with echocardiography until euthanasia and organ removal. **(B)** TAC surgery will be performed in adult mice 3-4 days before IV injection of vascular EC- targeted AAV9 containing Bmp7, Apln or Nts. Cardiac function will be monitored regularly until euthanasia and organ collection. *Illustration created by using www.biorender.com.*

11.4. Study Limitations

The main limitation faced during this study in the exclusion of the other abundant cardiac cell types, such as immune cells, pericytes and vascular smooth muscle cells. Hence, additional experimental work involving these cells needs to be further conducted.

Additionally, due to the limited capacity of the applied isolation protocol for ECs isolation after a certain age, I had to isolate ECs from murine pups at the 10th post-natal day as the latest time point. Hence, a late non-regenerative (10dp7dTAC) EC population could not be isolated using the same protocol. However, this could be compensated by performing the investigations on tissue cryosection or whole heart isolated from late non-regenerating mice.

12. Conclusion

My thesis set out an investigation about the role of endothelial cells during cardiac pressure overload in potentiating a maladaptive response in adult mice, while driving compensatory mechanisms in newborn mice.

Firstly, the comprehensive analysis of the RNA transcriptome of murine ECs, isolated during short term and chronic PO, revealed a distinct transcriptomic signature specific to each phase. Adult cardiac ECs initially adapt to increased pressure overload by transiently upregulating cell cycle and vascular genes. This finding comes in concordance with the enhanced myocardial angiogenesis observed 1-2 weeks after PO induction in adult mice. Besides, inflammatory genes' expression by ECs started as early as one week after PO induction and remained persistently elevated during the chronic stage of pressure overload. A major hallmark of my study is the transient and partial upregulation of mesenchymal genes by cardiac ECs during the first week after PO induction in adult mice. In other terms, 10-20% of ECs co-express both endothelial and matrix genes during the subacute phase of PO. This transient upregulation later returns to baseline expression during the chronic stage of PO. My results further validates the findings of other groups disputing the idea of complete transdifferentiation of ECs into fibroblasts (EndMT) upon cardiac injury, but rather a transient activation of collagen genes by ECs while maintaining their original identity. Computed interaction analysis of PO-induced ligands by endothelial cells further showed a strong involvement of ECM proteins, such as collagens and fibronectin. This latter strongly induced cardiomyocytes' hypertrophy and fibroblasts' migration in a paracrine manner. In addition, it exhibited an autocrine effect by enhancing ECs' proliferation and migration.

On the other hand, we previously showed that PO induction with nTAC in 1-day old mice (during their regenerative age) was accompanied by a strong cardiac adaptation to the injury with enhanced vascularization. Conversely, 7-days old mice (during non-regenerative age) failed to compensate to nTAC induction and showed a strong maladaptive phenotype. [35,66] In this study, my single-cell RNA transcriptome analysis of ECs, exhibiting an adaptive response to nTAC, revealed a significant enrichment of EC subpopulations associated with vasculature development and angiogenic sprouting. In addition, bioinformatic interaction analysis of ligands secreted from ECs with an adaptive phenotype shed the light on three main angiocrine factors: Bmp7, Apln and Nts. Overexpression of these factors in ECs exhibited a strong effect

on neighboring co-cultured cardiomyocytes by significantly boosting their proliferation and contractility in a paracrine manner. Moreover, these EC-secreted candidates enhanced vasculature coverage and endothelial function in monolayer cell culture systems as well as in 3D cardiac organoids in an autocrine manner. Collectively, my findings underscore a novel EC-derived interaction with cardiomyocytes in neonates through the expression of Bmp7, Apln, and Nts, which may drive the primary adaptive phenotype of ECs in response to nTAC in P1 mice. Additionally, ECs with an adaptive response to PO downregulate the expression of the inflammatory gene *Ccl21*. The overexpression of this factor in ECs significantly reduced cardiomyocytes' contractility and proliferation. These observations suggest potentially novel roles for these angiocrine factors in facilitating a compensatory mechanism to cardiac pressure overload.

Taken together, my findings reported in this study highlight the pivotal role of endothelial cells in intracardiac communication by secreting pro-regenerative angiocrine factors and matrix proteins during cardiac compensation and maladaptive remodeling to pressure overload, respectively. Re-directing the EC transcriptome toward adaptive signaling could offer promising therapeutic potential for heart failure in the future.

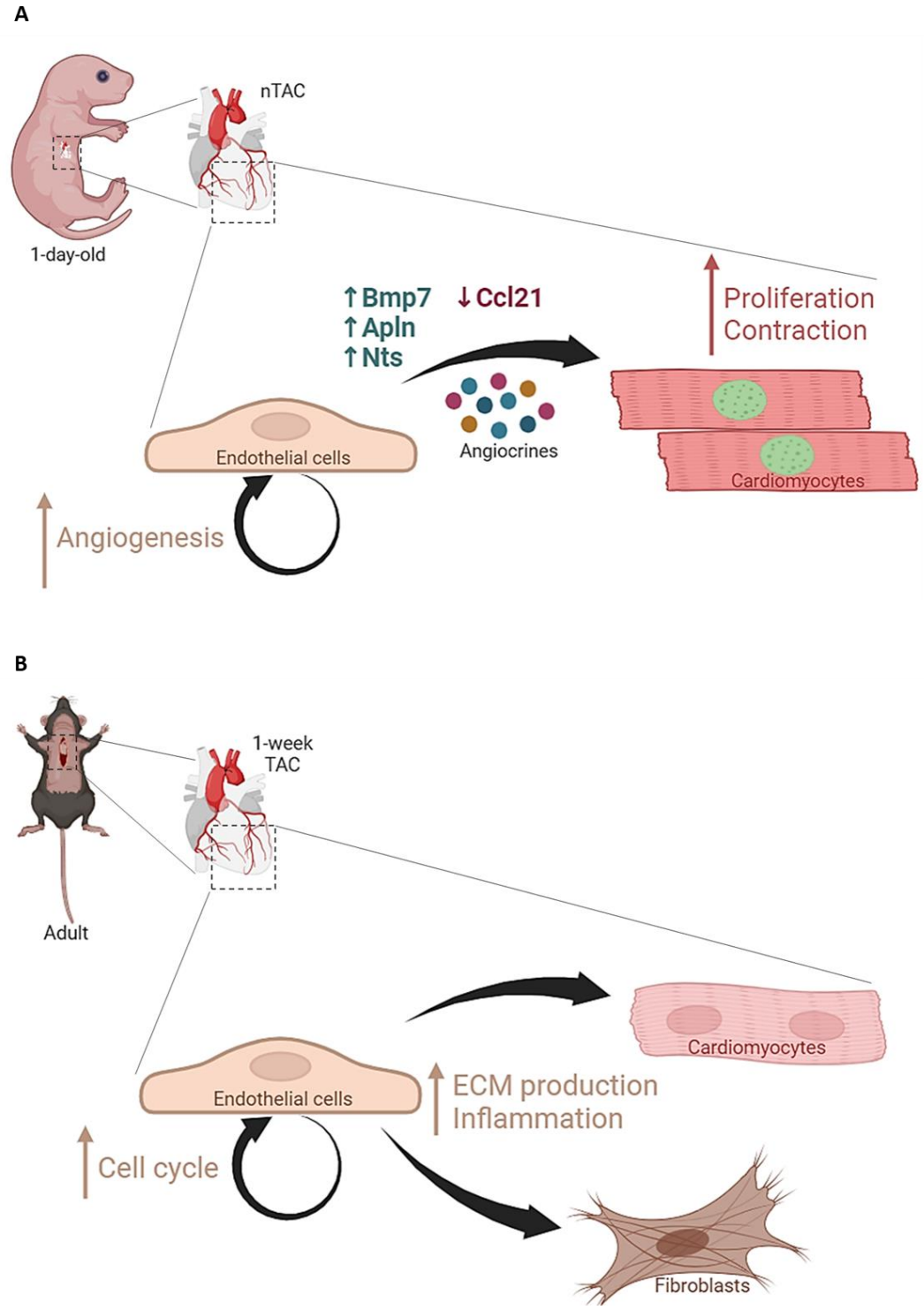

Figure 52 Schematic summary.

(A) Upon pressure overload induction in 1-day-old mice (P1, regenerating age) through nTAC, cardiac endothelial cells secrete the angiocrines Bmp7, Apln and Nts into their surrounding milieu. These factors enhance cardiomyocytes' proliferation and contractility, in addition to enhancing angiogenesis in an autocrine manner. **(B)** During the subacute phase of pressure overload in adult mice, endothelial cells transiently increase genes related to matrix production, inflammation and cell cycle. The alterations exert a significant effect on neighboring cells, mainly cardiomyocytes and fibroblasts. *Illustration created by using www.biorender.com.*

References

1. Cardiovascular diseases (CVDs). 2021; https://www.who.int/news-room/fact-sheets/detail/cardiovascular-diseases-(cvds).
2. Heart Diseases Prevalence. 2024; https://www.cdc.gov/heart-disease/data-research/facts-stats/?CDC_AAref_Val=https://www.cdc.gov/heartdisease/facts.htm.
3. Tsao CW, Aday AW, Almarzooq ZI, et al. Heart Disease and Stroke Statistics—2023 Update: A Report From the American Heart Association. *Circulation.* 2023;147(8):e93-e621.
4. Mosca L, Benjamin EJ, Berra K, et al. Effectiveness-Based Guidelines for the Prevention of Cardiovascular Disease in Women—2011 Update. *Circulation.* 2011;123(11):1243-1262.
5. Gilboa SM, Devine OJ, Kucik JE, et al. Congenital Heart Defects in the United States. *Circulation.* 2016;134(2):101-109.
6. Kavey R-EW, Daniels SR, Lauer RM, Atkins DL, Hayman LL, Taubert K. American Heart Association Guidelines for Primary Prevention of Atherosclerotic Cardiovascular Disease Beginning in Childhood. *Circulation.* 2003;107(11):1562-1566.
7. Savarese G, Lund LH. Global Public Health Burden of Heart Failure. *Card Fail Rev.* 2017;3(1):7-11.
8. Ponikowski P, Voors AA, Anker SD, et al. 2016 ESC Guidelines for the diagnosis and treatment of acute and chronic heart failure: The Task Force for the diagnosis and treatment of acute and chronic heart failure of the European Society of Cardiology (ESC)Developed with the special contribution of the Heart Failure Association (HFA) of the ESC. *European Heart Journal.* 2016;37(27):2129-2200.
9. Borlaug BA, Redfield MM. Diastolic and Systolic Heart Failure Are Distinct Phenotypes Within the Heart Failure Spectrum. *Circulation.* 2011;123(18):2006-2014.
10. Andersen MJ, Borlaug BA. Heart Failure with Preserved Ejection Fraction: Current Understandings and Challenges. *Current Cardiology Reports.* 2014;16(7):501.
11. Authors/Task Force M, McMurray JJV, Adamopoulos S, et al. ESC Guidelines for the diagnosis and treatment of acute and chronic heart failure 2012: The Task Force for the Diagnosis and Treatment of Acute and Chronic Heart Failure 2012 of the European Society of Cardiology. Developed in collaboration with the Heart Failure Association (HFA) of the ESC. *European Heart Journal.* 2012;33(14):1787-1847.
12. Mann DL, Felker GM. Mechanisms and Models in Heart Failure: A Translational Approach. *Circ Res.* 2021;128(10):1435-1450.
13. Ziaeian B, Fonarow G. Epidemiology and aetiology of heart failure. *Nature reviews Cardiology.* 2016;13.
14. Drazner MH. The Progression of Hypertensive Heart Disease. *Circulation.* 2011;123(3):327-334.
15. Heineke J, Molkentin JD. Regulation of cardiac hypertrophy by intracellular signalling pathways. *Nature Reviews Molecular Cell Biology.* 2006;7(8):589-600.
16. Carabello BA, Paulus WJ. Aortic stenosis. *The Lancet.* 2009;373(9667):956-966.
17. Vogelgesang A, Hasenfuss G, Jacobshagen C. Low-flow/low-gradient aortic stenosis-Still a diagnostic and therapeutic challenge. *Clin Cardiol.* 2017;40(9):654-659.
18. Puls M, Beuthner BE, Topci R, et al. Impact of myocardial fibrosis on left ventricular remodelling, recovery, and outcome after transcatheter aortic valve implantation in different haemodynamic subtypes of severe aortic stenosis. *European Heart Journal.* 2020;41(20):1903-1914.
19. Cuspidi C, Sala C, Negri F, Mancia G, Morganti A, on behalf of the Italian Society of H. Prevalence of left-ventricular hypertrophy in hypertension: an updated review of echocardiographic studies. *Journal of Human Hypertension.* 2012;26(6):343-349.
20. Hein S, Arnon E, Kostin S, et al. Progression From Compensated Hypertrophy to Failure in the Pressure-Overloaded Human Heart. *Circulation.* 2003;107(7):984-991.
21. Pinto AR, Ilinykh A, Ivey MJ, et al. Revisiting Cardiac Cellular Composition. *Circulation Research.* 2016;118(3):400-409.

22. Schiattarella GG, Hill JA. Inhibition of Hypertrophy Is a Good Therapeutic Strategy in Ventricular Pressure Overload. *Circulation.* 2015;131(16):1435-1447.
23. Nakamura M, Sadoshima J. Mechanisms of physiological and pathological cardiac hypertrophy. *Nature Reviews Cardiology.* 2018;15(7):387-407.
24. Burch GE, Ray CT, Cronvich JA. The George Fahr Lecture. *Circulation.* 1952;5(4):504-513.
25. Frey N, Katus HA, Olson EN, Hill JA. Hypertrophy of the Heart. *Circulation.* 2004;109(13):1580-1589.
26. Malek Mohammadi M, Kattih B, Grund A, et al. The transcription factor GATA4 promotes myocardial regeneration in neonatal mice. *EMBO Molecular Medicine.* 2017;9(2):265-279-279.
27. Toischer K, Zhu W, Hünlich M, et al. Cardiomyocyte proliferation prevents failure in pressure overload but not volume overload. *The Journal of Clinical Investigation.* 2017;127(12):4285-4296.
28. Bergmann O, Bhardwaj RD, Bernard S, et al. Evidence for Cardiomyocyte Renewal in Humans. *Science.* 2009;324(5923):98-102.
29. Secco I, Giacca M. Regulation of endogenous cardiomyocyte proliferation: The known unknowns. *Journal of Molecular and Cellular Cardiology.* 2023;179:80-89.
30. Porrello ER, Mahmoud AI, Simpson E, et al. Transient Regenerative Potential of the Neonatal Mouse Heart. *Science.* 2011;331(6020):1078-1080.
31. Zhu W, Zhang E, Zhao M, et al. Regenerative Potential of Neonatal Porcine Hearts. *Circulation.* 2018;138(24):2809-2816.
32. Ye L, D'Agostino G, Loo SJ, et al. Early Regenerative Capacity in the Porcine Heart. *Circulation.* 2018;138(24):2798-2808.
33. Senyo SE, Steinhauser ML, Pizzimenti CL, et al. Mammalian heart renewal by pre-existing cardiomyocytes. *Nature.* 2013;493(7432):433-436.
34. Bersell K, Arab S, Haring B, Kühn B. Neuregulin1/ErbB4 Signaling Induces Cardiomyocyte Proliferation and Repair of Heart Injury. *Cell.* 2009;138(2):257-270.
35. Malek Mohammadi M, Abouissa A, Azizah I, et al. Induction of cardiomyocyte proliferation and angiogenesis protects neonatal mice from pressure overload–associated maladaptation. *JCI Insight.* 2019;4(16).
36. Breckwoldt K, Weinberger F, Eschenhagen T. Heart regeneration. *Biochimica et Biophysica Acta (BBA) - Molecular Cell Research.* 2016;1863(7, Part B):1749-1759.
37. Mia MM, Singh MK. The Hippo Signaling Pathway in Cardiac Development and Diseases. *Frontiers in Cell and Developmental Biology.* 2019;7.
38. Wang J, Liu S, Heallen T, Martin JF. The Hippo pathway in the heart: pivotal roles in development, disease, and regeneration. *Nature Reviews Cardiology.* 2018;15(11):672-684.
39. Fu M, Hu Y, Lan T, Guan K-L, Luo T, Luo M. The Hippo signalling pathway and its implications in human health and diseases. *Signal Transduction and Targeted Therapy.* 2022;7(1):376.
40. Heallen T, Morikawa Y, Leach J, et al. Hippo signaling impedes adult heart regeneration. *Development.* 2013;140(23):4683-4690.
41. Lin Z, von Gise A, Zhou P, et al. Cardiac-Specific YAP Activation Improves Cardiac Function and Survival in an Experimental Murine MI Model. *Circulation Research.* 2014;115(3):354-363.
42. Del Re DP, Matsuda T, Zhai P, et al. Proapoptotic Rassf1A/Mst1 signaling in cardiac fibroblasts is protective against pressure overload in mice. *J Clin Invest.* 2010;120(10):3555-3567.
43. Xin M, Kim Y, Sutherland LB, et al. Regulation of insulin-like growth factor signaling by Yap governs cardiomyocyte proliferation and embryonic heart size. *Sci Signal.* 2011;4(196):ra70.
44. Talman V, Ruskoaho H. Cardiac fibrosis in myocardial infarction-from repair and remodeling to regeneration. *Cell Tissue Res.* 2016;365(3):563-581.
45. Gutiérrez E, Flammer AJ, Lerman LO, Elízaga J, Lerman A, Fernández-Avilés F. Endothelial dysfunction over the course of coronary artery disease. *European Heart Journal.* 2013;34(41):3175-3181.
46. Davignon J, Ganz P. Role of Endothelial Dysfunction in Atherosclerosis. *Circulation.* 2004;109(23_suppl_1):III-27-III-32.

47. Münzel T, Daiber A, Gori T. More answers to the still unresolved question of nitrate tolerance. *European Heart Journal.* 2013;34(34):2666-2673.
48. Landmesser U, Harrison DG. Oxidative stress and vascular damage in hypertension. *Coronary Artery Disease.* 2001;12(6).
49. Sano M, Minamino T, Toko H, et al. p53-induced inhibition of Hif-1 causes cardiac dysfunction during pressure overload. *Nature.* 2007;446(7134):444-448.
50. Mohammed SF, Hussain S, Mirzoyev SA, Edwards WD, Maleszewski JJ, Redfield MM. Coronary Microvascular Rarefaction and Myocardial Fibrosis in Heart Failure With Preserved Ejection Fraction. *Circulation.* 2015;131(6):550-559.
51. Carmeliet P. Angiogenesis in health and disease. *Nature Medicine.* 2003;9(6):653-660.
52. Marchant DJ, Boyd JH, Lin DC, et al. Inflammation in Myocardial Diseases. *Circulation Research.* 2012;110(1):126-144.
53. Zeisberg M, Kalluri R. Cellular Mechanisms of Tissue Fibrosis. 1. Common and organ-specific mechanisms associated with tissue fibrosis. *American Journal of Physiology-Cell Physiology.* 2012;304(3):C216-C225.
54. Trogisch FA, Abouissa A, Keles M, et al. Endothelial cells drive organ fibrosis in mice by inducing expression of the transcription factor SOX9. *Science Translational Medicine.* 2024;16(736):eabq4581.
55. Tombor LS, John D, Glaser SF, et al. Single cell sequencing reveals endothelial plasticity with transient mesenchymal activation after myocardial infarction. *Nature Communications.* 2021;12(1):681.
56. Travers JG, Kamal FA, Robbins J, Yutzey KE, Blaxall BC. Cardiac Fibrosis. *Circulation Research.* 2016;118(6):1021-1040.
57. Kong P, Christia P, Frangogiannis NG. The pathogenesis of cardiac fibrosis. *Cellular and Molecular Life Sciences.* 2014;71(4):549-574.
58. Khalil H, Kanisicak O, Prasad V, et al. Fibroblast-specific TGF-β–Smad2/3 signaling underlies cardiac fibrosis. *The Journal of Clinical Investigation.* 2017;127(10):3770-3783.
59. Fan D, Takawale A, Lee J, Kassiri Z. Cardiac fibroblasts, fibrosis and extracellular matrix remodeling in heart disease. *Fibrogenesis & Tissue Repair.* 2012;5(1):15.
60. Goldsmith EC, Bradshaw AD, Zile MR, Spinale FG. Myocardial fibroblast–matrix interactions and potential therapeutic targets. *Journal of Molecular and Cellular Cardiology.* 2014;70:92-99.
61. Li F, Wang X, Capasso JM, Gerdes AM. Rapid Transition of Cardiac Myocytes from Hyperplasia to Hypertrophy During Postnatal Development. *Journal of Molecular and Cellular Cardiology.* 1996;28(8):1737-1746.
62. Mahmoud AI, Porrello ER, Kimura W, Olson EN, Sadek HA. Surgical models for cardiac regeneration in neonatal mice. *Nature Protocols.* 2014;9(2):305-311.
63. Haubner BJ, Schuetz T, Penninger JM. A reproducible protocol for neonatal ischemic injury and cardiac regeneration in neonatal mice. *Basic Research in Cardiology.* 2016;111(6):64.
64. Blom JN, Lu X, Arnold P, Feng Q. Myocardial Infarction in Neonatal Mice, A Model of Cardiac Regeneration. *JoVE.* 2016(111):e54100.
65. Darehzereshki A, Rubin N, Gamba L, et al. Differential regenerative capacity of neonatal mouse hearts after cryoinjury. *Developmental Biology.* 2015;399(1):91-99.
66. Malek Mohammadi M, Abouissa A, Heineke J. A surgical mouse model of neonatal pressure overload by transverse aortic constriction. *Nature Protocols.* 2021;16(2):775-790.
67. Rockman HA, Ross RS, Harris AN, et al. Segregation of atrial-specific and inducible expression of an atrial natriuretic factor transgene in an in vivo murine model of cardiac hypertrophy. *Proceedings of the National Academy of Sciences.* 1991;88(18):8277-8281.
68. Grund A, Szaroszyk M, Korf-Klingebiel M, et al. TIP30 counteracts cardiac hypertrophy and failure by inhibiting translational elongation. *EMBO Molecular Medicine.* 2019;11(10):e10018.
69. Sahara M. Recent Advances in Generation of In Vitro Cardiac Organoids. *International Journal of Molecular Sciences.* 2023;24(7).

70. Wagner JUG, Pham MD, Nicin L, et al. Dissection of heterocellular cross-talk in vascularized cardiac tissue mimetics. *Journal of Molecular and Cellular Cardiology.* 2020;138:269-282.
71. Grune T, Ott C, Häseli S, Höhn A, Jung T. The "MYOCYTER" – Convert cellular and cardiac contractions into numbers with ImageJ. *Scientific Reports.* 2019;9(1):15112.
72. Ovchinnikova S, Anders S. Exploring dimension-reduced embeddings with Sleepwalk. *Genome Research.* 2020;30(5):749-756.
73. Babyplots R Package. https://bp.bleb.li/documentation/r.
74. Froese N, Cordero J, Abouissa A, et al. Analysis of myocardial cellular gene expression during pressure overload reveals matrix based functional intercellular communication. *iScience.* 2022;25(3):103965.
75. Lewis-Israeli YR, Wasserman AH, Aguirre A. Heart Organoids and Engineered Heart Tissues: Novel Tools for Modeling Human Cardiac Biology and Disease. *Biomolecules.* 2021;11.
76. Wang L, Yu P, Zhou B, et al. Single-cell reconstruction of the adult human heart during heart failure and recovery reveals the cellular landscape underlying cardiac function. *Nature Cell Biology.* 2020;22(1):108-119.
77. Cleuren ACA, van der Ent MA, Jiang H, et al. The in vivo endothelial cell translatome is highly heterogeneous across vascular beds. *Proceedings of the National Academy of Sciences.* 2019;116(47):23618-23624.
78. Farbehi N, Patrick R, Dorison A, et al. Single-cell expression profiling reveals dynamic flux of cardiac stromal, vascular and immune cells in health and injury. *eLife.* 2019;8:e43882.
79. Skelly DA, Squiers GT, McLellan MA, et al. Single-Cell Transcriptional Profiling Reveals Cellular Diversity and Intercommunication in the Mouse Heart. *Cell Reports.* 2018;22(3):600-610.
80. Heineke J, Auger-Messier M, Xu J, et al. Cardiomyocyte GATA4 functions as a stress-responsive regulator of angiogenesis in the murine heart. *The Journal of Clinical Investigation.* 2007;117(11):3198-3210.
81. Izumiya Y, Shiojima I, Sato K, Sawyer DB, Colucci WS, Walsh K. Vascular Endothelial Growth Factor Blockade Promotes the Transition From Compensatory Cardiac Hypertrophy to Failure in Response to Pressure Overload. *Hypertension.* 2006;47(5):887-893.
82. Kanisicak O, Khalil H, Ivey MJ, et al. Genetic lineage tracing defines myofibroblast origin and function in the injured heart. *Nature Communications.* 2016;7(1):12260.
83. Moore-Morris T, Guimarães-Camboa N, Banerjee I, et al. Resident fibroblast lineages mediate pressure overload–induced cardiac fibrosis. *The Journal of Clinical Investigation.* 2014;124(7):2921-2934.
84. Manavski Y, Lucas T, Glaser SF, et al. Clonal Expansion of Endothelial Cells Contributes to Ischemia-Induced Neovascularization. *Circulation Research.* 2018;122(5):670-677.
85. Gan X, Ramesh L, Nair N, Sundararaman A. Fibronectin Fibrillogenesis During Angiogenesis. In: Papadimitriou E, Mikelis CM, eds. *Matrix Pathobiology and Angiogenesis.* Cham: Springer International Publishing; 2023:1-27.
86. Zhou F, Sun J, Ye L, et al. Fibronectin promotes tumor angiogenesis and progression of non-small-cell lung cancer by elevating WISP3 expression via FAK/MAPK/ HIF-1α axis and activating wnt signaling pathway. *Experimental Hematology & Oncology.* 2023;12(1):61.
87. Konstandin MH, Völkers M, Collins B, et al. Fibronectin contributes to pathological cardiac hypertrophy but not physiological growth. *Basic Research in Cardiology.* 2013;108(5):375.
88. Valiente-Alandi I, Potter SJ, Salvador AM, et al. Inhibiting Fibronectin Attenuates Fibrosis and Improves Cardiac Function in a Model of Heart Failure. *Circulation.* 2018;138(12):1236-1252.
89. Quaife-Ryan GA, Sim CB, Ziemann M, et al. Multicellular Transcriptional Analysis of Mammalian Heart Regeneration. *Circulation.* 2017;136(12):1123-1139.
90. Fan Y, Cheng Y, Li Y, et al. Phosphoproteomic Analysis of Neonatal Regenerative Myocardium Revealed Important Roles of Checkpoint Kinase 1 via Activating Mammalian Target of Rapamycin C1/Ribosomal Protein S6 Kinase b-1 Pathway. *Circulation.* 2020;141(19):1554-1569.
91. Wang Z, Cui M, Shah AM, et al. Mechanistic basis of neonatal heart regeneration revealed by transcriptome and histone modification profiling. *Proceedings of the National Academy of Sciences.* 2019;116(37):18455-18465.

92. Wang M, Hu S, Nie Y, Song J. Proteomic profiling of key transcription factors in the process of neonatal mouse cardiac regeneration capacity loss. *Cell Biology International.* 2019;43(12):1435-1442.
93. Wang Z, Cui M, Shah AM, et al. Cell-Type-Specific Gene Regulatory Networks Underlying Murine Neonatal Heart Regeneration at Single-Cell Resolution. *Cell Reports.* 2020;33(10):108472.
94. Cui M, Wang Z, Chen K, et al. Dynamic Transcriptional Responses to Injury of Regenerative and Non-regenerative Cardiomyocytes Revealed by Single-Nucleus RNA Sequencing. *Developmental Cell.* 2020;53(1):102-116.e108.
95. Long H, Steimle JD, Grisanti Canozo FJ, et al. Endothelial cells adopt a pro-reparative immune responsive signature during cardiac injury. *Life Science Alliance.* 2024;7(2):e202201870.
96. Malektaj H, Nour S, Imani R, Siadati MH. Angiogenesis induction as a key step in cardiac tissue Regeneration: From angiogenic agents to biomaterials. *International Journal of Pharmaceutics.* 2023;643:123233.
97. Marín-Juez R, El-Sammak H, Helker CSM, et al. Coronary Revascularization During Heart Regeneration Is Regulated by Epicardial and Endocardial Cues and Forms a Scaffold for Cardiomyocyte Repopulation. *Developmental Cell.* 2019;51(4):503-515.e504.
98. Marín-Juez R, Marass M, Gauvrit S, et al. Fast revascularization of the injured area is essential to support zebrafish heart regeneration. *Proceedings of the National Academy of Sciences.* 2016;113(40):11237-11242.
99. Ptashne M, Gann A. Transcriptional activation by recruitment. *Nature.* 1997;386(6625):569-577.
100. Zhao L, Yu Y. Editorial: Transcription factors in cardiovascular development and remodeling. *Front Cell Dev Biol.* 2023;11:1225947.
101. Potente M, Urbich C, Sasaki K-i, et al. Involvement of Foxo transcription factors in angiogenesis and postnatal neovascularization. *The Journal of Clinical Investigation.* 2005;115(9):2382-2392.
102. Li Y, Li Z, Zhang C, et al. Cardiac Fibroblast–Specific Activating Transcription Factor 3 Protects Against Heart Failure by Suppressing MAP2K3-p38 Signaling. *Circulation.* 2017;135(21):2041-2057.
103. Dittrich GM, Froese N, Wang X, et al. Fibroblast GATA-4 and GATA-6 promote myocardial adaptation to pressure overload by enhancing cardiac angiogenesis. *Basic Research in Cardiology.* 2021;116(1):26.
104. Yamada Y, Pannell R, Forster A, Rabbitts TH. The oncogenic LIM-only transcription factor Lmo2 regulates angiogenesis but not vasculogenesis in mice. *Proceedings of the National Academy of Sciences.* 2000;97(1):320-324.
105. Kappel A, Schlaeger TM, Flamme I, Orkin SH, Risau W, Breier G. Role of SCL/Tal-1, GATA, and Ets transcription factor binding sites for the regulation of Flk-1 expression during murine vascular development. *Blood.* 2000;96(9):3078-3085.
106. El Omari K, Hoosdally SJ, Tuladhar K, et al. Structure of the leukemia oncogene LMO2: implications for the assembly of a hematopoietic transcription factor complex. *Blood.* 2011;117(7):2146-2156.
107. Wadman IA, Osada H, Grütz GG, et al. The LIM-only protein Lmo2 is a bridging molecule assembling an erythroid, DNA-binding complex which includes the TAL1, E47, GATA-1 and Ldb1/NLI proteins. *The EMBO Journal.* 1997;16(11):3145-3157-3157.
108. Yamada Y, Zhong Y, Miki S, Taura A, Rabbitts TH. The transcription factor complex LMO2/TAL1 regulates branching and endothelial cell migration in sprouting angiogenesis. *Scientific Reports.* 2022;12(1):7226.
109. Deleuze V, Chalhoub E, El-Hajj R, et al. TAL-1/SCL and Its Partners E47 and LMO2 Up-Regulate VE-Cadherin Expression in Endothelial Cells. *Molecular and Cellular Biology.* 2007;27(7):2687-2697.
110. Coma S, Allard-Ratick M, Akino T, van Meeteren LA, Mammoto A, Klagsbrun M. GATA2 and Lmo2 control angiogenesis and lymphangiogenesis via direct transcriptional regulation of neuropilin-2. *Angiogenesis.* 2013;16(4):939-952.

111. Deleuze V, El-Hajj R, Chalhoub E, et al. Angiopoietin-2 Is a Direct Transcriptional Target of TAL1, LYL1 and LMO2 in Endothelial Cells. *PLOS ONE.* 2012;7(7):e40484.
112. Choi H-J, Rho S-S, Choi D-H, Kwon Y-G. LDB2 regulates the expression of DLL4 through the formation of oligomeric complexes in endothelial cells. *BMB Rep.* 2018;51(1):21-26.
113. Santoyo-Suarez MG, Mares-Montemayor JD, Padilla-Rivas GR, et al. The Involvement of Krüppel-like Factors in Cardiovascular Diseases. *Life (Basel).* 2023;13(2).
114. Wang Y, Yang C, Gu Q, et al. KLF4 Promotes Angiogenesis by Activating VEGF Signaling in Human Retinal Microvascular Endothelial Cells. *PLOS ONE.* 2015;10(6):e0130341.
115. Sweet DR, Padmanabhan R, Liao X, et al. Krüppel-Like Factors Orchestrate Endothelial Gene Expression Through Redundant and Non-Redundant Enhancer Networks. *J Am Heart Assoc.* 2023;12(4):e024303.
116. Yang H, Xi X, Zhao B, Su Z, Wang Z. KLF4 protects brain microvascular endothelial cells from ischemic stroke induced apoptosis by transcriptionally activating MALAT1. *Biochemical and Biophysical Research Communications.* 2018;495(3):2376-2382.
117. Zhang X, Wang L, Han Z, et al. KLF4 alleviates cerebral vascular injury by ameliorating vascular endothelial inflammation and regulating tight junction protein expression following ischemic stroke. *Journal of Neuroinflammation.* 2020;17(1):107.
118. Wang D, Zhao Y, Zhou Y, Yang S, Xiao X, Feng L. Angiogenesis—An Emerging Role in Organ Fibrosis. *International Journal of Molecular Sciences.* 2023;24(18).
119. François M, Caprini A, Hosking B, et al. Sox18 induces development of the lymphatic vasculature in mice. *Nature.* 2008;456(7222):643-647.
120. Darby IA, Bisucci T, Raghoenath S, Olsson J, Muscat GEO, Koopman P. Sox18 Is Transiently Expressed during Angiogenesis in Granulation Tissue of Skin Wounds with an Identical Expression Pattern to Flk-1 mRNA. *Laboratory Investigation.* 2001;81(7):937-943.
121. Matsui T, Kanai-Azuma M, Hara K, et al. Redundant roles of Sox17 and Sox18 in postnatal angiogenesis in mice. *Journal of Cell Science.* 2006;119(17):3513-3526.
122. Ribeiro I, Kawakami Y, Büscher D, et al. Tbx2 and Tbx3 Regulate the Dynamics of Cell Proliferation during Heart Remodeling. *PLOS ONE.* 2007;2(4):e398.
123. Khan SF, Damerell V, Omar R, et al. The roles and regulation of TBX3 in development and disease. *Gene.* 2020;726:144223.
124. Graveline R, Marcinkiewicz K, Choi S, et al. The Chromatin-Associated Phf12 Protein Maintains Nucleolar Integrity and Prevents Premature Cellular Senescence. *Mol Cell Biol.* 2017;37(5).
125. Thompson M, Sakabe M, Verba M, et al. PRDM16 regulates arterial development and vascular integrity. *Frontiers in Physiology.* 2023;14.
126. Talman V, Kivelä R. Cardiomyocyte—Endothelial Cell Interactions in Cardiac Remodeling and Regeneration. *Frontiers in Cardiovascular Medicine.* 2018;5.
127. Ding B-S, Cao Z, Lis R, et al. Divergent angiocrine signals from vascular niche balance liver regeneration and fibrosis. *Nature.* 2014;505(7481):97-102.
128. Ding B-S, Nolan Daniel J, Guo P, et al. Endothelial-Derived Angiocrine Signals Induce and Sustain Regenerative Lung Alveolarization. *Cell.* 2011;147(3):539-553.
129. Kobayashi H, Butler JM, O'Donnell R, et al. Angiocrine factors from Akt-activated endothelial cells balance self-renewal and differentiation of haematopoietic stem cells. *Nature Cell Biology.* 2010;12(11):1046-1056.
130. McMullen JR, Shioi T, Huang W-Y, et al. The Insulin-like Growth Factor 1 Receptor Induces Physiological Heart Growth via the Phosphoinositide 3-Kinase(p110α) Pathway *. *Journal of Biological Chemistry.* 2004;279(6):4782-4793.
131. Troncoso R, Ibarra C, Vicencio JM, Jaimovich E, Lavandero S. New insights into IGF-1 signaling in the heart. *Trends in Endocrinology & Metabolism.* 2014;25(3):128-137.
132. Macvanin M, Gluvic Z, Radovanovic J, Essack M, Gao X, Isenovic ER. New insights on the cardiovascular effects of IGF-1. *Frontiers in Endocrinology.* 2023;14.
133. Abubakar M, Rasool HF, Javed I, et al. Comparative Roles of IL-1, IL-6, IL-10, IL-17, IL-18, 1L-22, IL-33, and IL-37 in Various Cardiovascular Diseases With Potential Insights for Targeted Immunotherapy. *Cureus.* 2023;15(7):e42494.

134. Meléndez GC, McLarty JL, Levick SP, Du Y, Janicki JS, Brower GL. Interleukin 6 Mediates Myocardial Fibrosis, Concentric Hypertrophy, and Diastolic Dysfunction in Rats. *Hypertension.* 2010;56(2):225-231.
135. Alter C, Henseler AS, Owenier C, et al. IL-6 in the infarcted heart is preferentially formed by fibroblasts and modulated by purinergic signaling. *J Clin Invest.* 2023;133(11).
136. Tanaka T, Narazaki M, Kishimoto T. Interleukin (IL-6) Immunotherapy. *Cold Spring Harbor Perspectives in Biology.* 2018;10(8):a028456.
137. Mayfield AE, Kanda P, Nantsios A, et al. Interleukin-6 Mediates Post-Infarct Repair by Cardiac Explant-Derived Stem Cells. *Theranostics.* 2017;7(19):4850-4861.
138. Su J-H, Luo M-Y, Liang N-, et al. Interleukin-6: A Novel Target for Cardio-Cerebrovascular Diseases. *Frontiers in Pharmacology.* 2021;12.
139. Alter C, Henseler A-S, Owenier C, et al. IL-6 in the infarcted heart is preferentially formed by fibroblasts and modulated by purinergic signaling. *The Journal of Clinical Investigation.* 2023;133(11).
140. Tian M, Yuan Y-C, Li J-Y, Gionfriddo MR, Huang R-C. Tumor necrosis factor-α and its role as a mediator in myocardial infarction: A brief review. *Chronic Diseases and Translational Medicine.* 2015;1(1):18-26.
141. Qian Y, Mao M, Nian F. The Effect of TNF-α on CHD and the Relationship between TNF-α Antagonist and CHD in Rheumatoid Arthritis: A Systematic Review. *Cardiology Research and Practice.* 2022;2022(1):6192053.
142. Sieber C, Kopf J, Hiepen C, Knaus P. Recent advances in BMP receptor signaling. *Cytokine & Growth Factor Reviews.* 2009;20(5):343-355.
143. Kawabata M, Imamura T, Miyazono K. Signal transduction by bone morphogenetic proteins. *Cytokine & Growth Factor Reviews.* 1998;9(1):49-61.
144. Aluganti Narasimhulu C, Singla DK. The Role of Bone Morphogenetic Protein 7 (BMP-7) in Inflammation in Heart Diseases. *Cells.* 2020;9(2):280.
145. Luo G, Hofmann C, Bronckers AL, Sohocki M, Bradley A, Karsenty G. BMP-7 is an inducer of nephrogenesis, and is also required for eye development and skeletal patterning. *Genes & Development.* 1995;9(22):2808-2820.
146. Israel DI, Nove J, Kerns KM, et al. Heterodimeric Bone Morphogenetic Proteins Show Enhanced Activity In Vitro and In Vivo. *Growth Factors.* 1996;13(3-4):291-300.
147. Agnew C, Ayaz P, Kashima R, et al. Structural basis for ALK2/BMPR2 receptor complex signaling through kinase domain oligomerization. *Nature Communications.* 2021;12(1):4950.
148. Boon MR, van der Horst G, van der Pluijm G, Tamsma JT, Smit JWA, Rensen PCN. Bone morphogenetic protein 7: A broad-spectrum growth factor with multiple target therapeutic potency. *Cytokine & Growth Factor Reviews.* 2011;22(4):221-229.
149. Ye D, Liu Y, Pan H, et al. Insights into bone morphogenetic proteins in cardiovascular diseases. *Frontiers in Pharmacology.* 2023;14.
150. Rocher C, Singla R, Singal PK, Parthasarathy S, Singla DK. Bone morphogenetic protein 7 polarizes THP-1 cells into M2 macrophages. *Canadian Journal of Physiology and Pharmacology.* 2012;90(7):947-951.
151. Rocher C, Singla DK. SMAD-PI3K-Akt-mTOR Pathway Mediates BMP-7 Polarization of Monocytes into M2 Macrophages. *PLOS ONE.* 2013;8(12):e84009.
152. Singla DK, Singla R, Wang J. BMP-7 Treatment Increases M2 Macrophage Differentiation and Reduces Inflammation and Plaque Formation in Apo E-/- Mice. *PLOS ONE.* 2016;11(1):e0147897.
153. Giannarelli C, Fernandez DM. Manipulating Macrophage Polarization to Fix the Broken Heart: Challenges and Hopes∗. *Journal of the American College of Cardiology.* 2018;72(8):905-907.
154. Nikiforov NG, Wetzker R, Kubekina MV, Petukhova AV, Kirichenko TV, Orekhov AN. Trained Circulating Monocytes in Atherosclerosis: Ex Vivo Model Approach. *Frontiers in Pharmacology.* 2019;10.

155. Wang W, Hu Y-F, Pang M, et al. BMP and Notch Signaling Pathways differentially regulate Cardiomyocyte Proliferation during Ventricle Regeneration. *International Journal of Biological Sciences.* 2021;17(9):2157-2166.
156. Jin Y, Cheng X, Lu J, Li X. Exogenous BMP-7 Facilitates the Recovery of Cardiac Function after Acute Myocardial Infarction through Counteracting TGF-β1 Signaling Pathway. *The Tohoku Journal of Experimental Medicine.* 2018;244(1):1-6.
157. Wu C-C, Kruse F, Vasudevarao MD, et al. Spatially Resolved Genome-wide Transcriptional Profiling Identifies BMP Signaling as Essential Regulator of Zebrafish Cardiomyocyte Regeneration. *Developmental Cell.* 2016;36(1):36-49.
158. Bongiovanni C, Bueno-Levy H, Posadas Pena D, et al. BMP7 promotes cardiomyocyte regeneration in zebrafish and adult mice. *Cell Reports.* 2024;43(5).
159. Merino D, Villar AV, García R, et al. BMP-7 attenuates left ventricular remodelling under pressure overload and facilitates reverse remodelling and functional recovery. *Cardiovascular Research.* 2016;110(3):331-345.
160. Deckers MML, van Bezooijen RL, van der Horst G, et al. Bone Morphogenetic Proteins Stimulate Angiogenesis through Osteoblast-Derived Vascular Endothelial Growth Factor A. *Endocrinology.* 2002;143(4):1545-1553.
161. Janusz J, Janusz A, Kondera-Anasz Z, et al. Participation of Selected Soluble BMP-2 and BMP-7 Bone Morphogenetic Proteins and Their Soluble Type I ALK-1 and Type II BMPR2 Receptors in Formation and Development of Endometriosis. *Biomedicines.* 2021;9(10):1292.
162. Akiyama I, Yoshino O, Osuga Y, et al. Bone Morphogenetic Protein 7 Increased Vascular Endothelial Growth Factor (VEGF)-A Expression in Human Granulosa Cells and VEGF Receptor Expression in Endothelial Cells. *Reproductive Sciences.* 2014;21(4):477-482.
163. Tatemoto K, Hosoya M, Habata Y, et al. Isolation and Characterization of a Novel Endogenous Peptide Ligand for the Human APJ Receptor. *Biochemical and Biophysical Research Communications.* 1998;251(2):471-476.
164. Zhong J-C, Zhang Z-Z, Wang W, McKinnie SMK, Vederas JC, Oudit GY. Targeting the apelin pathway as a novel therapeutic approach for cardiovascular diseases. *Biochimica et Biophysica Acta (BBA) - Molecular Basis of Disease.* 2017;1863(8):1942-1950.
165. Maguire JJ, Kleinz MJ, Pitkin SL, Davenport AP. [Pyr1]Apelin-13 Identified as the Predominant Apelin Isoform in the Human Heart. *Hypertension.* 2009;54(3):598-604.
166. Kleinz MJ, Skepper JN, Davenport AP. Immunocytochemical localisation of the apelin receptor, APJ, to human cardiomyocytes, vascular smooth muscle and endothelial cells. *Regulatory Peptides.* 2005;126(3):233-240.
167. Boucher Jrm, Masri B, Daviaud Dl, et al. Apelin, a Newly Identified Adipokine Up-Regulated by Insulin and Obesity. *Endocrinology.* 2005;146(4):1764-1771.
168. Wang W, McKinnie SMK, Farhan M, et al. Angiotensin-Converting Enzyme 2 Metabolizes and Partially Inactivates Pyr-Apelin-13 and Apelin-17. *Hypertension.* 2016;68(2):365-377.
169. Akcılar R, Turgut S, Caner V, et al. Apelin Effects on Blood Pressure and RAS in DOCA-Salt-Induced Hypertensive Rats. *Clinical and Experimental Hypertension.* 2013;35(7):550-557.
170. Yang X, Zhu W, Zhang P, et al. Apelin-13 stimulates angiogenesis by promoting cross-talk between AMP-activated protein kinase and Akt signaling in myocardial microvascular endothelial cells. *Mol Med Rep.* 2014;9(5):1590-1596.
171. Helker CSM, Eberlein J, Wilhelm K, et al. Apelin signaling drives vascular endothelial cells toward a pro-angiogenic state. *eLife.* 2020;9:e55589.
172. Liu Q, Hu T, He L, et al. Genetic targeting of sprouting angiogenesis using Apln-CreER. *Nature Communications.* 2015;6(1):6020.
173. Farkasfalvi K, Stagg MA, Coppen SR, et al. Direct effects of apelin on cardiomyocyte contractility and electrophysiology. *Biochemical and Biophysical Research Communications.* 2007;357(4):889-895.
174. Liu W, Yan J, Pan W, Tang M. Apelin/Elabela-APJ: a novel therapeutic target in the cardiovascular system. *Ann Transl Med.* 2020;8(5):243.

175. Barchetta I, Baroni MG, Melander O, Cavallo MG. New Insights in the Control of Fat Homeostasis: The Role of Neurotensin. *International Journal of Molecular Sciences.* 2022;23(4):2209.
176. Osadchii OE. Emerging role of neurotensin in regulation of the cardiovascular system. *European Journal of Pharmacology.* 2015;762:184-192.
177. Januzzi JL, Lyass A, Liu Y, et al. Circulating Proneurotensin Concentrations and Cardiovascular Disease Events in the Community. *Arteriosclerosis, Thrombosis, and Vascular Biology.* 2016;36(8):1692-1697.
178. Li J, Yang L, Song J, et al. Neurotensin accelerates atherosclerosis and increases circulating levels of short-chain and saturated triglycerides. *Atherosclerosis.* 2024;392:117479.
179. Ramirez-Virella J, Leinninger GM. The Role of Central Neurotensin in Regulating Feeding and Body Weight. *Endocrinology.* 2021;162(5).
180. Cimini FA, Barchetta I, Bertoccini L, et al. High pro-neurotensin levels in individuals with type 1 diabetes associate with the development of cardiovascular risk factors at follow-up. *Acta Diabetologica.* 2022;59(1):49-56.
181. Bakirtzi K, West G, Fiocchi C, Law IKM, Iliopoulos D, Pothoulakis C. The Neurotensin–HIF-1α–VEGFα Axis Orchestrates Hypoxia, Colonic Inflammation, and Intestinal Angiogenesis. *The American Journal of Pathology.* 2014;184(12):3405-3414.
182. Pearson AC, Shrestha K, Curry Jr TE, Duffy DM. Neurotensin modulates ovarian vascular permeability via adherens junctions. *The FASEB Journal.* 2024;38(7):e23602.
183. Simões FC, Riley PR. Immune cells in cardiac repair and regeneration. *Development.* 2022;149(8).
184. Osadchii OE. Emerging role of neurotensin in regulation of the cardiovascular system. *Eur J Pharmacol.* 2015;762:184-192.
185. Förster R, Davalos-Misslitz AC, Rot A. CCR7 and its ligands: balancing immunity and tolerance. *Nature Reviews Immunology.* 2008;8(5):362-371.
186. Damås JK, Smith C, Øie E, et al. Enhanced Expression of the Homeostatic Chemokines CCL19 and CCL21 in Clinical and Experimental Atherosclerosis. *Arteriosclerosis, Thrombosis, and Vascular Biology.* 2007;27(3):614-620.
187. Pierce EM, Carpenter K, Jakubzick C, et al. Idiopathic pulmonary fibrosis fibroblasts migrate and proliferate to CC chemokine ligand 21. *European Respiratory Journal.* 2007;29(6):1082.
188. Nykänen AI, Sandelin H, Krebs R, et al. Targeting Lymphatic Vessel Activation and CCL21 Production by Vascular Endothelial Growth Factor Receptor-3 Inhibition Has Novel Immunomodulatory and Antiarteriosclerotic Effects in Cardiac Allografts. *Circulation.* 2010;121(12):1413-1422.
189. Marsland BJ, Bättig P, Bauer M, et al. CCL19 and CCL21 Induce a Potent Proinflammatory Differentiation Program in Licensed Dendritic Cells. *Immunity.* 2005;22(4):493-505.
190. Finsen AV, Ueland T, Sjaastad I, et al. The Homeostatic Chemokine CCL21 Predicts Mortality in Aortic Stenosis Patients and Modulates Left Ventricular Remodeling. *PLOS ONE.* 2014;9(11):e112172.
191. Jiang Y, Bai J, Tang L, Zhang P, Pu J. Anti-CCL21 Antibody Attenuates Infarct Size and Improves Cardiac Remodeling After Myocardial Infarction. *Cellular Physiology and Biochemistry.* 2015;37(3):979-990.
192. Báez-Díaz C, Blanco-Blázquez V, Sánchez-Margallo F-M, et al. Microencapsulated Insulin-Like Growth Factor-1 therapy improves cardiac function and reduces fibrosis in a porcine acute myocardial infarction model. *Scientific Reports.* 2020;10(1):7166.
193. Tate M, Perera N, Prakoso D, et al. Bone Morphogenetic Protein 7 Gene Delivery Improves Cardiac Structure and Function in a Murine Model of Diabetic Cardiomyopathy. *Frontiers in Pharmacology.* 2021;12.
194. Salido-Medina AB, Gil A, Expósito V, et al. BMP7-based peptide agonists of BMPR1A protect the left ventricle against pathological remodeling induced by pressure overload. *Biomedicine & Pharmacotherapy.* 2022;149:112910.

195. Bozoglu T, Lee S, Ziegler T, et al. Endothelial Retargeting of AAV9 In Vivo. *Advanced Science.* 2022;9(7):2103867.